VITAMIN D-INDEPENDENT REGULATION OF INTESTINAL CALCIUM ABSORPTION AND SKELETAL MINERALIZATION DURING PREGNANCY

NEVA JENNIFER FUDGE

VITAMIN D-INDEPENDENT REGULATION OF INTESTINAL CALCIUM ABSORPTION AND SKELETAL MINERALIZATION DURING PREGNANCY

by

©Neva Jennifer Fudge

A thesis submitted to the School of Graduate Studies in partial fulfillment of the requirements for the degree of Master of Science

Faculty of Medicine
Memorial University of Newfoundland

May 6, 2010

St. John's Newfoundland and Labrador

ABSTRACT

Pregnancy and lactation create a large physiological demand for calcium. Normally, 1,25 dihydroxyvitamin D ($1,25(OH)_2D_3$) and the vitamin D receptor (VDR) are critical for the regulation of calcium and bone metabolism. Without $1,25(OH)_2D_3$ and/or the VDR, intestinal calcium absorption is reduced, leading to hypocalcemia, secondary hyperparathyroidism, rickets, and osteomalacia. This project assessed whether $1,25(OH)_2D_3$ and the VDR were required for the regulation of calcium and bone metabolism during the reproductive periods.

Mice lacking the gene encoding for the VDR (*Vdr* null) and wild-type (WT) mice were raised on a regular 1% calcium diet until 10 weeks of age and then switched to a 2% calcium, 20% lactose enriched diet. Bone mineral content (BMC) was measured at baseline, late pregnancy, late lactation and 21 days after weaning. Duodenal ^{45}Ca absorption and gene expression, parameters of calcium homeostasis, bone turnover markers and bone histomorphometry were measured at baseline and late pregnancy.

Vdr null mice had a significantly lower BMC at baseline as compared to WT siblings. WT mice gained 7% BMC during pregnancy, lost 18% during lactation and recovered to baseline post weaning. In contrast, *Vdr* null sisters gained 57% BMC during pregnancy ($p \leq 0.05$) resulting in a BMC that was equal to WT. *Vdr* nulls lost 31% BMC during lactation and recovered post-weaning to a value that was 49% higher than the pre-pregnancy baseline. Duodenal ^{45}Ca absorption and the expression of the calcium channel transient receptor potential, vanilloid type 6 (*Trpv6*) was lower in *Vdr* nulls at baseline but significantly increased to WT levels during pregnancy. *Vdr* null serum parathyroid

hormone (PTH) levels and bone turnover were elevated at baseline but normalized to WT levels by late pregnancy. Urine calcium concentration was reduced at baseline in *Vdr* null mice but similar to WT values during pregnancy. *Vdr* null rachitic tibias were not morphologically repaired during pregnancy but had increased mineralization of osteoid.

In summary, pregnancy increased intestinal calcium absorption in *Vdr* null mice, possibly through an increase in duodenal *Trpv6* expression. This led to a normalizing of serum PTH levels, bone turnover and ultimately an increase in BMC. In conclusion, intestinal calcium absorption and skeletal mineralization are regulated independently of 1,25 $(OH)_2D_3$ and the VDR during pregnancy.

ACKNOWLEDGEMENTS

I have many reasons to thank my supervisor Dr. Christopher Kovacs. First of all, I would like to thank him for believing in my research potential and agreeing to take me on as his master's student, even when it meant that he would be loosing a research assistant. I'd also like to thank him for being so understanding about the fact that I have a family. During the first six months of my program, he allowed me to work in the evenings so that I could stay home with my infant daughter during the day. Finally, I would like to thank him for his outstanding supervision. His support and guidance allowed me to win various awards, publish my data and attend 5 national and international conferences. Studying in his lab has been a positive experience that has led me to continue to pursue a career in science.

I would like to thank my supervisory committee, Dr. Daniel MacPhee and Dr. Donald McKay. Their valuable comments and criticisms also played a key role in the success of my program and thesis.

I would like to thank my labmates and friends Beth, Charlene, Darryl, Andrea and the rest of the lunchtime crew for their friendship, support (lol) and comic relief.

Finally, I would like to thank my family, especially my husband Adam and my children, Brandon and Naya. Without their love, support and understanding, this entire adventure would not have been possible.

TABLE OF CONTENTS

ABSTRACT ii
ACKNOWLEDGEMENTS iv
TABLE OF CONTENTS v
LIST OF FIGURES vii
LIST OF TABLES ix
LIST OF ABBREVIATIONS x
1. Introduction 1
1.1 Vitamin D 1
1.2 Calcium and bone metabolism 2
1.2.1 Calcium distribution 2
1.2.2 The physiological importance of calcium 2
1.2.3 Calcium homeostasis 3
1.2.3.1 Intestinal calcium absorption 5
1.2.3.2 Renal calcium excretion 9
1.2.3.3 The skeleton 9
1.2.3.3.1 Bone remodeling-activation 10
1.2.3.3.2 Bone remodeling-resorption 11
1.2.3.3.3 Bone remodeling-reversal 12
1.2.3.3.4 Bone remodeling-formation 13
1.2.4 Adaptations during pregnancy 14
1.2.5 Adaptations during lactation 15
1.2.6 Skeletal recovery after weaning 17
1.2.7 Vdr knockout mouse model 17
1.2.8 Project description 19
2. Methods 21
2.1 Animal husbandry 21
2.3.1 Tagging and tailing 23
2.3.2 DNA extraction from tail samples 23
2.3.3 Polymerase chain reaction (PCR) 24
2.3.4 Gel electrophoresis 25
2.4 Bone mineral content 25
2.5 Intestinal ^{45}Ca transfer 26
2.6 RNA expression analysis in the duodenum and vertebrae 27
2.6.1 Tissue collection 27
2.6.2 RNA extraction 27
2.6.3 Whole genome microarray analysis 29
2.6.4 Validation of microarray results using real time RT-PCR. 30
2.7 Serum analysis 31
2.7.1 Serum ionized calcium 31
2.7.2 Serum PTH 31
2.7.3 Serum osteocalcin 32

2.8. Urine analysis 33
2.8.1 Urine deoxypyridinoline (DPD) 33
2.8.2 Urine creatinine 34
2.8.3 Urine total calcium 34
2.9 Histology 35
2.9.1 Goldner's trichrome method 35
2.9.2 Von Kossa method 36
2.9.3 Toluidine blue stain 37
2.10 Histomorphometry 37
3. Results 39
3.1 Bone mineral content 39
3.2 Duodenal ^{45}Ca absorption 47
3.3 Duodenal gene expression 47
3.4 Calcium homeostasis 50
3.4.1 Serum ionized calcium 53
3.4.2 Urine calcium 53
3.4.3 Secondary hyperparathyroidism 57
3.5 Bone histology and histomorphometry 61
4. Discussion 64
4.1 Bone mineral content 64
4.2 Duodenal calcium absorption and gene expression 68
4.2.1 Duodenal calcium absorption 68
4.2.2 Duodenal gene expression 71
4.3 Impact on calcium homeostasis 76
4.3.1 Serum calcium 76
4.3.2 Urine calcium 78
4.3.3 Secondary hyperparathyroidism and bone turnover 78
4.4 Bone histology and histomorphometry 80
4.6 Summary and conclusion 85
REFERENCES 86

LIST OF FIGURES

Figure 1.1: Active transcellular and passive paracellular intestinal calcium absorption..6

Figure 3.1: Relative changes in BMC throughout the reproductive periods in WT and *Vdr* null mice.....40

Figure 3.2: Relative changes in spine BMC throughout the reproductive periods in WT and *Vdr* null mice.....41

Figure 3.3: Relative change in hindlimb BMC throughout the reproductive periods in WT and *Vdr* null mice.....42

Figure 3.4: Changes in absolute BMC in *Vdr* null and WT mice throughout the reproductive periods.....44

Figure 3.5: Relative change in BMC in non-pregnant *Vdr* null mice after receiving the enriched diet as compared to their pre-diet baseline.....45

Figure 3.6: Duodenal ^{45}Ca absorption in *Vdr* null and WT mice at baseline and gestation day 16.5 of pregnancy.....48

Figure 3.7: Relative expression of duodenal *Trpv6* in WT and *Vdr* null mice at baseline and throughout pregnancy as determined using Real Time RT-PCR.....52

Figure 3.8: Preliminary results for serum ionized calcium levels at baseline and late pregnancy in *Vdr* null mice.....53

Figure 3.9: Serum ionized calcium in virgin *Vdr* null mice while on a regular diet (10 weeks) and while receiving the enriched diet.....55

Figure 3.10: Urine total calcium levels in WT and *Vdr* null mice at baseline and throughout pregnancy.....56

Figure 3.11: Serum PTH levels in WT and *Vdr* null mice at baseline and during pregnancy.....58

Figure 3.12: Serum osteocalcin levels in WT and *Vdr* null mice at baseline and during pregnancy.....59

Figure 3.13: Urine DPD levels in WT and *Vdr* null mice at baseline and during pregnancy.....60

Figure 3.14: Undecalcified tibia histology.....62

Figure 4.1: Proposed model for the increase in transcellular absorption in *Vdr* null mice during pregnancy.....83

Figure 4.2: Proposed model for the effect of the calcium and lactose enriched diet on paracellular absorption.....84

LIST OF TABLES

Table 3.1: The time between baseline and late pregnancy scans for each *Vdr* null and WT mice and the amount of BMC gained.....46

Table 3.2: Relative duodenal mRNA expression of *Trpv6*, *Pmca1b* and *Sg100* as determined by whole genome microarray analysis.....49

Table 3.3: Relative duodenal mRNA expression of *Trpv6*, *Pmca1b* and *Sg100* as determined by real time RT-PCR.....51

Table 3.4: Histomorphometry results for *Vdr* null tibias at baseline and late pregnancy.....63

LIST OF ABBREVIATIONS

Bone mineral content	BMC
Bone mineral density	BMD
Bone volume	BV/TV
Ca^{2+}ATPase gene	*Pmca1b*
Calbindin-D_{9K}	*Sg100*
Calcium sensing receptor	CaSR
Cholecalciferol	D_3
Complementary DNA	cDNA
Deoxypyridinoline	DPD
Deoxyribonucleic acid	DNA
Deoxyribonucleotide triphophates	dNTPs
Enzyme linked immunoassay	ELISA
Enzyme immunoassay	EIA
Ergocalciferol	D_2
Glutaraldehyde-3-phosphate dehydrogenase	*Gapdh*
Gonadotrophin releasing hormone	GnRH
Immunoradiometric assay	IRMA
Intraperitoneal	i.p.
Osteoblast number	N.Ob/BPm
Osteoclast number	N.Oc/BPm
Osteoclast surface	OcS/BS

Osteoid surface	OS/BS
Osteoprotegerin	OPG
Parathryroid hormone	PTH
Parathyroid hormone-like protein	PTHrP
Parathyroid hormone receptor	PTHR
Phosphate Buffered Saline	PBS
Polymerase chain reaction	PCR
Receptor activator of nuclear factor-κβ	RANK
Receptor activator of nuclear factor-κβ ligand	RANKL
Reverse transcriptase polymerase chain reaction	RT-PCR
Rho-associated coiled-coil forming kinase	ROCK
Ribonucleic acid	RNA
RNA integrity number	RIN
Threshold cycle	C_T
Trabecular number	Tb.N
Trabecular thickness	Tb.Th
Trabecular spacing	Tb.Sp
Transforming growth factor beta	TGF-β
Transient receptor potential, vanilloid type 6	TRPV6
Transient receptor potential, vanilloid type 6 gene	*Trpv6*
Vitamin D receptor	VDR
Vitamin D receptor gene	*Vdr*

1,25 dihydroxyvitamin D	$1,25(OH)_2D_3$
25, hydroxyvitamin D	25(OH)D
Wild-type	WT

1. Introduction

1.1 Vitamin D

The "sunshine vitamin", vitamin D, is required for normal calcium and bone metabolism. Vitamin D deficiency results in secondary hyperparathyroidism, rickets and osteomalacia. Vitamin D levels are also positively correlated with bone mineral density (BMD) (1). Moreover, supplementation with calcium and vitamin D improves BMD and prevents fractures in older people (2).

The term vitamin D refers to two biologically inactive precursors, ergocalciferol (D_2) and cholecalciferol (D_3) (3). Vitamin D_2 (obtained from dietary supplements) or vitamin D_3 (obtained from the diet or synthesized in the skin during sun exposure) must undergo many enzymatic conversions to become calcitriol, the active form of vitamin D (1,25 dihydroxyvitamin D or $1,25(OH)_2D_3$). D_2 and D_3 become bound by serum vitamin D binding proteins and enter the circulation. They are then converted to the pro-hormone, 25 hydroxyvitamin D (25(OH)D) by cytochrome P450 enzymes that are primarily located in the liver and released back into the blood stream (3). This is the form that is measured clinically because it is the most reliable indicator of vitamin D levels (4). 25(OH)D is converted to $1,25(OH)_2D_3$ by the 1,α hydroxylase enzyme, located in the kidney (3) and many other target tissues. The expression of the renal enzyme is stimulated by parathyroid hormone (PTH), a peptide hormone that is produced by the parathyroids which has an important role in regulating calcium metabolism.

The importance of $1,25(OH)_2D_3$ and the VDR in the regulation of calcium and bone metabolism is well known. Its role in regulating calcium and bone metabolism during the reproductive periods, however, is controversial. Here I use a mouse model to investigate the importance of $1,25(OH)_2D_3$ and the VDR on calcium and bone metabolism during pregnancy.

1.2 Calcium and bone metabolism

1.2.1 Calcium distribution

The adult human contains approximately 1000 grams of calcium, of which ~99% exists as hydroxyapatite in the mineralized portion of the skeleton. The final 1% of the body's calcium exists in the blood (or serum), extracellular fluid and soft tissues. In the serum, approximately 45% of total serum calcium is bound to proteins such as albumin, 10% is complexed to anions such as citrate or phosphate. The final 45% is ionized calcium, which is the physiologically active portion (5).

1.2.2 The physiological importance of calcium

The blood provides ionized calcium for many cellular processes, including neuronal excitability, skeletal and cardiac muscle contraction, and bone formation. Calcium also serves as a signal transducer. It activates pathways that are involved in hormone secretion, neurotransmission, and kinase phosphorylation. Calcium

insufficiency disrupts these vital physiological processes and can lead to muscle cramps, tetany, seizures and fatal arrythmias (6).

Maintenance of skeletal calcium is also important. Flat bones, such as ribs and the skull, support and protect vital organs. Long bones, such as the femur and humorus, serve as levers for the muscles and support locomotion and movement.

1.2.3 Calcium homeostasis

To meet the needs of biochemical processes and skeletal mineral requirements, the amount of calcium in the blood and in the skeleton is tightly regulated. Normally in humans, total serum calcium is maintained between 2.1 – 2.5 mM and ionized calcium between 1.1-1.3 mM (7). Presuming that calcium intake is adequate, calcium balance is achieved through the coordinated actions of the intestine, bone and kidney. Adults ingesting 1 gram of calcium per day, typically absorb only 200 mg in the small intestine and egest 800mg in the feces. The skeleton, which contains 1 kg of calcium, acts as a nearly inexhaustible calcium storage site and there is a constant exchange of calcium between the bone and the extracellular fluid. The skeleton will release about 500 mg of calcium into the blood daily due to resorption and also deposit 500mg during bone formation. The kidneys typically filter 10 g of calcium out of the blood per day but reabsorb almost 100% of this calcium back into the circulation. As a result, only 200mg of calcium is lost in the urine daily (5).

Calcium absorption in the intestine, excretion by the kidneys and exchange between the blood and bone is, in part, maintained through the action of the calcium sensing receptor (CaSR). The CaSR is a G-protein coupled receptor that is most prominently expressed on the surface of the chief cells of the parathyroid gland (8) and to a lesser extent on segments of the nephron in the kidney. This receptor contains multiple Ca^{2+} binding elements in its extracellular domain and signaling determinants in its cytoplasmic region (7). The CaSR detects changes in extracellular calcium and mediates the minute to minute secretion of PTH. When there is a decrease in the extracellular calcium concentration, less calcium binds to the CaSR. As a result, the CaSR is less activated, releasing its inhibition on PTH synthesis and release by the parathyroid gland (7).

PTH acts to increase extracellular calcium levels in three ways. Within minutes, PTH acts on the kidneys, to enhance calcium's return to the blood (9). In minutes to hours, PTH increases bone resorption, liberating calcium into the blood. PTH also indirectly increases intestinal calcium absorption by stimulating an increase in the renal synthesis of $1,25(OH)_2D_3$ (10). All three actions help restore normocalcemia, which in turn, inhibits further production of PTH and $1,25(OH)_2D_3$. Certain disorders in the intestine, kidneys or bone may interfere with this homeostatic process (11). In these cases, PTH levels remain elevated (secondary hyperparathyroidism) (11).

Conversely, an increase in serum calcium activates the CaSR, which suppresses the release of PTH by the parathyroid gland. As a result, the renal synthesis of $1,25(OH)_2D_3$ also decreases. Decreased PTH and $1,25(OH)_2D_3$ levels result in decreased

bone resorption and intestinal calcium absorption. An increase in serum calcium level is also detected by the renal CaSR, which stimulates an increase in calcium excretion by the kidney, thus removing excess calcium from the circulation, returning serum calcium to normal levels (5).

1.2.3.1 Intestinal calcium absorption

Absorption of dietary calcium occurs chiefly (90%) in the small intestine (5). Calcium intake is typically 1000mg daily but only 20 to 60% of dietary calcium is absorbed (5). The efficiency of absorption is influenced by age, calcium intake, vitamin D status, the state of the calcium homeostatic system and the bioavailability of calcium in the diet (12).

Calcium is absorbed in the small intestine by two different processes, active transcellular transport and passive paracellular diffusion (*Figure 1.1*). During adulthood or when calcium intake is low, active transcellular transport of calcium is high in the duodenum (13) which normally accounts for 10-15% absorption of the dietary load. Transcellular absorption of calcium involves the movement of calcium directly through the mucosal cells of the intestinal epithelial layer. Differences in calcium concentrations of the intestinal lumen (10^{-3}M) and the cytosol of the mucosal cell (10^{-6}M) create a 1000-fold chemical and electrical gradient across the plasma membrane. This favors calcium entry into the cell via a transmembrane calcium ion channel, transient receptor potential, vanilloid type 6 (TRPV6), which is located on the apical membrane (14-16). When

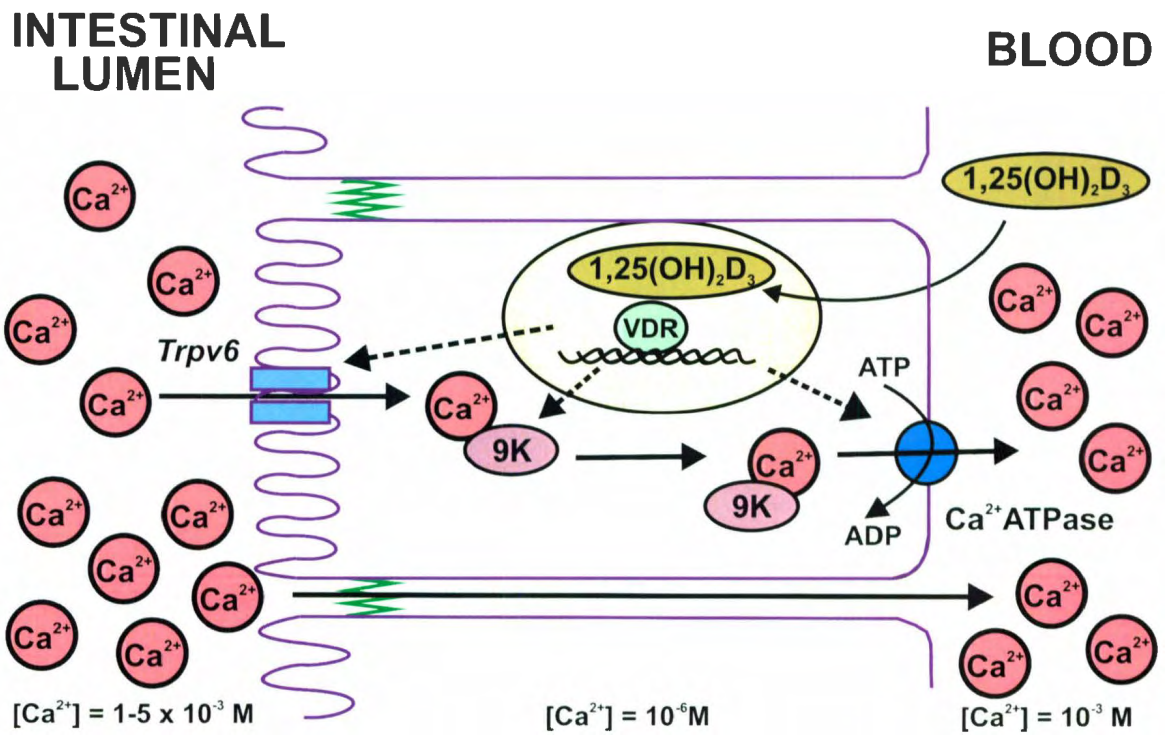

Figure 1.1 **Active transcellular and passive paracellular intestinal calcium absorption.** Active absorption involves the movement of calcium ions across the mucosal cell via a calcium ion channel (TRPV6), a calcium binding protein (calbindin-D_{9K}) and an energy dependent, high affinity, limited capacity Ca^{2+}ATPase. Passive diffusion, a process driven by transepithelial electrochemical gradients, involves the movement of calcium ions between the membranes of adjacent intestinal mucosal cells and into the extracellular fluid.

calcium enters the cytoplasm it becomes bound by calbindin-D_{9K}, a calcium binding protein (16, 17), which is sequestered in vesicles (9). Calbindin-D_{9K} transports calcium ions from the apical membrane to the basolateral membrane of the absorptive enterocyte. The vesicles then fuse with the basolateral membrane (9). Calcium is extruded out of the cell and into the blood via an energy dependent, high affinity, limited capacity Ca^{2+}ATPase (9). A low affinity, high capacity sodium-calcium exchanger may play a minor role in transporting calcium out of the intestinal cell (18).

1,25$(OH)_2D_3$ is a key regulator of transcellular calcium transport. The steroid hormone diffuses out of the blood, across the basolateral membrane and into the musosal cell. It forms a complex with the nuclear VDR, a ligand dependent transcription factor (19). This initiates the transcription of *Trpv6*, calbindin-D_{9K} (encoded by the gene *Sg100*) and Ca^{2+}ATPase (encoded by the gene *Pmca1b*), thus stimulating all three components involved in the active absorption of calcium across the intestine (20-23).

PTH regulates transcellular calcium absorption indirectly. It stimulates 1-α hydroxylase in the kidney to convert circulating 25-hydroxyvitamin D to 1,25 dihydroxyvitamin D_3. This increases serum 1,25$(OH)_2D_3$ levels, which leads to increased intestinal calcium absorption.

Other hormones have been shown to stimulate intestinal calcium absorption. Prolactin, a hormone that stimulates mammary milk production and estrogen, the primary female sex hormone, may interact with their receptors to induce *Trpv6* expression and stimulate transcellular calcium transport independently of 1,25$(OH)_2D_3$ (24-26).

Calcium also crosses the intestinal epithelium via passive diffusion. Passive diffusion involves the movement of calcium ions between the membranes of adjacent intestinal mucosal cells and into the extracellular fluid. This process is driven by transepithelial electrochemical gradients. The higher the concentration of calcium in the lumen of the intestine, the greater the diffusion of calcium between the mucosal cells.

Paracellular calcium absorption can be regulated through the manipulation of tight junction proteins which control epithelial permeability (27). $1,25(OH)_2D_3$ stimulates paracellular calcium absorption (28-30) through either VDR-dependent mechanisms, by increasing in the expression of the claudin family of tight junction proteins (30) or non-genomic mechanisms, by stimulating signaling pathways (29). Prolactin increases passive calcium absorption (31, 32) possibly through the activation of the Rho-associated coiled-coil forming kinase (ROCK) signaling pathway (33, 34). Lactose, a component of milk, has also been shown to increase intestinal calcium absorption (35). The mechanism of how this occurs is unknown but its degradation to glucose and galactose is involved (36).

The importance of paracellular absorption has been debated. Several studies indicate that when calcium intake is normal or high, calcium is primarily absorbed by passive mechanisms in the ileum or jejunum (12, 37, 38). Conversely, a review by McCormick (39) suggests that the passive diffusion is not the major mechanism by which calcium is absorbed in normal adult humans.

1.2.3.2 Renal calcium excretion

The kidney plays a central role in maintaining calcium balance. Calcium is filtered out of the blood in the capillaries of the glomerulus. Approximately 85% of filtered calcium is passively reabsorbed in the proximal tubule and the thick ascending loop of Henle. 15% of filtered calcium is actively reabsorbed in the distal convoluted tubule (5). This portion of calcium reabsorption is regulated by PTH. When there is a decrease in serum calcium levels, PTH binds to the PTH receptor (PTHR) on the kidney tubules and stimulates calcium reabsorption (40). As a result, less calcium is excreted in the urine. An increase in serum calcium activates the renal CaSR, which stimulates an increase in calcium excretion by the kidney, thus normalizing serum calcium (5).

1.2.3.3 The skeleton

In addition to support and locomotion, the skeleton also acts as a storage site for calcium and plays an important role in the maintenance of extracellular calcium balance. This is achieved through the process of bone remodeling. Bone remodeling is a complex coordination of cellular events that ultimately results in the formation of new bone through two processes, bone breakdown or resorption and bone formation or mineralization. Bone remodeling occurs in small packets of cells which are referred to as bone remodeling units (41). The skeleton is composed mainly of two bone types: dense cortical bone and spongy, metabolically active trabecular bone. Bone remodeling is more active near the marrow cavity, on the surface of trabecular bone and occurs in cycles

(42). When calcium demand is high, the activation of new remodeling units may be required (41). This increases the number of bone resorption sites and liberates more calcium into the blood. Conversely, when calcium intake is high, excess calcium is stored in the bone through the process of bone formation. These processes do not occur randomly. They are regulated by a variety of systemic hormones and local cytokines that act on bone forming cells or osteoblasts and bone resorbing cells, or osteoclasts. A complete remodeling cycle will take 3-6 months (43). Rates of remodeling may also differ depending on the location of the bone, age and activities. Bone resorption and formation rates are not always equal and may result in a net change in the total amount of BMC in the skeleton. When formation dominates over resorption, such as during childhood, there will be a net increase in BMC. When bone resorption dominates over bone formation, as it does in late adulthood, there will be a net decrease in BMC.

1.2.3.3.1 Bone remodeling-activation

Bone is broken down by bone resorbing cells called osteoclasts. These cells originate from macrophages in the bone marrow (44). Two cytokines are essential for the initiation of osteoclastogenesis; receptor activator of nuclear factor-κβ ligand (RANKL) (45) and macrophage colony stimulating factor (46). RANKL, a member of the Tumor Necrosis Factor superfamily, is a key cytokine required for osteoclastogenesis. Osteoblasts, or bone forming cells, stimulate the differentiation of osteoclast precursors when RANKL is expressed on their surface. RANKL binds to the

receptor activated nuclear factor (RANK) receptor on the surface of pre-osteoclasts and stimulates their differentiation. Several activated pre-osteoclasts fuse to form a mature, multinucleated osteoclast. RANKL also stimulates mature osteoclasts to resorb bone.

Activation of bone remodeling is negatively regulated by a local cytokine, osteoprotegerin (OPG). OPG is secreted by the osteoblast and binds to RANKL, thus preventing RANK-RANKL interactions (47, 48). This inhibits the formation of new osteoclasts and the initiation of bone resorption.

Continuous administration of PTH leads to bone loss in humans. PTH binds to the PTHR on pre-osteoblasts and induces RANKL expression. As a result, OPG expression decreases, which encourages the proliferation and differentiation of pre-osteoclasts, and the stimulation of bone resorption (49).

Despite its pharmacological use to increase BMC, $1,25(OH)_2D_3$ stimulates bone resorption (50, 51). When present at supraphysiological levels, $1,25(OH)_2D_3$ increases mesenchymal cell transcription of the RANKL gene and decreases transcription of OPG (48).

1.2.3.3.2 Bone remodeling-resorption

The activated osteoclast migrates to bone and attaches to it. $\alpha v\beta 3$ is the principle integrin mediating the attachment of osteoclasts to bone (52). This integrin recognizes the Arg-Gly-Asp amino acid motif which is present in many bone matrix proteins, such as osteopontin and bone sialoprotein. Contact with the bone surface induces the

formation of the sealing zone, which is caused by the rearrangement of the cytoskeleton to form the "actin ring". This enables the osteoclast to form an isolated microenvironment between itself and the underlying bone matrix. Vesicles containing cathepsin K, tartrate-resistent acid phosphatase and matrix metalloproteases are then transported to and fused with the plasma membrane that is adjacent to the bone (53). This results in the formation of the "ruffled border", a villus structure that is unique to osteoclasts. The ruffled border contains a proton pump and a Cl^- channel that together acidify the isolated resorptive compartment to a pH of ~4.5 (54). This acidic environment removes the mineral from the bone. The exposed bone matrix, composed mainly of type I collagen, is then degraded by the lysosomal enzyme, cathepsin K. The resulting protein fragments are endocytosed by the osteoclast and discharged from the opposite basal surface into the extracellular environment (55). The presence of degraded protein fragments in the serum (C-telopeptide), or in the urine (deoxypyridinoline (DPD)) are often used as biomarkers to determine the physiological rate of bone resorption.

1.2.3.3.3 Bone remodeling-reversal

During the intermediate phase between resorption and formation, uncharacterized macrophage-like mononuclear cells form a cement line over the resorption site. This line marks the limit of resorption and helps to bind the new bone to the old bone. A spectrum of signaling proteins accumulate in the extracellular matrix which play key roles in the commitment and differentiation of mesenchymal stem cells in the bone marrow to

become osteoblasts (56). Pre-osteoblasts are recruited to the site to begin the bone formation stage. The signals that recruit osteoblasts have not been identified but it is likely that transforming growth factor beta, insulin growth factor I and II, bone morphogenic proteins, platelet derived growth factor and fibroblast growth factor may be involved (57-59).

1.2.3.3.4 Bone remodeling-formation

Upon arrival at the remodeling site, osteoblasts synthesize and secrete the organic matrix, composed mostly of collagen I. During this process, other proteins secreted by the osteoblasts, such as osteocalcin and alkaline phosphatase, will 'leak' into the circulation and are often used as serum biomarkers of bone formation. After the matrix is secreted, the osteoblasts release small membrane bound 'matrix vesicles' that contain highly concentrated calcium and phosphate and other factors which create optimal conditions for bone mineralization (41). Osteocalcin has a high binding affinity for calcium. When sufficient calcium is available, it binds to the osteocalcin resulting in the mineralization of the matrix. Osteoblasts eventually become entombed in the mineralized matrix as osteocytes but maintain communication with other osteocytes by extending their cytoplasm through tunnel-like canaliculae (41). When calcium is not readily available, the osteoid may remain unmineralized or mineralization may be prolonged.

1,25$(OH)_2D_3$ may play a direct role in the regulation of bone formation. Oral supplementation with vitamin D_3 decreases rates of bone loss in older adult humans (60).

Higher serum $1,25(OH)_2D_3$ levels have been associated with a higher BMD of the hip (1). $1,25(OH)_2D_3$ also enhances the synthesis of osteocalcin by osteoblasts (42), promotes exocytosis of bone materials and increases osteoblast survival (61). Furthermore, this is suppported by the fact that the *Vdr* is expressed in osteoblasts (62). Other findings suggest that the anabolic actions of $1,25(OH)_2D_3$ are indirect, resulting from the suppression of PTH (63) and the stimulation of intestinal calcium absorption, which both encourage bone formation.

PTH has also been used as a pharmacological stimulator of bone formation (64). The administration of short pulses of PTH activates the PTHR and stimulates the proliferation, differentiation and activation of osteoblasts, leading to an increase in bone formation.

1.2.4 Adaptations during pregnancy

During human pregnancy, the mineralizing fetal skeleton will require approximately 30g of calcium, 80% of this during the third trimester. This imposes a high demand for calcium on the maternal circulation. The mother primarily adapts to this demand through a doubling in intestinal calcium absorption (65, 66). Total circulating $1,25(OH)_2D_3$ is doubled early in pregnancy but free $1,25(OH)_2D_3$ levels are not increased until the third trimester (67). The increase in $1,25(OH)_2D_3$ may mediate an increase in TRPV6, calbindin-D_{9K} and Ca^{2+} ATPase, resulting in an increase in intestinal calcium absorption during pregnancy. There is evidence to suggest, however, that the increase in

intestinal calcium absorption can occur independently of $1,25(OH)_2D_3$. The doubling in intestinal calcium absorption precedes the rise in free $1,25(OH)_2D_3$ levels in humans and other mammals (67). Also, intestinal calcium absorption was increased in vitamin D deficient rats during pregnancy (68, 69). Studies by Takeuchi *et al.* (70) suggest that placental lactogen, a hormone that is produced by the placenta, may stimulate intestinal calcium absorption.

Studies in our laboratory in normal mice found that the mother may experience increases in BMC during pregnancy (71, 72). This suggests that BMC may increase during pregnancy in preparation for the large skeletal losses that occur during lactation. Evidence in humans suggests that there is a small decrease in BMD by the end of pregnancy due to small increases in bone resorption (73, 74). These human studies are limited for many reasons. For example, due to concerns of fetal radiation exposure, BMD scans have been done months before a planned pregnancy and 1-6 weeks after, but not during pregnancy. Many studies lack baseline measurements and therefore the controls that are needed to properly interpret data. Serum and urine biomarker studies are also not reliable during pregnancy because of different factors such as hemodilution and increased glomerular filtration rate in the kidney (67).

1.2.5 Adaptations during lactation

During lactation, humans secrete between 0.2-0.5g of calcium in the breast milk daily. This greatly increases the physiological demand for calcium in the lactating

woman. In contrast to pregnancy, lactating mothers maintain calcium balance by rapidly demineralizing their skeletons. Women who lactate exclusively for three to six months lose 5-10% bone mineral content. Female mice normally lose 25-30% of BMD during three weeks of lactation. The amount of BMD lost during lactation is proportional to the amount of calcium lost in the milk (75).

The mechanism by which skeletal resorption is regulated is only partially understood. PTH levels are reduced 50% or more during the first few months of lactation, suggesting that skeletal demineralization is not regulated by mechanisms found in non-pregnant, non-lactating females (67). There is evidence that the effects of high levels of parathyroid hormone related protein (PTHrP) and low estradiol levels combine to elevate bone resorption during lactation. PTHrP is produced by the breast during lactation. Its levels are elevated in the serum of lactating women and are 10,000 times higher in the breast milk. Studies by VanHouten *et al.* (76) have shown that mice lacking mammary PTHrP expression during lactation, lost less BMC during this time. This suggests that PTHrP produced by mammary tissue drives bone resorption during this time. Suckling and high prolactin levels suppress gonadotropins, which in turn, reduces the production of estradial by the ovary (67). Estradiol deficiency is well known to stimulate bone resorption in humans and rodents. For example, postmenopausal women have losses of 1.4%/year at the hip and 1.6%/year at the spine (77). Also, six months of estrogen deficiency induced by gonadotropin releasing hormone agonist therapy leads to1-4% losses in trabecular bone mineral density (73). Although the above findings are consistent with a role for estrogen deficiency in bone resorption, this alone cannot

account for the 5-10% losses that occur in women during lactation. It is likely that PTHrP and low estradiol levels act together to achieve this degree of bone resorption.

1.2.6 Skeletal recovery after weaning

After weaning, the maternal skeletal mineral content is rapidly and completely regained (73, 78, 79). During post weaning recovery, women will experience increases of 0.5-2% BMC per month. This is unique because BMC losses experienced as an adult are normally followed by a slow and incomplete recovery, as opposed to the rapid recovery observed post-weaning. One study by Halloran *et al.* (80) suggests that $1,25(OH)_2D_3$ may play a role. They reported that vitamin D-deficient rats replaced some mineral after lactation but failed to recover to baseline. Further understanding the mechanism of rapid increase in bone mineral content after lactation may prove useful in the development of new strategies to increase BMC and treat conditions such as osteoporosis in the future.

1.2.7 Vdr knockout mouse model

As there is no '$1,25(OH)_2D_3$ gene', several strategies have been used to study the absence of $1,25(OH)_2D_3$ *in vivo*. Rats have been rendered vitamin D deficient when raised in darkness and fed a diet lacking vitamin D (69, 81, 82). The 1-α hydroxylase gene has been ablated in mice so that they are unable to enzymatically produce

$1,25(OH)_2D_3$, the form of vitamin D with the highest amount of physiological activity (83). *Vdr* knockout mouse models have been created independently by scientists in Boston (84), Leuwen (20) and Tokyo (85). In these models, the mice lack the receptor that is required for $1,25(OH)_2D_3$ function.

For my experiments, I used the *Vdr* knockout mouse that was created in the laboratory of Marie Demay at Boston. A 5kb fragment of DNA encoding the second zinc finger of the receptor DNA-binding domain was deleted and replaced with a neomycin cassette to generate *Vdr* null mice (84). Without a functional DNA-binding domain, the VDR cannot bind to DNA and is therefore unable to activate vitamin D-dependent transcription. As a result, *Vdr* null mice have high serum $1,25(OH)_2D_3$ levels but cannot utilize it.

Vdr mice provide an animal model of the human condition, vitamin D-dependent rickets type II. Similar to humans, these mice are born phenotypically normal but develop alopecia, hypocalcemia, secondary hyperparathyroidism, rickets and osteomalacia by adulthood (84). This data is consistent with other *Vdr* knockouts (85). Fertility and litter sizes are also reduced in *Vdr* null mice (86). The phenotype, excluding alopecia, is a consequence of the absence of the *Vdr* in the intestine (87). Kollenkirchen *et al.* (88) formulated an enriched diet, high in calcium, phosphorus and lactose which achieved normocalcemia, without raising PTH levels, in vitamin D deficient rats. When *Vdr* null mice are fed this diet immediately after weaning from the mother, the hypocalcemia, hypophosphatemia, secondary hyperparathyroidism and skeletal

abnormalities are prevented (87, 89). The mechanism of how this occurs has not been determined but it is thought that the lactose enhances passive absorption of calcium.

The fact that *Vdr* null mice do not develop abnormalities in mineral metabolism until post-weaning is not unexpected. In rats, during gestation and in the neonate, calcium absorption in the intestine occurs primarily by passive mechanisms (90). After 18 days of age, these passive mechanisms become less important and are replaced by active, $1,25(OH)_2D_3$-dependent absorptive mechanisms. Without the *Vdr*, active mechanisms are impaired and calcium absorption is reduced in the adult, resulting in severe consequences on calcium metabolism. This would explain why *Vdr* nulls, despite genetic ablations, are born phenotypically normal but develop abnormalities in calcium homeostasis as they mature.

1.2.8 Project description

$1,25(OH)_2D_3$ and the VDR play an important role in regulating calcium homeostasis. Without $1,25(OH)_2D_3$ and the VDR, intestinal calcium absorption is reduced, calcium homeostasis is impaired and the skeleton is stripped of mineral. Pregnancy and lactation create a large change in calcium homeostasis. Studies have indicated that the $1,25(OH)_2D_3$ and the VDR may be less important in regulating calcium metabolism during the reproductive periods (68-70). I wanted to determine the role of $1,25(OH)_2D_3$ and the VDR in regulating calcium and bone metabolism during pregnancy. To accomplish this, I analysed the Boston *Vdr* knockout mouse model during this period

and I hypothesized that intestinal calcium absorption and calcium and bone homeostasis are regulated independently of $1,25(OH)_2D_3$ and the VDR during pregnancy.

For my Master's project, I first determined the consequences of pregnancy and lactation on skeletal mineral content. From there, I focused on how pregnancy affected calcium absorption and gene expression in the duodenum, calcium homeostasis and skeletal morphology in *Vdr* null mice.

2. Methods

2.1 Animal husbandry

All studies were approved by the Institutional Animal Care Committee at Memorial University of Newfoundland. The animals were maintained in facilities operated by Animal Care services of Memorial University of Newfoundland, in accordance with the guidelines of the Canadian Council on Animal Care. The original heterozygous mice were initially backcrossed for 3 generations with normal Black Swiss mice and periodically thereafter, such that they were at least six generations in Black Swiss prior to the beginning of these experiments. *Vdr* heterozygous males and females were mated to produce heterozygous, homozygous (*Vdr* null) and wild-type (WT) offspring.

2.2 Experimental design

WT and *Vdr* null females were weaned at 21 days, genotyped and raised on a regular (1% calcium) laboratory mouse diet for 10 weeks after which time the nulls fully developed hypocalcemia, secondary hyperparathryroidism and rickets. Both genotypes were then switched to a 2% calcium, 1.25% phosphorus and 10% lactose enriched diet for the remainder of the experiment. Studies by Johnson *et al.* (91) have shown that *Vdr* null fertility was restored to WT levels when fed a high calcium diet. Other than

improving fertility, it was not known how this diet would affect the mice in my experiments since they were not receiving the enriched diet until ten weeks of age.

After at least one week on the enriched diet, baseline BMC measurements, whole blood (ionized calcium), serum, urine, duodenal (for microarray) and bone (for histomorphometry) samples were obtained. The mice were then mated overnight. The presence of a vaginal plug in the morning was designated as gestation day 0.5 of pregnancy. Serial BMC measurements were obtained at late pregnancy (gestation day 18.5), late lactation (lactation day 21) and post-weaning recovery (recovery day 21). Serum and urine were further collected during early (gestation day 7) and late (gestation day 18.5) pregnancy. Duodenal samples for microarray analysis and tibias for histomorphometry were collected at gestation day 16.5 in order to analyze the molecular/cellular events that lead to the phenotype at the end of pregnancy.

Experiments involving non-pregnant mice differed slightly. Baseline BMC and ionized calcium measurements were obtained while the non-pregnant *Vdr* nulls were receiving the regular 1% calcium diet. The mice were then switched to the enriched diet and serial BMC and ionized calcium measurements were obtained at 12, 14, 20 and 22 weeks of age.

Results are displayed as mean ± the standard error as determined using analysis of variance followed by Tukey's Test.

2.3 Genotyping

2.3.1 Tagging and tailing

Mice were exposed to isoflurane (Baxter corporation) for approximately 8 seconds after which time they were anaesthetized for approximately 5-8 seconds. An ear tag containing an ID number was implanted in each animal's right ear. Approximately 0.5 cm of tail was removed using a razor blade, placed in 0.5 ml of lysis buffer (100mM Tris (pH 8.0), 5mM EDTA (pH 8.0), 0.2% SDS, 200mM NaCl) and incubated at 55°C overnight.

2.3.2 DNA extraction from tail samples

After the overnight incubation in lysis buffer, the tail sample was centrifuged at 18,300 x g for 10 minutes to pellet the hair. The sample was then decanted into 0.5 ml of 2-propanol (HPLC grade, Fisher Scientific) and inverted 5 to 10 times to precipitate the DNA. The precipitate was removed with a pipette tip, placed in a clean 1.5 ml centrifuge tube containing 0.5 ml of deionized water and hand shaken for 5 minutes to dissolve the DNA. 0.5 ml of phenol: chloroform: isoamyl alcohol (25:24:1) pH 6.7 (Fisher Scientific) was added, the sample was shaken by hand for 1 minute and centrifuged at 18,300 x g for 2 minutes. The aqueous layer was removed, placed in a clean 1.5 ml centrifuge tube and 1ml of 0.12M sodium acetate (Fisher Scientific) in reagent alcohol (Histological grade, Fisher Scientific) was added. This was then inverted 5 to 10 times to precipitate the

DNA and centrifuged for 10 minutes at 18,300 x g. The sodium acetate solution was decanted and 1 ml of 70% ethanol was added to wash the pellet. The sample was shaken by hand for approximately 10 seconds and again centrifuged at 18,300 x g for 10 minutes. The solution was decanted and the remaining ethanol was discarded. The pellet was air dried for 5 to 10 minutes and resuspended in 200 µl TE (10mM Tris, 1mM EDTA, pH 8.0).

2.3.3 Polymerase chain reaction (PCR)

A ~450bp region of exon 3 of the WT *Vdr* gene and a 308bp region of the neomycin gene were amplified by PCR using two primer sets. The primers used to amplify the WT product were as follows: forward primer: 5'-CTG CCC TGC TCC ACA GTC CTT-3', reverse primer: 5'-GCA GAC TCT CCA ATG TGA AGC-3'. The primers used to amplify the neomycin cassette are as follows: forward primer: 5'-GGA GAG GCT ATT CGG CTA TGA C-3', reverse primer: 5'-CGC ATT CGA TCA GCC ATG ATG G-3'. 1 µl of genomic DNA was added to 49µl of a PCR cocktail containing 1X PCR Buffer (20mM Tris-HCl (pH 8.4), 50mM KCl), 2mM MgCl, 0.2mM deoxynucleotide triphosphates (dNTPs). 1U Taq DNA polymerase) in a 0.6 ml thin walled PCR tube (Fisher Scientific). For each experiment, DNA was omitted from one tube to serve as a negative control. The samples were then loaded into a Peltier Thermal Cycler (MJ Research). The PCR program included the followed conditions: denaturation at 94°C for 4 minutes, 35 cycles of denaturation at 94°C for 1 minute, annealing at 62°C

for 1 minute, polymerization at 72°C for 1 minute. After these 35 cycles, the program was completed with a 7 minute polymerization at 72°C. The PCR products were stored at 4°C until gel electrophoresis was performed.

2.3.4 Gel electrophoresis

PCR products were separated by gel electrophoresis. Agarose (1.2g) (Invitrogen) was added to 100 ml of buffer (0.4M Tris, 20mM EDTA, 1.14% Acetic Acid, pH 8.5) in a 500ml Fleaker and boiled in the microwave. The solution was cooled slightly and 20 µl of SYBR® Safe DNA gel stain (Invitrogen) was added. The solution was mixed gently and poured into a gel electrophoresis chamber (Easy Cast) containing a loading well comb. The solution was cooled for 20 minutes during which time it solidified to form a gel. Orange G loading dye (5 µl) was added to the 50µl PCR sample and mixed. The PCR sample/orange G mixture (10µl) was loaded into each well. The PCR product ran on the gel for 30 minutes at 200 volts. A digital picture of the gel was taken using a Gel Logic 100 Imaging system (Mandel Scientific).

2.4 Bone mineral content

WT and *Vdr* null mice were switched from the enriched 2% calcium diet to a regular 1% calcium diet 18 hours prior to scanning for BMC. In advance of the scan, each mouse was anaesthetized (40µl of 83.3mg/ml Ketamine, 3.3 mg/ml xylazine, i.p.).

After at least one week on the enriched diet, baseline total (whole body, excluding the head) BMC was measured using a Lunar Piximus2 bone densitometer (General Electric). Regional measurements (spine and hindlimb), were derived from the whole body scans. The mice were then mated and pregnancies were achieved within 0-12 weeks. Additional BMC measurements were obtained during early pregnancy (gestation day 7), late pregnancy (gestation day 18.5), early lactation (lactation day 7), late lactation (lactation day 21) and recovery (21 days after weaning). The results are expressed as the relative change in BMC from the non-pregnant baseline, which has been set to zero. The densitometer was calibrated daily using a Phantom quality control composed of a known amount of fat (11.9%) and BMC (0.063 grams).

2.5 Intestinal ^{45}Ca transfer

Intestinal calcium absorption was measured using the duodenal ligated loop technique (adapted from Song *et al*, 2003). The mouse was anaesthetized using a 30µl i.p. injection (83.3 mg/ml ketamine/3.3 mg/ml xylazine). The abdomen was shaved and the peritoneal cavity was opened. One suture was tied around the duodenum adjacent to the pyloric sphincter and a second suture was placed approximately two centimetres distal to the first. ^{45}Ca buffer (40µl of ^{45}Ca (16 µCi/ml), NaCl (150mM), $CaCl_2$ (2mM), Tris-HCl (30mM, pH 7.2)) was injected into the lumen of the closed loop of duodenum. 16µCi of ^{45}Ca was also injected into a scintillation vial to serve as a negative control. The mouse's abdomen was kept warm with gauze soaked in warm phosphate buffered

saline (PBS) and the heartbeat was monitored. After 10 minutes, the loop was excised external to the sutures, placed in a scintillation vial and solubilized overnight in 5ml Scintigest (Fisher Scientific) at 65°C on a shaker. Loops that appeared non-viable (purple) or deflated were discarded. The samples were then pulse vortexed until they were disrupted. After scintillation fluid (10 ml, Fisher Scientific) was added, the vials were counted in a LS 6500 Multi-purpose liquid scintillation counter (Beckman Coulter). The results are expressed as a percentage of the initial amount of ^{45}Ca that was injected into the loop.

2.6 RNA expression analysis in the duodenum and vertebrae.

2.6.1 Tissue collection

At each timepoint, tissue samples were collected for RNA, protein and histology. Mice were killed by cervical dislocation. The tissues were dissected, snap frozen in liquid nitrogen and stored at -80°C.

2.6.2 RNA extraction

The homogenizer was cleaned between samples by rinsing with an RNA wash solution (2mmol EDTA, 0.1% SDS, 0.1% Diethyl pyrocarbonate, (DEPC)(Sigma)) and Ribonuclease-free deionized water.

1ml of Trizol reagent (Invitrogen) was added to each sample in a 14ml polystyrene centrifuge tube and the tissue was disrupted using a Polytron homogenizer (Kinematica) for 1 minute at high speed in a fume hood. The samples were incubated at room temperature for 5 minutes.

Chloroform (0.2ml, Fisher Scientific) was added to the samples. The tubes were covered with Parafilm and shaken for 15 seconds. The samples were incubated at room temperature for 3 minutes and centrifuged at 12,000 x g for 15 minutes at 4°C. The RNA (upper aqueous layer) was transferred to a clean 1.5ml centrifuge tube.

Isopropanol (0.5 ml, HPLC grade, Fisher Scientific) was added to precipitate the RNA. Each tube was mixed, incubated on ice for 10 minutes and centrifuged at 12,000 x g for 10 minutes at 4°C. The RNA pellet was washed with 80% ethanol (treated with), vortexed and centrifuged at 7500 x g for 5 minutes, at 4°C. The ethanol was decanted and the RNA pellet was air dried for 30 minutes at room temperature. The RNA was resuspended in 500µl of RNase-free water by passing the solution through a pipette tip a few times.

Impurities were removed from the RNA sample by performing RNA clean up using the RNeasy Midi kit (Qiagen). This resulted in a 150µl total RNA sample, ranging in concentration from 0.5-2.0µg/µl. RNA quality was determined at the Hospital for Sick Children (Toronto, ON) using a Bioanalyser 2100 (Agilent Technologies). RNA samples with an RNA Integrity Number (RIN)>7 were used for microarray analysis and real time RT-PCR.

2.6.3 Whole genome microarray analysis

WT and *Vdr* null total RNA samples from baseline and late pregnancy were analyzed at the Centre for Applied Genomics, Microarray Facility, Hospital for Sick Children (Toronto, ON). The Mouse Gene ST 1.0 Array (Affymetrix) was completed on 8 samples (1sample per chip), representing 2 samples for each of the 4 groups: WT and *Vdr* null at baseline (pre-pregnancy) and pregnancy (gestation day 18.5).

Primary data analysis at the Statistical Analysis Core Facility of The Centre for Applied Genomics used the March 2008 gene annotation information from Affymetrix. Probesets without gene names/gene assignments were removed, leaving 22158 probesets. Raw data were normalized using the robust multi-array average (RMA) algorithm (92). Statistical analysis involved four comparisons of raw data; *Vdr* null baseline vs. WT baseline, *Vdr* null late pregnancy vs. *Vdr* null baseline, WT pregnancy vs. WT baseline and *Vdr* null pregnancy vs. WT pregnancy. Differentially expressed genes were then identified using the Local-Pooled-Error Test (LPE) (93). False discovery rate (FDR) (94) was set at 0.05 such that genes with adjusted p-values < 0.1 were considered to be statistically significant. A p-value of 0.1 was chosen because of the small sample size. The genes that showed significant changes in expression among timepoints (ie. *Vdr* null pregnancy vs. *Vdr* null baseline) are shown in Appendix A. To identify common genes that were differentially expressed, I compared each statistical group comparison and listed the similarities and differences among common genes (Appendix B). My analysis, however, focused on the expression of genes that are known to be involved in the active transport of calcium across the duodenum (*Trpv6*, *Sg100*, *Pmca1b*).

2.6.4 Validation of microarray results using real time RT-PCR.

Real time RT-PCR was performed on each RNA sample to validate the expression of *Trpv6*, *Sg100* and *Pmca1b* mRNA as determined by microarray. cDNA synthesis and amplification were performed in one step using TaqMan® RNA-to-C_T™ 1-Step Kit and TaqMan® Gene Expression Assays (Applied Biosystems). A reaction cocktail containing approximately 12.5ηg of total RNA, 1X TaqMan® RT Enzyme Mix, 1X TaqMan® RT-PCR Mix and 1X TaqMan® Gene Expression Assays for either *Trpv6*, *Sg100*, *Pmca1b* or glutaraldehyde-3-phosphate dehydrogenase (*Gapdh*). Each assay was run in triplicate, three times for each gene. The cocktail (20µl) was loaded onto an Optical 96-Well Thermal Cycling plate (Applied Biosystems). Each well was covered using Optical Caps (Applied Biosystems) and the plate was centrifuged at 2000 x g for 1 minute. The plate was then transferred to an ABI 7000 Thermocycler (Applied Biosystems) and an absolute quantification document was selected. The RT-PCR program included cDNA synthesis: 48°C for 15 minutes, enzyme activation: 95°C for 10 minutes and 40 cycles of denaturing: 95°C for 15 seconds and annealing/extension: 60°C for 1 minute. The resulting amplification curves were used to determine the threshold cycle (C_T) values for each sample. The data for each gene was normalized to the 'housekeeping' gene *Gapdh* and expressed relative to another genotype or reproductive timepoint, depending on the comparison.

2.7 Serum analysis

The tail was nicked using a razor blade, whole blood was collected into a capillary tube and then transferred into a 1.5 ml polypropylene centrifuge tube. The blood was incubated at room temperature for 30 minutes and then centrifuged for 10 minutes at 15,800 x g. The clear serum layer was removed with a pipette, placed in a fresh 0.6ml centrifuge and stored at -80°C. Prior to each assay performed on the sample, the sample was thawed and centrifuged for 10 minutes at 15,800 x g.

2.7.1 Serum ionized calcium

Serum ionized calcium (Ca^{2+}) was determined using the 634 Ca^{2+}/ pH analyzer (Chiron Diagnostics). Whole tail blood samples were collected in a 60µl capillary tube (Bayer) and capped with an adaptor. The blood sample was immediately loaded in to the machine and the ionized calcium results (corrected for pH 7.4) were obtained.

2.7.2 Serum PTH

Serum PTH was measured using a rat intact PTH enzyme linked immunosorbet assay (ELISA) kit (Immutopics, Inc). This kit is cross-reactive to mouse PTH. 25µl of undiluted serum, standards and controls were loaded into a streptavidin coated 96 well plate. Two antibodies; a biotinylated rat anti-PTH and a horseradish peroxidase conjugated rat anti-PTH, were added and incubated for three hours. As a result, the PTH

in the serum sample is captured and immobilized on the surface of the well and tagged with HRP. After five washes with a buffer, an HRP substrate was added and the enzymatic activity of HRP was measured by reading the absorbance at 450ηm using a kinetic microplate reader (Molecular Devices). The amount of HRP activity is directly proportional to the amount of PTH in the sample. The absorbance of each standard was plotted against their known concentration on a linear-linear standard curve. This standard curve was used to determine the concentration of PTH in the serum samples. Samples with apparent values below the detection limit (1.6 pg/ml) were assigned values equal to the detection limit.

2.7.3 Serum osteocalcin

Serum osteocalcin was measured using the mouse osteocalcin IRMA kit (Immutopics, Inc) according to the manufacturer's protocol. Serum was diluted 1:11 with zero standard prior to the assay. A standard, control or diluted serum (25µl) was added to a 2 ml polystyrene tube. ^{125}I labeled anti-mouse osteocalcin antibody (200µl) was dispensed into the tubes. The tubes were mixed by vortexing on low and one bead coated with anti-mouse osteocalcin antibodies was added to each tube. The tubes were incubated at room temperature for 18-24 hours. The liquid was aspirated and the beads were washed three times with 0.1M PBS. Each tube was counted in a gamma counter for one minute. The counts per minute (cpm) were plotted against the known concentration for each standard to produce a log-log standard curve. This standard curve

was used to determine the concentration of osteocalcin in the diluted serum samples. These values were then multiplied by the dilution factor.

2.8. Urine analysis

Mice were placed in empty sterile cages until they produced urine. The urine was collected, placed in a 0.6ml polypropylene centrifuge tube and stored at -20°C. Prior to each of the following assays, the urine was centrifuged at 15,800 x g for 5 minutes.

2.8.1 Urine deoxypyridinoline (DPD)

Urine DPD was measured using the Metra DPD Enzyme Immunoassay (EIA) (Quidel). Standards, controls and urine were diluted 1:10 with assay buffer. 50µl of each was added to wells coated with monoclonal anti-DPD antibody. DPD conjugated to alkaline phosphatase (100µl) was added to wells and incubated at room temperature for 2 hours in the dark. The wells were washed three times with buffer and inverted for 5 minutes. 150µl of pNPP substrate was added to the wells and incubated for 1 hour at room temperature. 100µl of stop solution was added and the absorbance at 405ηm was obtained using a kinetic microplate reader (Molecular Devices) to determine the amount of alkaline phosphatase activity in each well. Due to the competitive nature of the assay, the amount of alkaline phosphatase activity was inversely proportional to the amount of DPD in the sample. The absorbances of the known standards were used to construct a

standard curve (4 parameter). This standard curve was used to determine the concentration of DPD in the diluted urine samples. These DPD values were then multiplied by the dilution factor and expressed relative to the urine creatinine concentration (nmol DPD/mmol creatinine) to correct for urinary concentration.

2.8.2 Urine creatinine

Urine creatinine was determined using the Creatinine-S spectrophotometric assay (Diagnostic Chemicals Limited (DCL)). Urine samples were diluted 1/10 in 0.9% NaCl. 100µl of creatinine standard, control (DC-Trol, DCL) or urine were added to 4ml cuvettes (Fisher Scientific). Creatinine working reagent (2.0ml) was added to the cuvette and mixed. An Ultraspec 2000 spectrophotometer (Pharmacia Biotech) was used to obtain the absorbance at 510ηm at 20 and 80 seconds after the reagent was added. The change in absorbance of the unknown urine sample relative to the change in absorbance of the known standard was used to calculate the concentration of the unknown. These values were then multiplied by the dilution factor.

2.8.3 Urine total calcium

Urine total calcium was measured using a calcium spectrophotometric assay (Diagnostic Chemical Limited (DCL). Depending on the concentration, urine samples were diluted 1/2 or 1/10 in 0.9% NaCl. 10µl of standard, control (DC-Trol, DCL) or

urine and 1.0 ml of reagent were combined in a 1.0ml polystyrene semi-cuvette, mixed and incubated at room temperature for at least 30 seconds. An Ultraspec 2000 spectrophotometer (Pharmacia Biotech) was used to measure the absorbance of the solution at 650ηm using water as a reagent blank. The absorbance of the known calcium standard was used to calculate the concentration of calcium in the serum samples. These values were then multiplied by the dilution factor and expressed relative to the urine creatinine concentration (mmol calcium/mmol creatinine) to correct for urinary concentration.

2.9 Histology

Tibias were removed, stripped of muscle and other soft tissues and fixed in 10% buffered formalin. The samples were embedded in methacrylate by my supervisor, Dr. Christopher Kovacs while on sabbatical in the laboratory of Dr. Natalie Simms in St. Vincent's Institute, Melbourne, Victoria, Australia. Undecalcified 5-micron sections were stained with either the Goldner's trichrome and von Kossa methods or toluidine blue stain.

2.9.1 Goldner's trichrome method

Undecalcified tibia sections were deplasticized in cellosolve (Acros organics) for 2 X 25 minutes, rehydrated in decreasing ethanol series and tap water (3 minutes each).

The sections were stained with Ponceau/Acid Fuchsin/Azophloxine for 5 minutes and rinsed in 1% acetic acid for 10 seconds. The sections were placed in phosphomolybdic acid/ Orange G for 5 minutes and rinsed in 1% acetic acid for 10 seconds. The slides were then stained with Light Green for 5 minutes, rinsed in 1% acetic acid for 3 minutes and blotted dry. The sections were passed through two changes of butanol, one butanol/toluene mixture, two changes of toluene, mounted with Depex and coverslipped. Goldner's trichrome stains nuclei blue/black, mineralized bone/muscle green and osteoid red.

2.9.2 Von Kossa method

Undecalcified tibia sections were deplasticized in cellosolve (Acros organics) for 2 X 25 minutes, rehydrated in decreasing ethanol series and deionized water (3 minutes each). The slides were then incubated in 2% silver nitrate for 30 minutes under a strong light and washed in deionized water for five minutes. Sodium thiosulfate (2.5%) followed for 5 minutes and rinsed three times in deionized water. The sections were counterstained with methyl green (3 minutes) and blotted. The stain was cleared with two passes through butanol. The sections were then mounted with Depex and coverslipped. Mineralized bone stains black using the Von Kossa method.

2.9.3 Toluidine blue stain

Tibia sections were deplasticized in cellosolve (Acros organics) for 2 X 25 minutes and rehydrated in decreasing ethanol series and tap water (3 minutes each). The sections were stained in toluidine blue for 5 minutes, dipped in two changes of toluidine blue buffer and blotted. The stain was cleared by passing through butanol twice, a 1:1 butanol/toluene solution and toluene twice. The sections were mounted with Depex and coverslipped. Toluidine blue stains nuclei blue, mineralized bone light purple and osteoid colourless to pale blue.

2.10 Histomorphometry

Histomorphometric analysis of *Vdr* null proximal tibias (stained with toluidine blue) was carried out according to standard procedures using the Osteomeasure system (Osteometrics, Decatur, GA). Due to the sinuous nature of the *Vdr* null growth plate the analyzed region began immediately below the lowest arc of the chondroosseous junction and extended toward the diaphysis. The parameters analyzed were as follows: Bone volume (BV/TV): the total bone marrow volume occupied by trabecular bone; Trabecular number (Tb.N): the amount of trabeculae present in the field; Trabecular thickness (Tb.Th): the average thickness of the trabeculae present in the field; Trabecular spacing (Tb.Sp): the average distance between trabecular midpoints; Osteoblast number (N.Ob/BPm): the number of osteoblasts (defined as blue/grey cuboidal cells aligned in clusters at the bone surface) per bone perimeter; Osteoclast number (N.Oc/BPm): the

number of osteoclasts (defined by the standard criterion of multinucleated cells residing in resorptive lacunae) per bone perimeter; Osteoclast surface (OcS/BS): the amount of bone surface containing osteoclasts per total bone surface; Osteoid surface (OS/BS): the amount of osteoid surface per bone surface.

3. Results

3.1 Bone mineral content

In order to determine how the rachitic *Vdr* null skeleton would respond to the challenges of pregnancy and lactation, I first investigated the changes in total BMC in *Vdr* null and WT mice throughout the reproductive cycle. Regional measurements of the spine and tibia were also analysed to determine if the changes in BMC involved trabecular bone, cortical bone, or both.

Relative changes in total BMC in *Vdr* null and WT mice throughout the reproductive periods are shown in *Figure 3.1*. WT mice gained 7.1% BMC during pregnancy, lost 18.1% during lactation and recovered to baseline post weaning. Regional measurements showed that WT mice gained 1.1% spine BMC during pregnancy, lost 17.7% during lactation and recovered 8.3% above baseline post-weaning (*Figure 3.2*). WT mice also gained 12.7% hindlimb BMC during pregnancy, lost 18.3% during lactation and recovered post-weaning 8.3% above baseline (*Figure 3.3*). In contrast, *Vdr* null sisters gained 57.2% BMC by late pregnancy ($p<0.05$), lost 31.2% during lactation and recovered post-weaning to a value that was 49.1% higher than the pre-pregnancy baseline (*Figure 3.1*). Changes in spine BMC were even greater, with a 61.5% ($p<0.05$) increase during pregnancy, a 52.8% ($p<0.05$) decrease during lactation and a recovery to 48.9% above baseline (*Figure 3.2*). *Vdr* nulls also gained 34.0% hindlimb BMC during pregnancy, lost 25.7% during lactation and recovered post weaning, 29.5% above baseline (*Figure 3.3*).

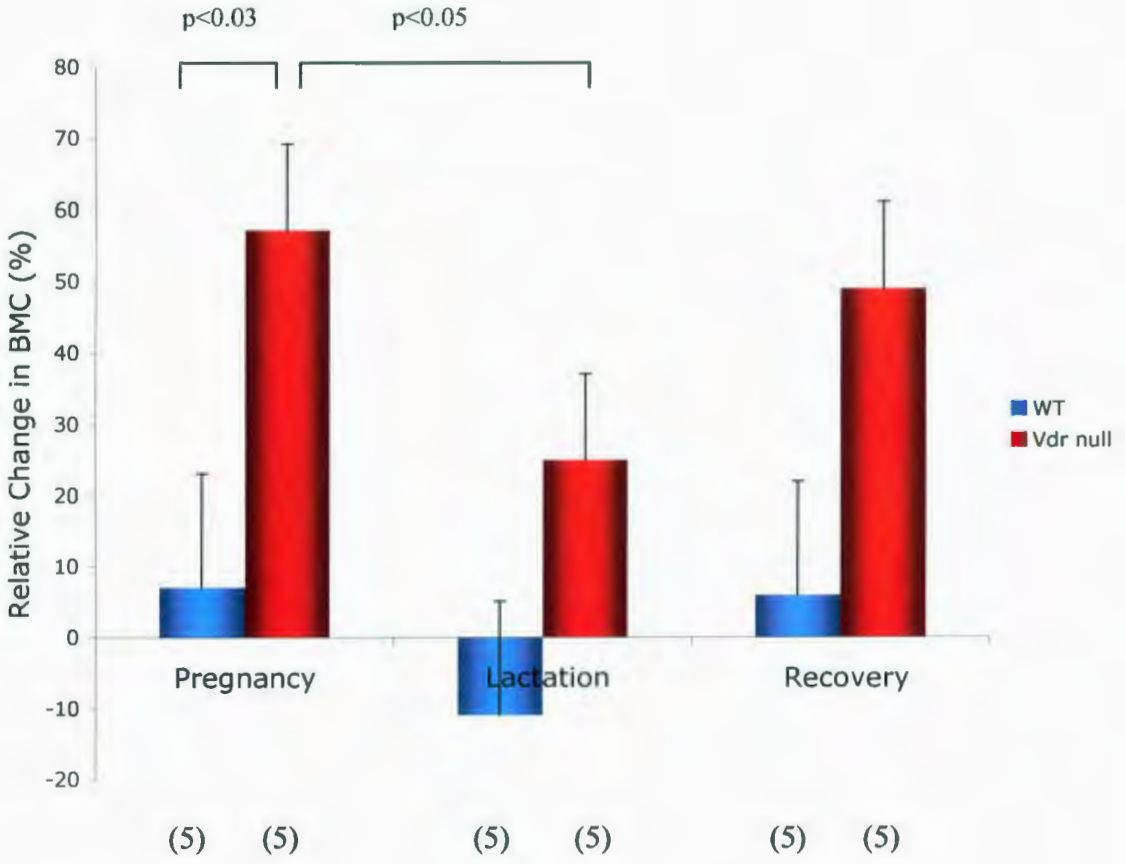

Figure 3.1 **Relative changes in BMC throughout the reproductive periods in WT (blue) and *Vdr* null (red) mice.** Mice were raised on a normal 1% calcium diet for 10 weeks. They were then switched to a 2% calcium, 1.25% phosphorus and 20% lactose enriched diet. After at least 7 days on the enriched diet, baseline BMC measurements were obtained using the Lunar *Piximus2* bone densitometer. The mice were then mated and allowed to follow through the entire reproductive cycle with additional BMC measurements obtained at late pregnancy, late lactation and post-weaning recovery. The results at each time point are displayed as the mean relative change in BMC (±SE) as compared to baseline measurements.

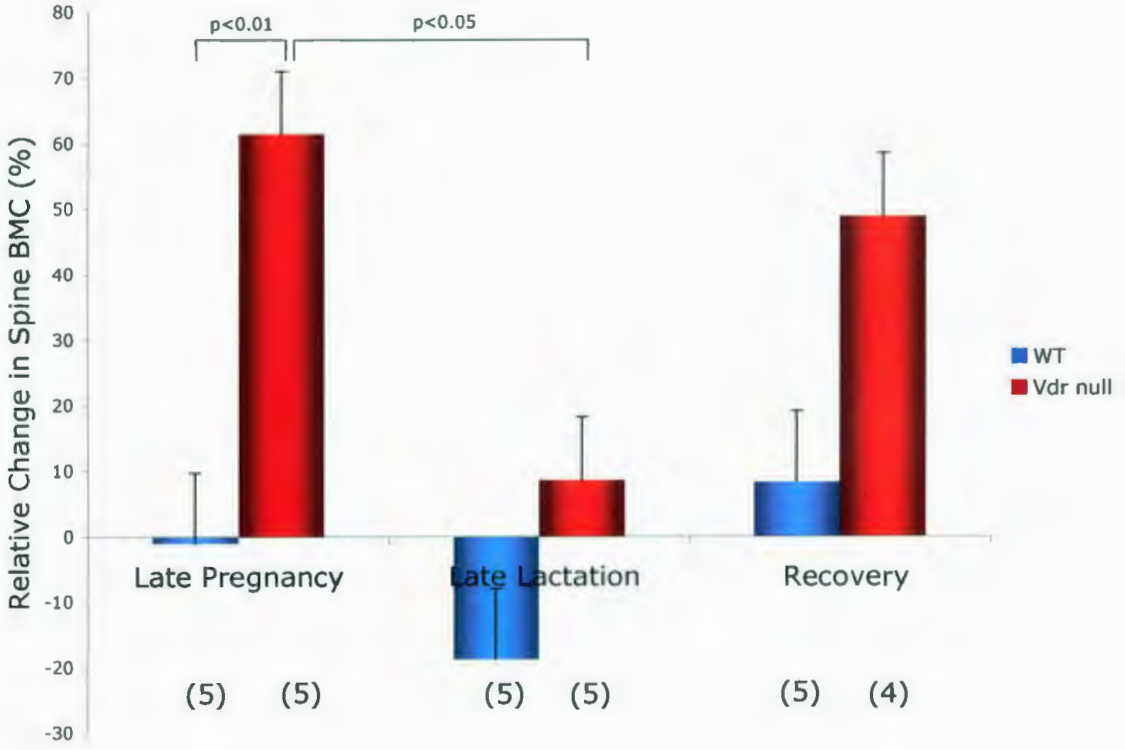

Figure 3.2 **Relative changes in spine BMC throughout the reproductive periods in WT (blue) and *Vdr* null (red) mice.** Mice were raised on a normal 1% calcium diet for 10 weeks. They were then switched to a 2% calcium, 1.25% phosphorus and 20% lactose enriched diet. After at least 7 days on the enriched diet, baseline BMC measurements were obtained using the Lunar *Piximus*2 bone densitometer. The mice were then mated and allowed to follow through the entire reproductive cycle with additional BMC measurements obtained at late pregnancy, late lactation and post-weaning recovery. The results at each time point are displayed as the mean relative change in spine BMC (±SE) as compared to baseline measurements.

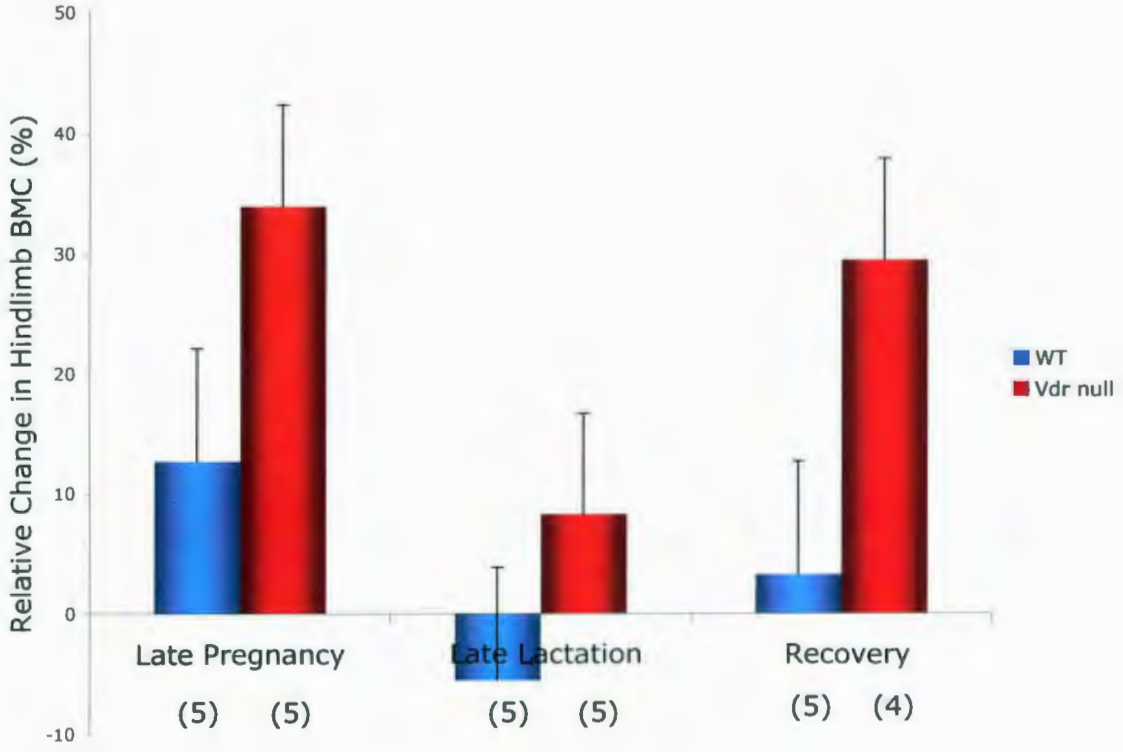

Figure 3.3 **Relative changes in hindlimb BMC throughout the reproductive periods in WT (blue) and *Vdr* null (red) mice.** Mice were raised on a normal 1% calcium diet for 10 weeks. They were then switched to a 2% calcium, 1.25% phosphorus and 20% lactose enriched diet. After at least 7 days on the enriched chow, baseline BMC measurements were obtained using the Lunar *Piximus*2 bone densitometer. The mice were then mated and allowed to follow through the entire reproductive cycle with additional BMC measurements obtained at late pregnancy, late lactation and post-weaning recovery. The results at each time point are displayed as the mean relative change in hindlimb BMC (±SE) as compared to baseline measurements.

Absolute values of baseline total bone mineral content (BMC) in *Vdr* null and WT mice throughout the reproductive periods are shown in *Figure 3.4*. At pre-pregnancy baseline, *Vdr* null sisters had a significantly reduced BMC (0.38g) as compared to their WT sisters (0.53g). During pregnancy and recovery from lactation, *Vdr* nulls increased their BMC significantly to equal WT levels.

In order to separate the effect of the enriched diet from that of pregnancy on BMC, I assessed changes in BMC in non-pregnant *Vdr* nulls from 10 to 22 weeks of age. Relative changes in total BMC in non-pregnant *Vdr* nulls while receiving the enriched chow as compared to the pre-diet baseline (10 weeks) are shown in *Figure 3.5*. *Vdr* nulls significantly increased BMC at 12, 14, 18 and 22 weeks of age. During the 12 weeks of scanning, BMC increased 58% by 22 weeks, which was equal to the amount gained during pregnancy and recovery from lactation (indicated by dotted line).

To further assess the effect of the enriched diet on BMC, I wanted to determine if there was a relationship between the amount of time between baseline and late pregnancy scans and the amount of BMC gained (*Table 3.1*). WT mice had a mean 3 weeks on the enriched diet and gained only 7.1% BMC during pregnancy. Three *Vdr* null mice had a mean 3.5 weeks on the enriched diet and gained 41% BMC during that time. Two *Vdr* null mice had a mean 14 weeks on the diet and gained 71%.

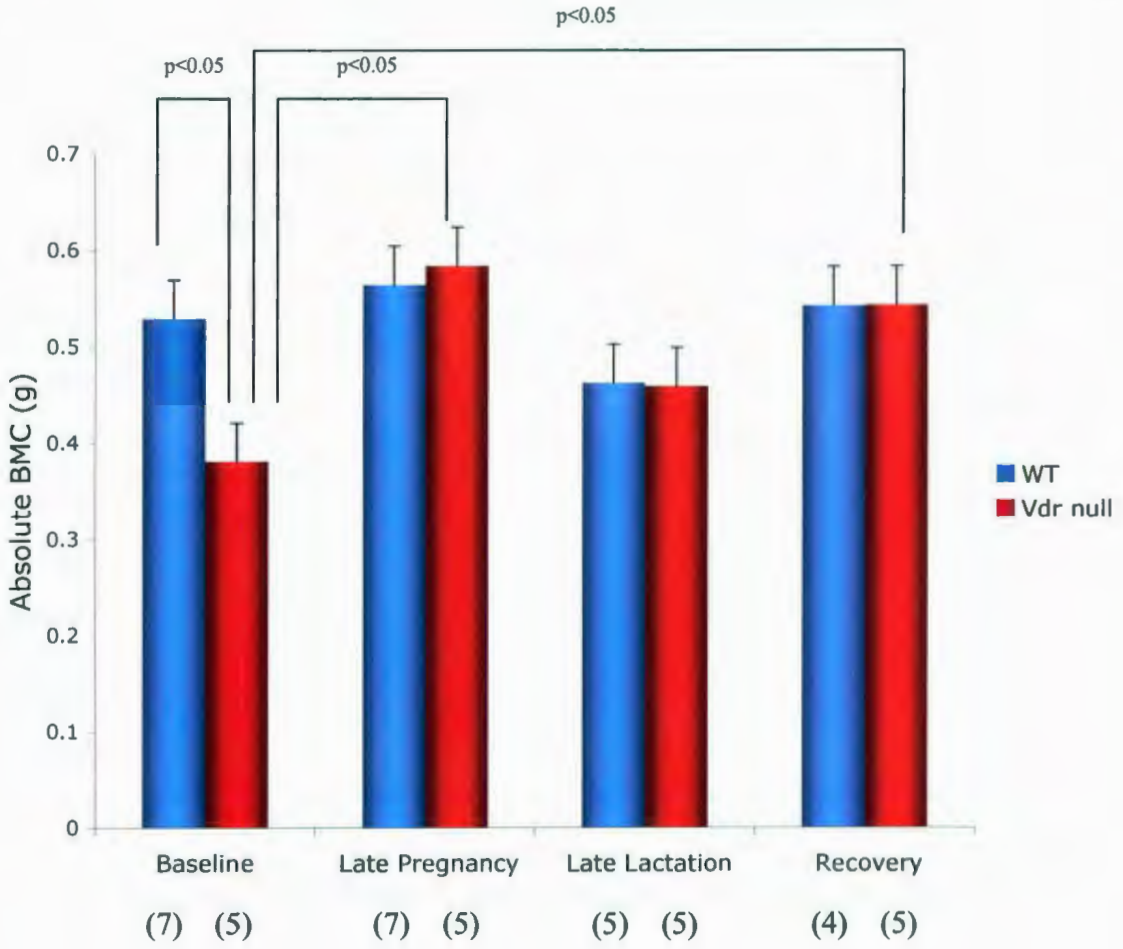

Figure 3.4 **Changes in absolute BMC in *Vdr* null (red) and WT (blue) mice throughout the reproductive periods.** Mice were raised on a normal 1% calcium diet for 10 weeks. They were then switched to a 2% calcium, 1.25% phosphorus and 20% lactose enriched diet. After at least 7 days on the enriched diet, baseline bone mineral content measurements were obtained using the Lunar *Piximus2* bone densitometer. The mice were then mated and allowed to follow through the entire reproductive cycle with additional BMC measurements obtained at late pregnancy, late lactation and post-weaning recovery. The results are displayed as mean total BMC (±SE).

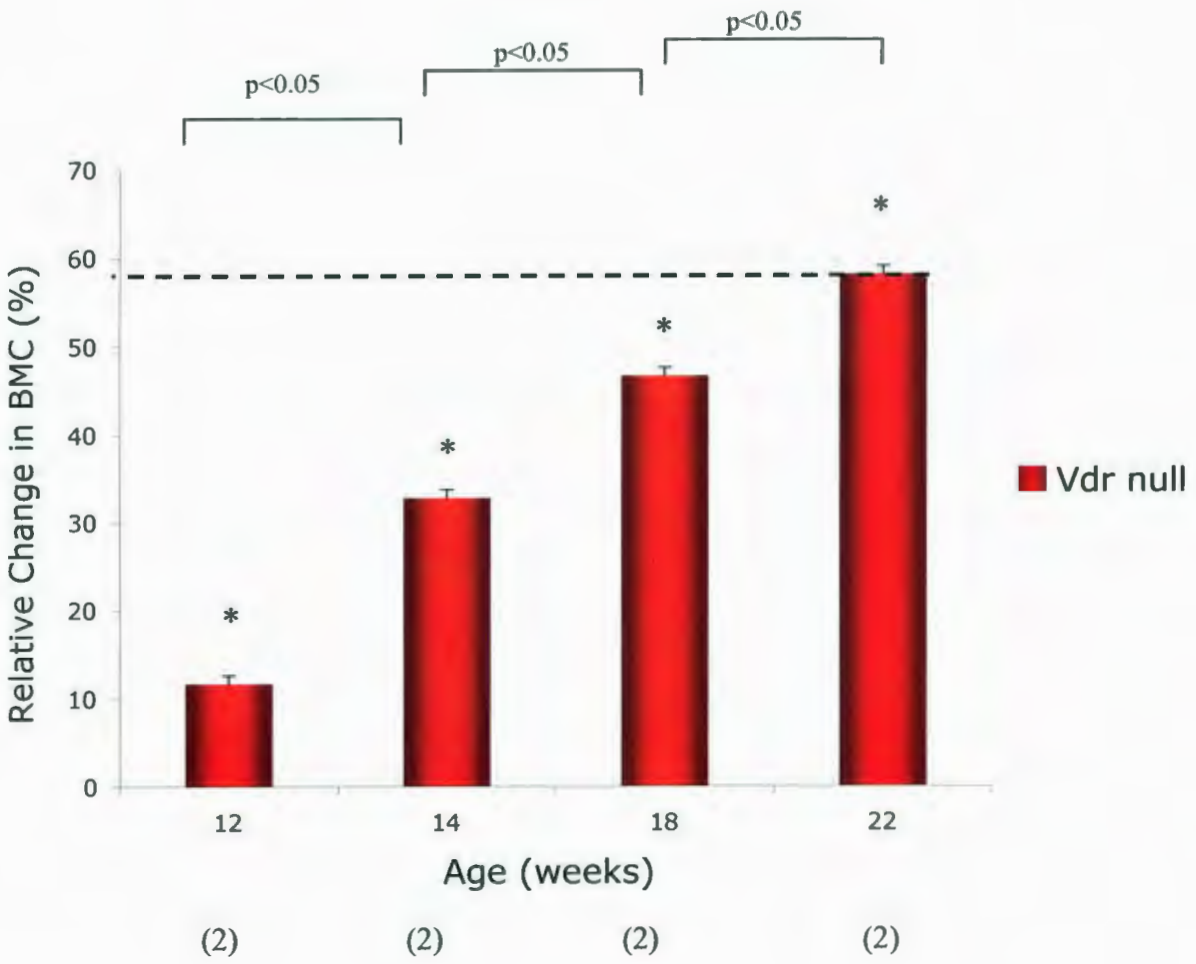

Figure 3.5 **Relative change in BMC in non-pregnant *Vdr* null mice after receiving the enriched chow as compared to their pre-diet baseline (10 weeks).** Mice were raised on a normal 1% calcium chow for 10 weeks. BMC measurements were obtained using the Lunar *Piximus2* bone densitometer. They were then switched to a 2% calcium, 1.25% phosphorus and 20% lactose enriched diet. Serial BMC measurements were obtained at 12, 20 and 22 weeks and expressed relative to their BMC at 10 weeks (mean±SE). *statistically different from baseline.

Mouse	Genotype	ID#	Time between Baseline and Late Pregnancy scans (weeks)	Average time (weeks)	Relative increase in BMC (%)	Average relative increase (%)
1	WT	X723	2.5	3±0.3	18.1	7.1±17
2	WT	X765	2.5		6.97	
3	WT	X742	4		1.18	
4	WT	X1309	3		4.91	
5	WT	X1310	3		4.47	
6	*Vdr* null	X740	2.5	3.5	28.2	41±13
7	*Vdr* null	X727	4		25.9	
8	*Vdr* null	X768	4		68.9	
9	*Vdr* null	X786	12	14±1.2	54.4	71±17
10	*Vdr* null	X769	16		87.3	

Table 3.1 **The time between baseline and late pregnancy scans for each *Vdr* null and WT mouse and the amount of BMC gained.** Mice were raised on a normal 1% calcium diet for 10 weeks. BMC measurements were obtained using the Lunar *Piximus2* bone densitometer. They were then switched to a 2% calcium, 1.25% phosphorus and 20% lactose enriched diet and mated. An additional scan was obtained at late pregnancy (gestation day 18.5). The time between baseline and pregnancy scans and the increase in BMC are expressed as mean ±SE.

3.2 Duodenal ^{45}Ca absorption

To determine if the increased BMC was due to an increase in calcium absorption that was independent of the *Vdr*, I measured duodenal ^{45}Ca absorption in *Vdr* null and WT mice (*Figure 3.6*). These results are displayed in *Figure 3.6*. At baseline, while consuming the enriched diet, duodenal ^{45}Ca absorption was reduced in *Vdr* nulls as compared to WT. In contrast, at the end of pregnancy ^{45}Ca absorption is significantly increased in *Vdr* null mice ($p<0.05$) as compared to baseline.

3.3 Duodenal gene expression

To examine the cellular mechanisms involved in the upregulation of intestinal calcium absorption in *Vdr* null mice during pregnancy, I performed a whole genome microarray analysis (Mouse Gene ST 1.0, Affymetrix) of gene expression in the duodenum at baseline and during pregnancy. All significant relative changes in gene expression ($p<0.1$) are listed in Appendix A for each statistical comparison. Relative changes in genes that were common among groups are listed in Appendix B.

My analysis focused on the results for genes that were known to be involved in the active transport of calcium across the duodenum. The relative changes in duodenal *Trpv6*, *Sg100* and *Pmca1b* mRNA expression as determined by microarray analysis are listed in *Table 3.2*. *Vdr* null *Trpv6* expression was reduced to 0.13 fold ($p<0.005$) at baseline as compared to WT. In contrast, *Trpv6* mRNA expression

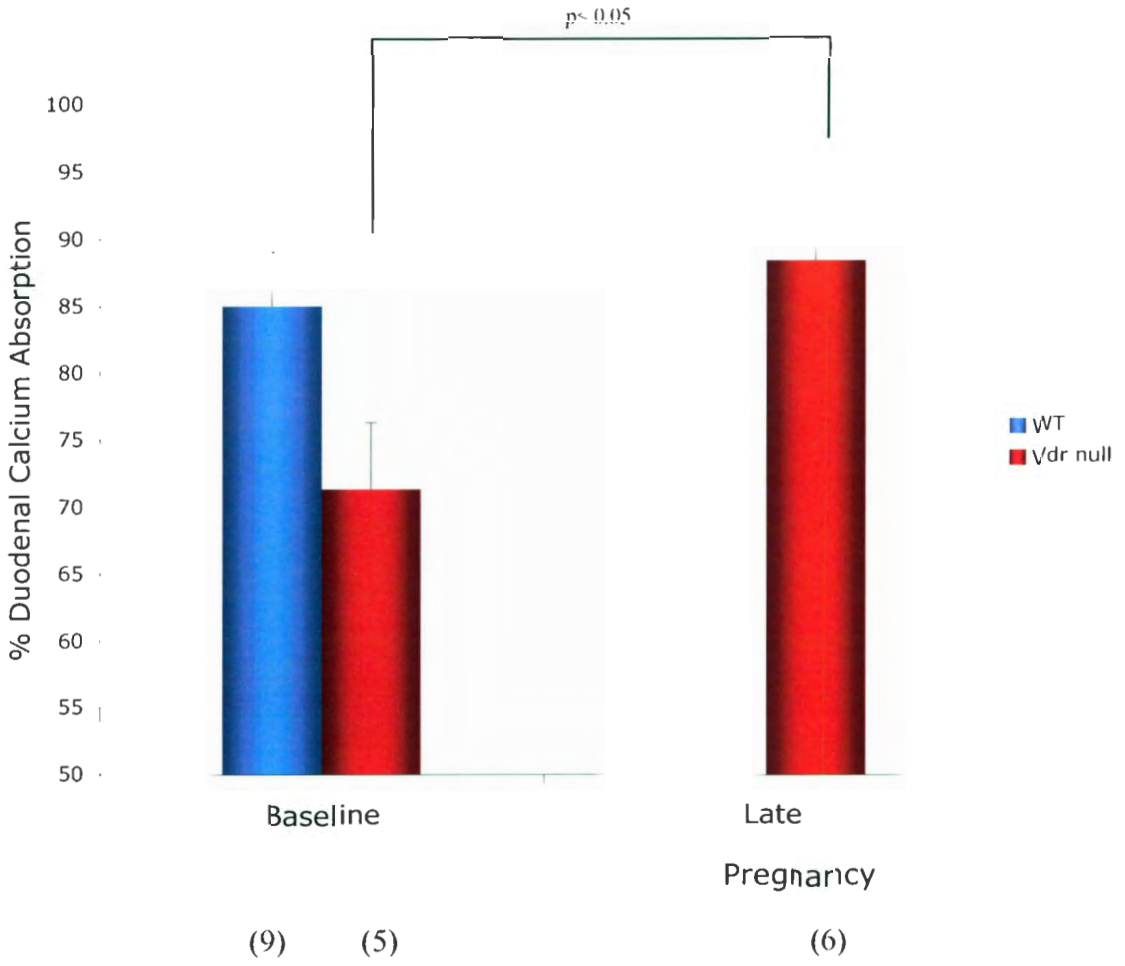

Figure 3.6 **Duodenal ^{45}Ca absorption in *Vdr* null (red) and WT (blue) mice at baseline and gestation day 16.5 of pregnancy.** Mice were raised on a normal 1% calcium diet for 10 weeks. They were then switched to a 2% calcium, 1.25% phosphorus and 20% lactose enriched diet. Duodenal ^{45}calcium absorption was measured at either baseline or late pregnancy using the *in situ* ligated loop technique. Mice were fasted for approximately 18 hours before the procedure. Duodenal ^{45}Ca absorption is expressed as the amount of calcium remaining in the loop as a percentage of the amount of ^{45}Ca that was initially injected into the loop (mean±SE).

Comparison	*Trpv6*	*Sg100*	*Pmca1b*
Vdr null baseline vs. WT baseline	0.13,p<0.005	0.85 (NS)	0.69 (NS)
Vdr null pregnancy vs. baseline	4.8,p<0.005	0.98 (NS)	1.02 (NS)
WT pregnancy vs. baseline	0.33,p<0.005	0.96 (NS)	0.78 (NS)
Vdr null pregnancy vs. WT pregnancy	1.91,p<0.005	0.88 (NS)	0.90 (NS)

Table 3.2 **Relative duodenal mRNA expression of *Trpv6*, *Sg100* and *Pmca1b* as determined by whole genome microarray analysis (Affymetrix).** Mice were raised on a normal 1% calcium chow for 10 weeks. They were then switched to a 2% calcium, 1.25% phosphorus and 20% lactose enriched diet. Duodenal samples were collected at either baseline or late pregnancy (gestation day 16.5) and total RNA was extracted. Microarray analysis and statistical analysis were performed at The Centre for Applied Genomics (Hospital for Sick Children, Toronto). The results are expressed as mean relative mRNA expression between each comparison.

significantly increased 4.8 fold ($P<0.005$) during pregnancy as compared to baseline. WT *Trpv6* mRNA expression decreased significantly during pregnancy as compared to WT baseline and pregnant *Vdr* nulls. Calbindin-D_{9K} and Ca^{2+}ATPase expression were not significantly different between *Vdr* null or WTs at baseline or late pregnancy.

To confirm the microarray results, I performed real time RT-PCR on the same *Vdr* null and WT baseline and late pregnancy RNA samples. The relative change in duodenal *Trpv6*, *Sg100* and *Pmca1b* mRNA expression as determined using real time RT-PCR are shown in *Table 3.3*. *Vdr* null *Trpv6* expression (*Figure 3.7*) was reduced at baseline as compared to WT. *Trpv6* mRNA expression significantly increased 13.5 fold during pregnancy as compared to baseline and was 3 fold higher ($p<0.01$) than pregnant WTs. WT *Trpv6* mRNA expression was decreased significantly during pregnancy as compared to WT baseline and pregnant *Vdr* nulls. *Sg100* and *Pmca1b* expression did not change significantly in *Vdr* null or WT at baseline or late pregnancy (*Table 3.3*).

3.4 Calcium homeostasis

To determine if the increase in duodenal calcium absorption in *Vdr* null during pregnancy affected maternal calcium homeostasis, I analyzed serum ionized calcium, urine calcium and parameters of secondary hyperparathyroidism (serum PTH and bone turnover markers).

Comparison	*Trpv6*	*Sg100*	*Pmca1b*
Vdr null baseline vs. WT baseline	0.04±0.00 NS	0.57±0.03 NS	0.34±0.02 NS
Vdr null pregnancy vs. baseline	13.5±2.37 p<0.001	0.70±0.08 NS	1.0±0.07 NS
WT pregnancy vs. baseline	0.18±0.05 p<0.06	0.81±0.1 NS	0.42±0.03 NS
Vdr null pregnancy vs. WT pregnancy	3.05±0.16 p<0.01	0.52±0.01 NS	0.82±0.01 NS

Table 3.3 **Relative duodenal mRNA expression of *Trpv6*, *Sg100* and *Pmca1b* as determined by real time RT-PCR.** Mice were raised on a normal 1% calcium diet for 10 weeks. They were then switched to a 2% calcium, 1.25% phosphorus and 20% lactose enriched diet. Duodenal samples were collected at either baseline or late pregnancy (gestation day 16.5). Duodenal total RNA was analyzed using TaqMan® RNA-to-C_T™ 1-Step Kit and TaqMan® Gene Expression Assays. The relative expression was calculated using the $2^{-\Delta\Delta CT}$ method and are expressed as mean relative expression ±SE.

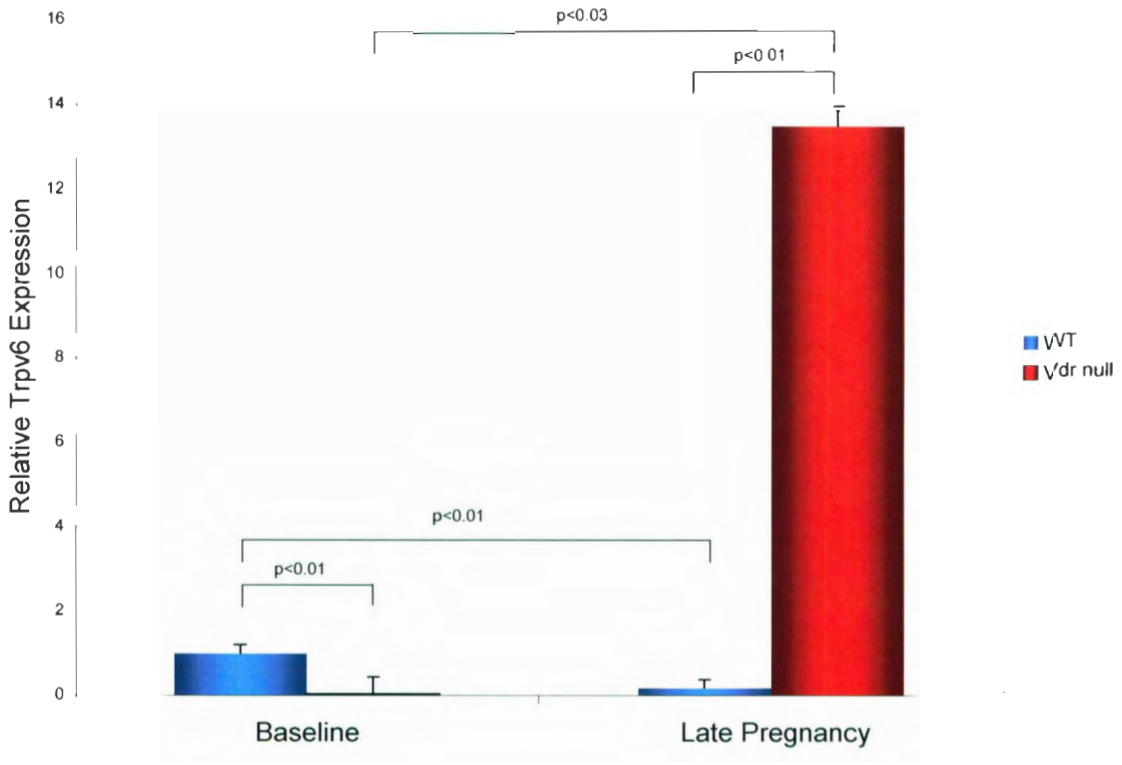

Figure 3.7 **Relative expression of duodenal *Trpv6* in WT (blue) and *Vdr* null (red) mice at baseline and pregnancy as determined using real time RT-PCR.** Mice were raised on a normal 1% calcium diet for 10 weeks. They were then switched to a 2% calcium, 1.25% phosphorus and 20% lactose enriched diet. Duodenal samples were collected at either baseline or late pregnancy (gestation day 16.5). Duodenal total RNA was analyzed using TaqMan® RNA-to-C_T™ 1-Step Kit and TaqMan® Gene Expression Assays. The results were calculated using the $2^{-\Delta\Delta}$CT method and displayed as mean relative expression ±SE.

3.4.1 Serum ionized calcium

Serum ionized calcium was measured to determine if the increase in duodenal calcium absorption in *Vdr* nulls during pregnancy caused serum calcium levels to normalize. *Figure 3.8* shows the preliminary results for ionized calcium in *Vdr* null mice at baseline and late pregnancy. WT baseline mean ionized calcium is indicated by the dotted line (1.17mmol/L). At baseline, the *Vdr* null was hypocalcemic (0.68 mmol/L). By late pregnancy, *Vdr* null ionized calcium increased to WT levels.

In order to determine the effect of the enriched diet on serum ionized calcium, I measured serum ionized calcium in non-pregnant *Vdr* nulls from 10-22 weeks of age (*Figure 3.9*). As shown, *Vdr* nulls were hypocalcemic while consuming both the regular (10 weeks) and enriched diets (12 weeks). By age 22 weeks, *Vdr* null ionized calcium significantly increased to WT levels.

3.4.2 Urine calcium

In order to determine if urine calcium excretion was altered in *Vdr* nulls during pregnancy, urine calcium was measured. *Figure 3.10* displays urine total calcium in WT and *Vdr* null mice throughout pregnancy. Although the difference was not statistically significant, the *Vdr* null value appeared lower than WT at baseline. Early in pregnancy, both WT and *Vdr* nulls have a trend toward increased urine calcium levels and the values become more similar. During late pregnancy, both genotypes have a trend toward

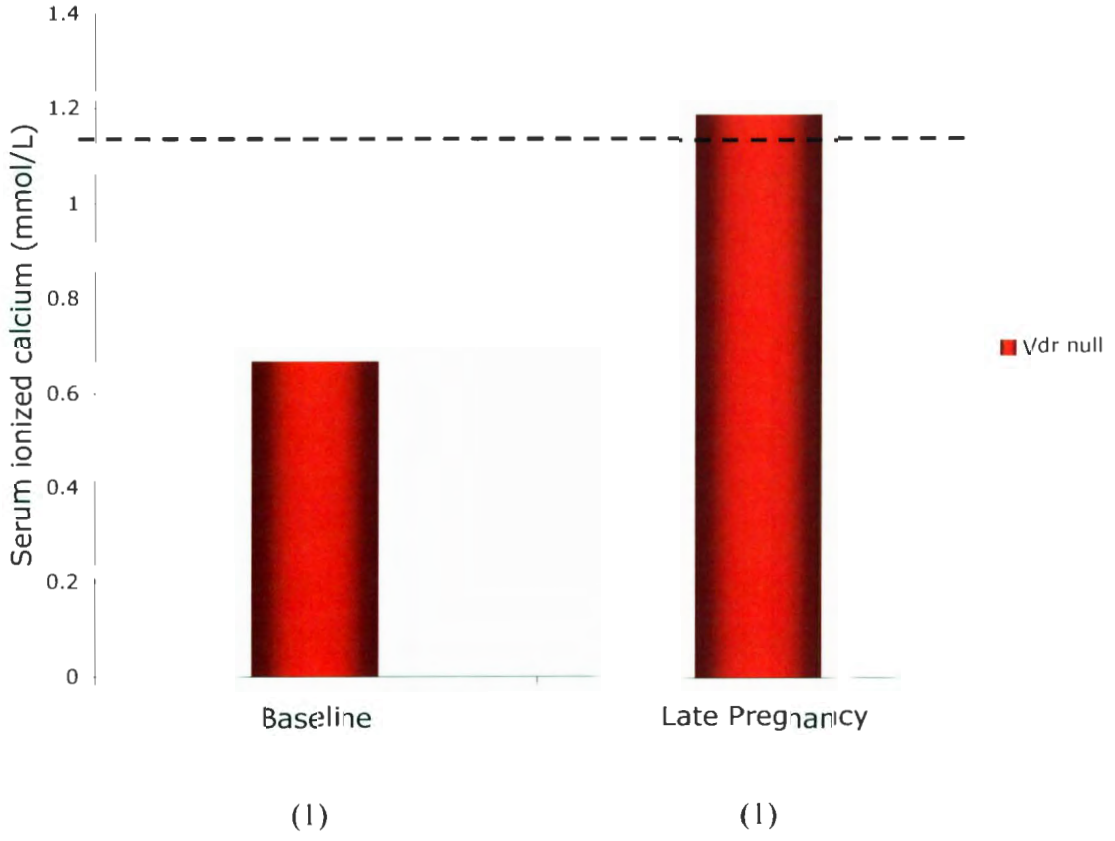

Figure 3.8 **Preliminary results for serum ionized calcium levels at baseline and late pregnancy in *Vdr* null mice.** Mice were raised on a normal 1% calcium diet for 10 weeks. Baseline whole tail blood was collected and analyzed immediately for ionized calcium. They were then switched to a 2% calcium, 1.25% phosphorus and 20% lactose enriched diet and mated. An additional ionized calcium measurement was obtained at late pregnancy. WT baseline serum ionized calcium (1.17mmol/L, N=8) is indicated by the dotted line.

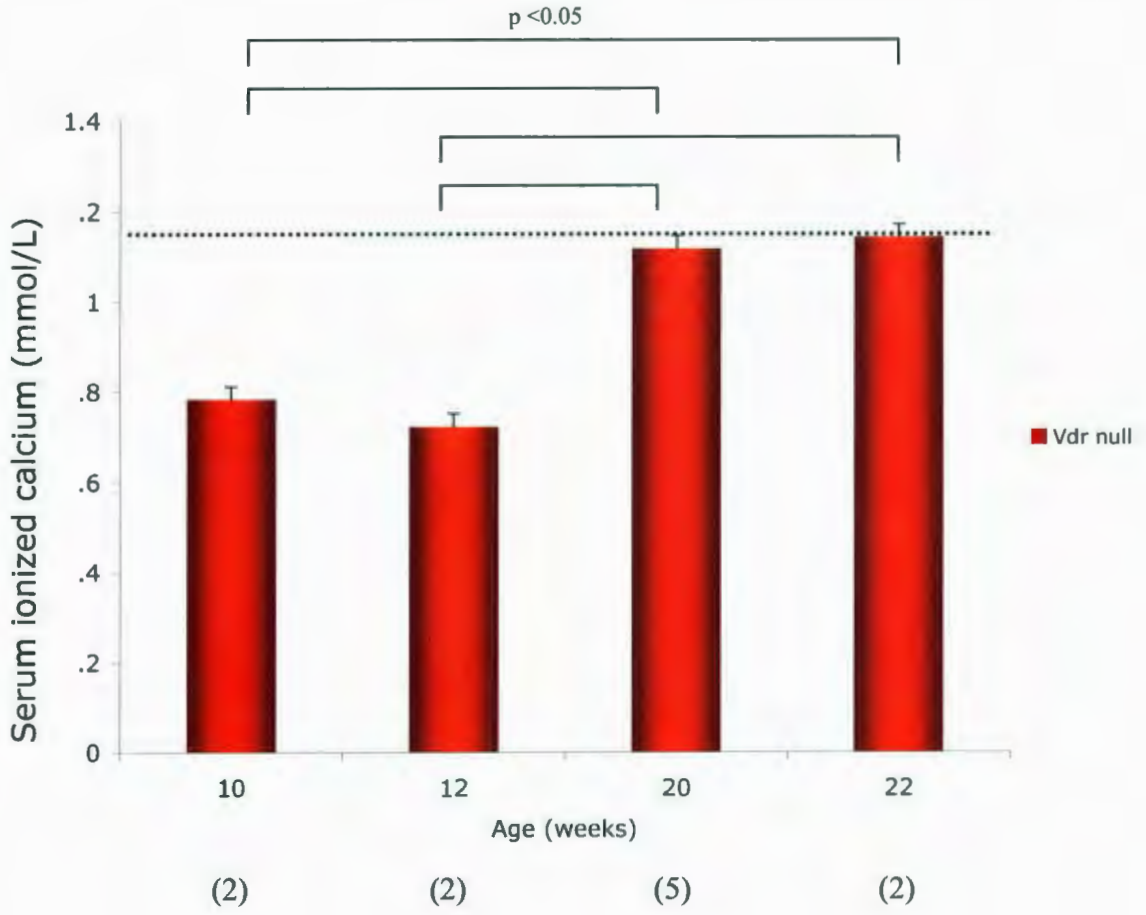

Figure 3.9 **Serum ionized calcium in virgin *Vdr* null mice while on regular diet (10 weeks) and while receiving the enriched diet.** Mice were raised on a normal 1% calciumdiet for 10 weeks. Whole tail blood was collected and analyzed immediately for ionized calcium. They were then switched to a 2% calcium, 1.25% phosphorus and 20% lactose enriched diet. Serial ionized calcium measurements were obtained at 12, 20 and 22 weeks and expressed as mean±SE. WT mean ionized calcium level (1.17mmol/L, N=8) is indicated by the dotted line.

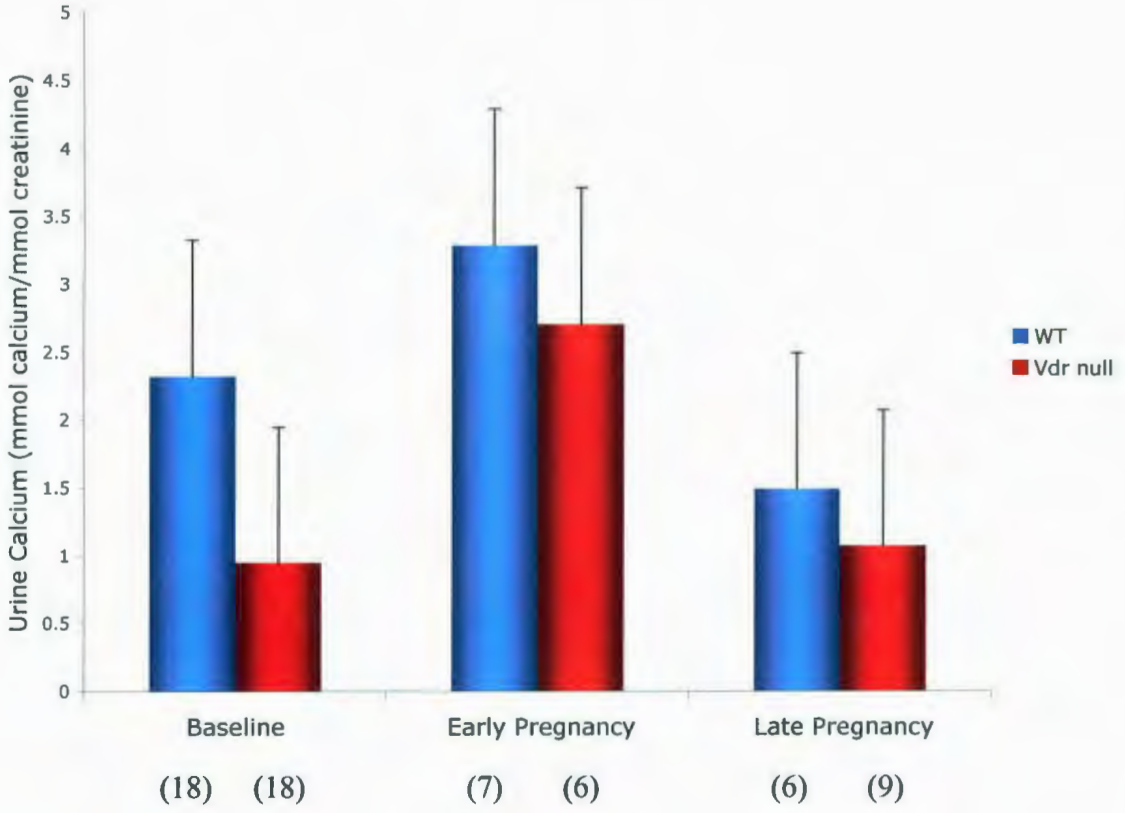

Figure 3.10 **Urine total calcium levels in WT (blue) and *Vdr* null (red) mice at baseline and throughout pregnancy.** Mice were raised on a normal 1% calcium diet for 10 weeks. They were then switched to a 2% calcium, 1.25% phosphorus and 20% lactose enriched diet. After at least 7 days, baseline urine was collected and the mice were mated. Serial urine samples were collected at gestation day 7 of pregnancy (early pregnancy), gestation day 18.5 of pregnancy (late pregnancy). Urine total calcium was measured using a calcium spectrophotometric assay (Diagnostic Chemical Ltd) and expressed relative to the urine creatinine concentration (mmol calcium/mmol creatinine, mean±SE).

decrease in urine calcium levels and the values remain similar, suggesting that *Vdr* null urine calcium excretion is becoming normalized.

3.4.3 Secondary hyperparathyroidism

Serum PTH was measured to determine if the increase in duodenal calcium absorption lessened secondary hyperparathyroidism in *Vdr* nulls during pregnancy. Serum PTH in *Vdr* null and WT mice at baseline and during pregnancy are shown in *Figure 3.11*. Baseline serum PTH levels were significantly higher in *Vdr* nulls as compared to WT. During pregnancy, serum PTH decreased in *Vdr* nulls to levels that were not significantly different from WT levels.

Since secondary hyperparathyroidism is associated with increased bone turnover, a decrease in serum PTH should be accompanied by a decrease in bone turnover. I measured serum osteocalcin and urine DPD, markers of bone formation and resorption respectively, to determine if bone turnover was decreased in *Vdr* nulls during pregnancy.

Serum osteocalcin levels in WT and *Vdr* null mice during pregnancy are displayed in *Figure 3.12*. At baseline, serum osteocalcin was elevated in *Vdr* null mice as compared to WT. By late pregnancy, *Vdr* null serum osteocalcin reduced significantly ($p<0.05$) to normal WT levels. WT osteocalcin levels did not change during pregnancy.

Urine DPD/creatinine levels in WT and *Vdr* null mice are shown in *Figure 3.13*. *Vdr* null DPD levels were significantly increased ($p<0.05$) at baseline but decreased significantly ($p<0.05$) to WT levels during pregnancy.

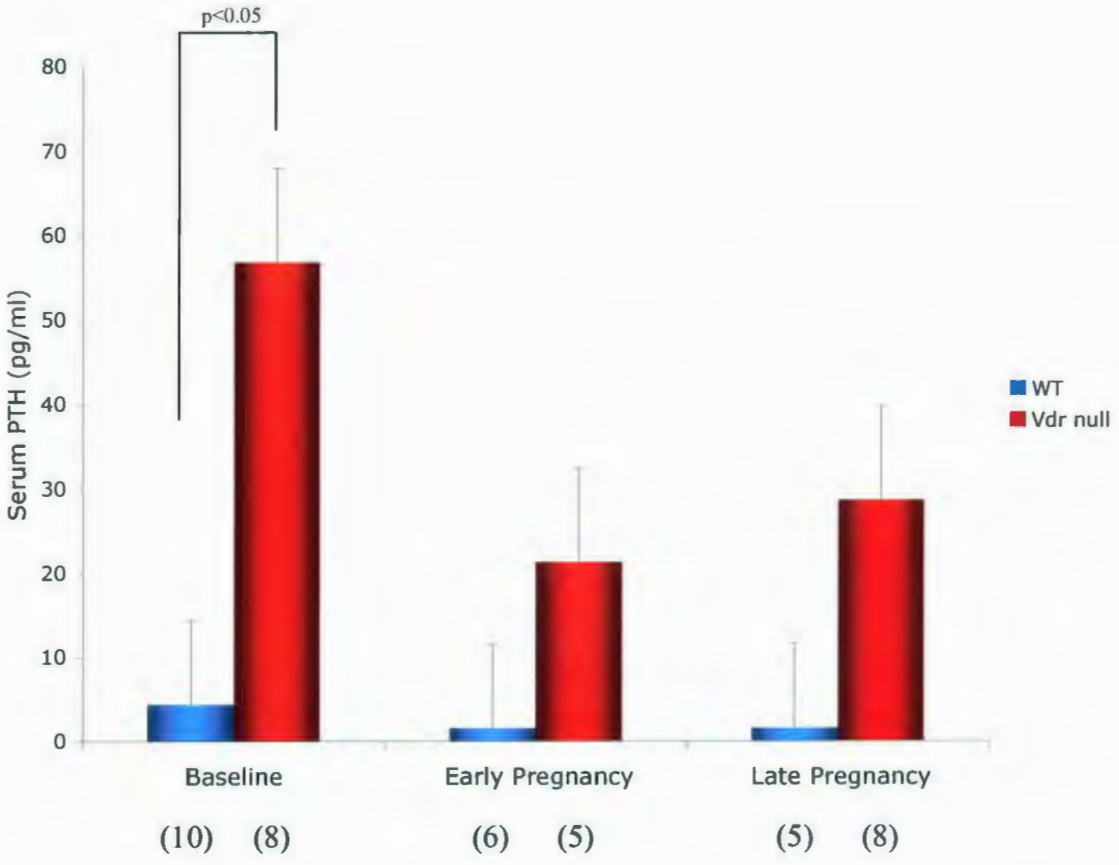

Figure 3.11 **Serum PTH levels in WT (blue) and *Vdr* null (red) mice at baseline and during pregnancy.** Mice were raised on a normal 1% calcium diet for 10 weeks. They were then switched to a 2% calcium, 1.25% phosphorus and 20% lactose enriched diet. After at least 7 days, baseline tail blood serum was collected and the mice were mated. Serial tail blood serum samples were collected at gestation day 7 (early pregnancy) and gestation day 18.5 (late pregnancy). Serum PTH levels were detected using a Rat Intact PTH ELISA kit (Immutopics, Inc) and expressed as mean±SE.

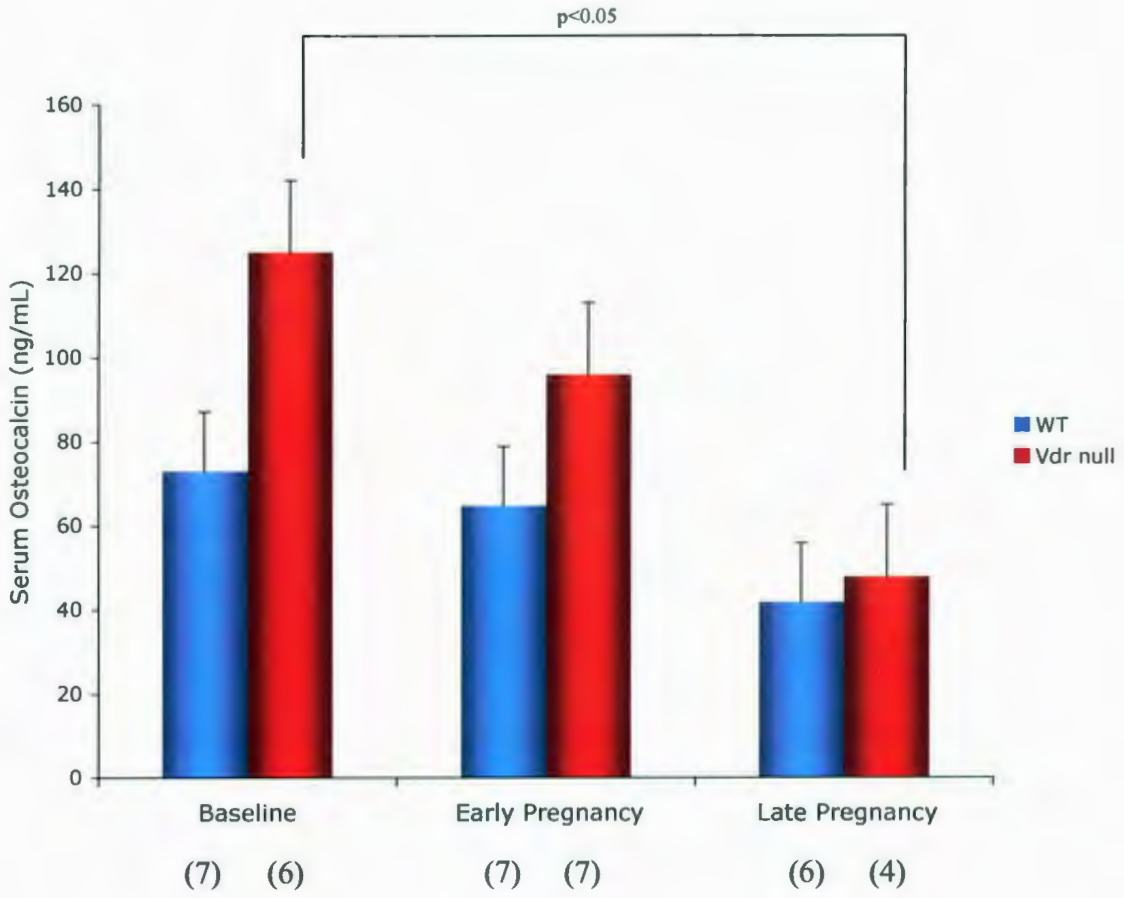

Figure 3.12 **Serum osteocalcin levels in WT (blue) and *Vdr* null (red) mice at baseline and during pregnancy.** Mice were raised on a normal 1% calcium diet for 10 weeks. They were then switched to a 2% calcium, 1.25% phosphorus and 20% lactose enriched diet. After 7 days, baseline tail serum was collected and the mice were mated. Serial tail serum samples were collected at gestation day 7 (early pregnancy) and gestation day 18.5 (late pregnancy). Serum osteocalcin was measured using the Mouse Osteocalcin IRMA kit (Immutopics, Inc) and expressed as mean±SE.

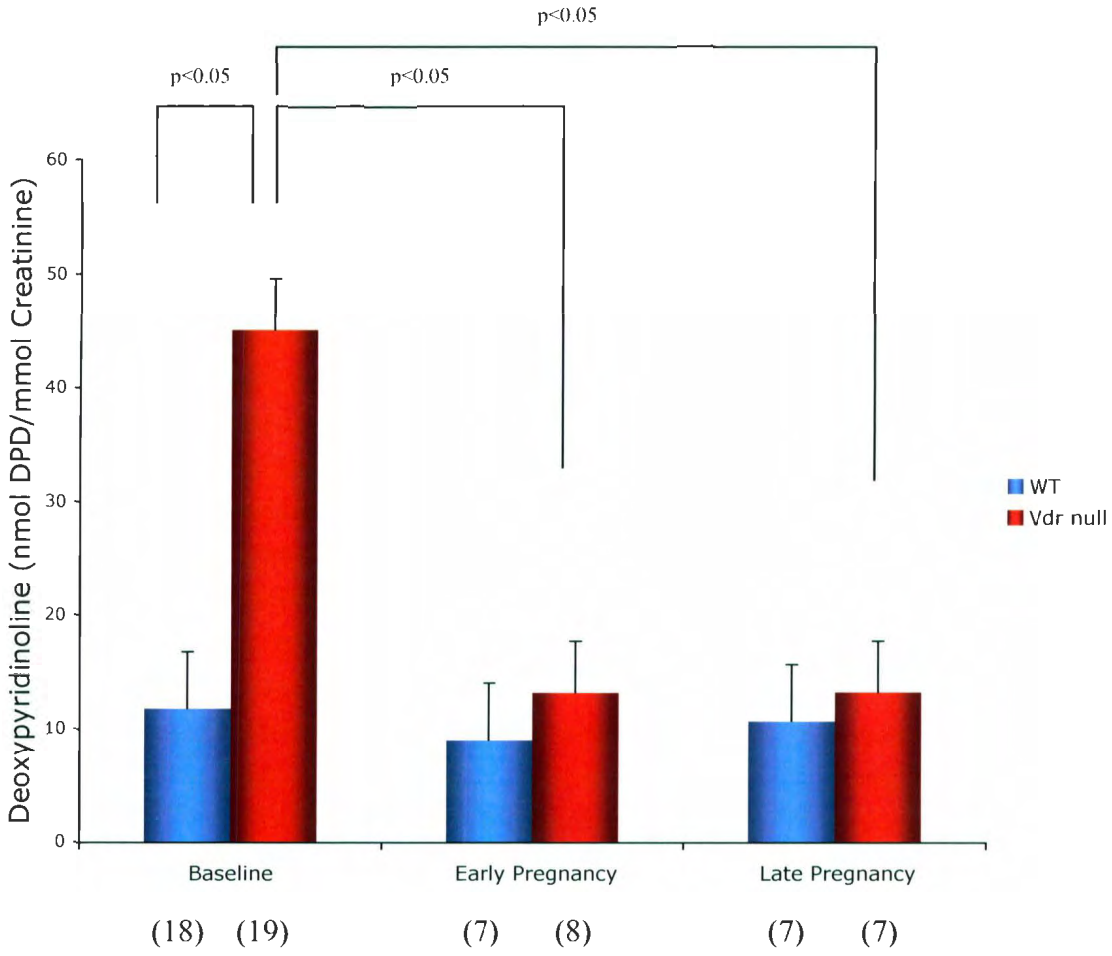

Figure 3.13 **Urine DPD levels in WT (blue) and *Vdr* null (red) mice at baseline and during pregnancy.** Mice were raised on a normal 1% calcium diet for 10 weeks. They were then switched to a 2% calcium, 1.25% phosphorus and 20% lactose enriched diet. After at least 7 days, baseline urine was collected and the mice were mated. Serial urine samples were collected at gestation day 7 (early pregnancy) and gestation day 18.5 of pregnancy (late pregnancy). Urine DPD was detected using the Metra DPD Enzyme Immunoassay (EIA) (Quidel) and Urine Creatinine was determined using the Creatinine-S spectrophotometric assay (Diagnostic Chemicals Limited). Urine DPD levels are expressed relative to the urine creatinine concentration as nmol DPD/mmol Creatinine (mean±SE).

3.5 Bone histology and histomorphometry

In order to determine if the rachitic *Vdr* null skeleton was repaired during pregnancy, the tibias were examined histologically. Goldner's trichrome stain of undecalcified tibia cross sections are shown in *Figure 3.14* (A-E). WT tibias (A,D) displayed a normal morphology and an organized growth plate (indicated by white arrows). *Vdr* null tibias had an abnormal rachitic morphology, disorganized growth plate (indicated by white arrows) and marked fibrosis (not shown) at both baseline (B,E) and pregnancy (C). Von Kossa stains of *Vdr* null tibia from baseline and late pregnancy are shown in *Figure 3.14* (H,I). Tibias from pregnant *Vdr* nulls displayed more mineral than baseline.

Vdr null undecalcified tibias were also examined histomorphometrically to determine if the increase in BMC in *Vdr* nulls during pregnancy was due to an increase in the formation of new bone or an increase in osteoid mineralization. *Table 3.4* displays the histomorphometry results for *Vdr* nulls at baseline and late pregnancy. Interestingly, there was no difference in bone volume, trabecular spacing, trabecular thickness or trabecular number during pregnancy as compared to baseline. In contrast, significant decreases were observed in osteoblast and osteoclast number, resorptive surface, osteoid surface and osteoid thickness in pregnant *Vdr* nulls as compared to baseline. This is also displayed histologically in *Figure 3.14* (F, G). Toluidine blue stains of *Vdr* null tibia trabeculae from baseline (F) showed more osteoid (arrows indicate clear layer of osteoid) than late pregnancy (G).

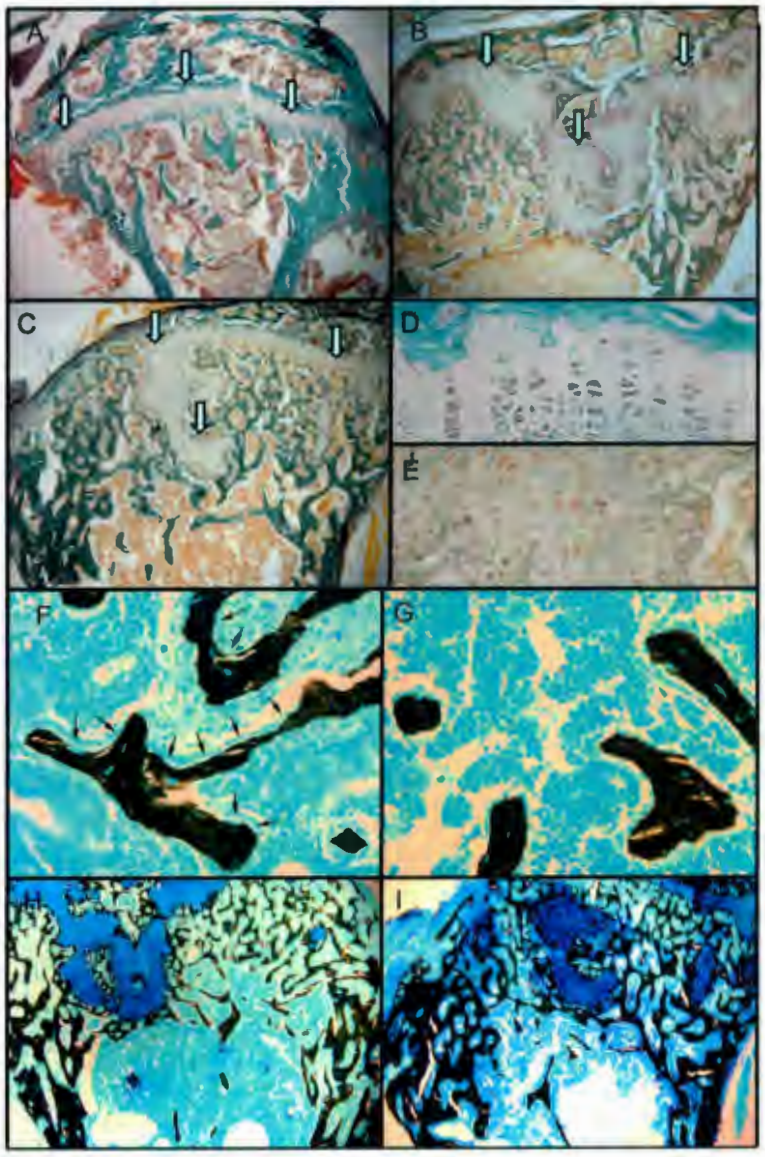

Figure 3.14 ***Undecalcified tibia histology.*** *A,B,C. Goldner's trichrome stain of WT baseline (A) Vdr null baseline (B) and Vdr null late pregnancy (C). D,E. Goldner's trichrome stain of WT baseline (D) and Vdr null baseline (E) growth plates. F,G.Toluidine blue stains of tibia trabeculae from Vdr null baseline (F, Arrows indicate clear layer of osteoid) and late pregnancy (G). H,I. Von Kossa stain of Vdr null tibias from baseline (H) and late pregnancy (I). Mice were raised on a normal 1% calcium chow for 10 weeks. They were then switched to a 2% calcium, 1.25% phosphorus and 20% lactose enriched diet. After at least 7 days (baseline) or at late pregnancy (gestation day 16.5) tibias were harvested, fixed, embedded, sectioned and stained.*

	Units	Baseline	Pregnancy
BV/TV	%	7.5±1.2	7.7±1.2
Tb.Th	μm	33.1±3.9	39.1±3.9
Tb.Sp	μm	471±133	502±133
Tb.N	#/mm	2.2±0.6	2.2±0.6
N.Ob/BPm	#/mm	18.3±3.7	0.3±3.7[b]
N.Oc/BPm	#/mm	2.6±0.5	0.8±0.5[d]
OcS/BS	%	9.5±1.6	3.0±1.6[c]
OS/BS	%	19.3±3.5	0.4±3.5[a]
O.Th	μm	3.9±0.7	0.9±0.7[c]

[a]$p<0.02$, [b]$p<0.03$, [c]$p<0.05$, [d]$p<0.08$

Table 3.4 **Histomorphometry results for *Vdr* null tibias at baseline and late pregnancy.** The parameters measured were as follows: Bone volume (BV/TV); Trabecular number (Tb.N); Trabecular thickness (Tb.Th); Trabecular spacing (Tb.Sp); Osteoblast number (N.Ob/BPm); Osteoclast number (N.Oc/BPm); Osteoclast surface (OcS/BS); Osteoid surface (OS/BS). The results are expressed as mean±SE.

4. Discussion

$1,25(OH)_2D_3$ and the VDR are essential for normal calcium and bone metabolism. Without the VDR, intestinal calcium absorption is reduced and the skeleton is stripped of calcium in order to maintain adequate levels in the serum. Vitamin D deficient rats and mice lacking either 1-α hydroxylase or the *Vdr* have poor intestinal calcium absorption, secondary hyperparathyroidism, hypocalcemia, rickets and an undermineralized skeleton (83-85). Pregnancy and lactation impose large demands on maternal calcium homeostasis. I investigated *Vdr* null mice to determine if $1,25(OH)_2D_3$ and the VDR were essential for calcium balance in females during the reproductive periods.

4.1 Bone mineral content

Adult *Vdr* null mice have rickets and osteomalacia. I wondered how these malformed, undermineralized skeletons would react when faced with the calcemic demands of pregnancy and lactation. I first investigated changes in BMC in *Vdr* null and WT mice during pregnancy, lactation and post-weaning recovery.

WT mice gained 7.13% total BMC during pregnancy, lost 18.05% during lactation and recovered to baseline post weaning. These data are consistent with previous research in WT mice in our lab (71, 72). The small increase in BMC during pregnancy may be an adaptation to prepare for the losses in BMC that occur during lactation in order

to provide calcium to the milk. After lactation, the BMC is rapidly regained without pathological consequences on the mother.

At baseline, *Vdr* nulls have approximately two thirds the amount of skeletal mineral as WT controls. This data is consistent with other studies involving vitamin D-depleted rats and *Vdr* null mice (80, 84, 85). Surprisingly, *Vdr* null mice experienced a 57% increase in BMC during pregnancy, which normalized their BMC to WT levels. These results suggest that there is an increase in either new bone formation or mineralization of osteoid during pregnancy so that the *Vdr* null skeleton contains the normal amount of mineral. Previous research supports these results. Rummens *et al.* (95) reported that bone density increased during pregnancy in the Leuwen *Vdr* knockout mouse on both regular calcium and enriched calcium diets. Furthermore, Halloran *et al.* (80) also documented that total bone calcium tended to increase in vitamin D deficient female rats during pregnancy.

Vdr nulls lost 36% BMC during lactation and recovered post-weaning to a value that was 49% higher than the pre-pregnancy baseline. These data do not agree with studies by Halloran *et al.* (80) or Miller *et al.* (96), who both observed that vitamin D deficient rats replaced some mineral after weaning but did not fully recover to baseline. This may be due to the fact that different models were used. It is possible that vitamin D deficient rats do not recover from lactation. These groups also used ash weight and histomorphometrical methods to estimate changes in bone mineral content which may provide a larger source of error and produce different results.

The skeleton is composed of both dense cortical bone and metabolically active spongy, trabecular bone. The hindlimb contains mostly cortical bone and the spine, trabecular bone. Regional changes in spine and hindlimb BMC were analyzed in order to determine if the changes in BMC affected involved one or both bone types. Gains and losses of BMC in the spine and hindlimb were similar to the changes in whole body BMC in *Vdr* null and WT mice. This suggests that the changes in BMC during the reproductive periods involve both trabecular and cortical bone.

Collectively, the results suggest that the VDR is not necessary for the maintenance of skeletal mineral metabolism during pregnancy and lactation. They also suggest that reproduction may be advantageous to the skeleton in mice lacking the *Vdr*. As bone is lost or resorbed during lactation, it is possible that new bone is formed to replace the abnormal bone, thus repairing the skeleton.

It was evident that the diet could be responsible, at least in part, for the increase in BMC. Rummens *et al.* (95) indicated that Leuwen *Vdr* nulls on a regular diet experienced an increase in trabecular bone while *Vdr* nulls who received the enriched diet at diagnosis of pregnancy, showed increases in both trabecular and cortical bone. For this reason, I measured changes in total BMC in non-pregnant *Vdr* nulls both before receiving the diet (10 weeks of age) and while on the diet (14, 18, 22 weeks). The preliminary data indicate that after 12 weeks on the diet, non-pregnant *Vdr* null mice experienced a gradual increase in BMC to a final value of 58%. This suggests that the enriched diet is responsible for at least some of the increase in BMC in *Vdr* nulls.

To further explore this issue, I also investigated the amount of time between baseline and late pregnancy scans and the amount of bone that was gained for each *Vdr* null. This would determine if there were a relationship between the amount of time consuming the diet and the amount of BMC gained. Three *Vdr* null mice had a mean 3.5 weeks on the enriched diet and gained 41% BMC during that time. Two *Vdr* null mice had a mean 14 weeks on the diet and gained 71%. These results show that pregnant *Vdr* null mice gained more BMC after both 3.5 and 14 weeks on the diet than non-pregnant *Vdr* null mice. Again, this suggests that the enriched diet is responsible for at least some of the increase in BMC but cannot account for all of the BMC that is achieved during pregnancy.

In future studies, it would be necessary to determine exactly how much the diet influences BMC during pregnancy and lactation in *Vdr* null mice. To achieve this, BMC measurements should be obtained during reproduction in *Vdr* nulls on a regular calcium diet, if it is physiologically possible. *Vdr* nulls are capable of completing pregnancy on a regular calcium diet (86) but it is not known if they can lactate normally. If the enriched diet were required for lactation, then the mice should be removed from the high calcium diet post weaning. This would at least determine if the enriched diet were necessary for the increase in BMC during post-weaning recovery.

4.2 Duodenal calcium absorption and gene expression

4.2.1 Duodenal calcium absorption

During pregnancy, there is an increase in intestinal calcium absorption in order to meet the demands of the mineralizing fetal skeleton. It has been presumed that the increase in calcium absorption is mediated by $1,25(OH)_2D_3$ and the VDR. I wondered if the increase in BMC in the *Vdr* nulls during pregnancy was due to an increase in calcium absorption that was independent of the VDR. This led me to investigate intestinal ^{45}Ca absorption in *Vdr* null and WT mice at baseline and late pregnancy (gestation day 16.5) using an *in situ* ligated loop technique. This technique utilizes a physiological concentration of calcium [$CaCl_2$, (2 mmol/L)] so that active transcellular calcium transport predominates (97, 98). The experiment was performed on gestation day 16.5 because it is the time when the transfer of calcium across the placenta to the fetus is at peak levels.

As shown in *Figure 3.6*, duodenal ^{45}Ca absorption was reduced in the non-pregnant *Vdr* null as compared to WT. This supports that a loss of VDR leads to a decrease in the active transport of calcium in the duodenum and it has also been observed in the Tokyo and Leuwen *Vdr* knockout strains (20, 99).

Surprisingly, ^{45}Ca absorption increased significantly in pregnant *Vdr* nulls as compared to baseline. This suggests that the increase in intestinal calcium absorption during pregnancy does not require the VDR. Previous evidence also indicates that $1,25(OH)_2D_3$ and the VDR are not required for intestinal calcium absorption during pregnancy. For example, the increase in calcium absorption during pregnancy has been

shown to precede the rise in $1,25(OH)_2D_3$ levels (67). In addition, Halloran *et al.* (68) and Brommage *et al.* (69) documented that intestinal calcium absorption was increased during pregnancy in vitamin D deficient rats.

The results suggest that during pregnancy, unique mechanisms may be activated to stimulate duodenal calcium absorption in order to achieve ideal physiological conditions for the fetus and to prepare for lactation. In addition, the increase in ^{45}Ca absorption in *Vdr* nulls may explain, at least in part, the increase in BMC during pregnancy. An increase in the active absorption of calcium would increase the amount of calcium that is available for bone formation or mineralization.

The increase in intestinal calcium absorption may be caused by hormones other than $1,25(OH)_2D_3$. Takeuchi *et al.* (70) reported that placental lactogen stimulates calcium transfer during pregnancy. Studies by Ajibade *et al.*(26), in non-pregnant vitamin D deficient mice, have shown that prolactin injections stimulated a 3 fold increase in duodenal calcium absorption. Placental lactogen is characteristically similar to prolactin and ultilizes the prolactin receptor. It is likely that both are capable of stimulating intestinal calcium absorption; however, placental lactogen is elevated during pregnancy while prolactin is not. Thus, placental lactogen could be responsible for increasing duodenal calcium absorption during this time.

Vdr null mice lack a functional *Vdr* but do not lack $1,25(OH)_2D_3$. Several studies have shown, however, that $1,25(OH)_2D_3$ may stimulate both active and passive intestinal calcium absorption through VDR-independent mechanisms (29, 30, 100, 101). It has been proposed that in these situations, $1,25(OH)_2D_3$ acts similar to growth factors or

peptide hormones to initiate signaling pathways to activate rapid responses (29). This may occur through a unique receptor on the plasma membrane (102). Intestinal calcium absorption also increases in vitamin D deficient rats during pregnancy (68) therefore, it is unlikely that non-genomic actions of $1,25(OH)_2D_3$ are responsible for the increase in intestinal calcium in *Vdr* null mice.

There is also increasing evidence that the VDR may have a unique non-transcriptional role in mediating plasma membrane signaling (103-105). Although the *Vdr* knockout model used in my experiments has a mutation in the second zinc finger of the VDR DNA binding domain, this may not inhibit non-transcriptional actions of the VDR in my null mice. It is possible that the mutated VDR initiates signaling to stimulate calcium absorption during pregnancy.

My values for percentage duodenal calcium absorption in non-pregnant mice were much higher than values recorded by Song *et al.* (99). I reported a 71% and 85% absorption in non-pregnant *Vdr* null and WT, respectively. Song *et al.* (99) observed 16% and 55% for *Vdr* null and WT mice on a 0.5% calcium diet and 20% and 18% on a 2% calcium diet. Their data suggested that the enriched calcium diet decreases the active transport of calcium. It is my belief, however, that the diet increased passive duodenal calcium absorption in my experiments, thus causing the high baseline values. Although the ligated loop technique is designed to measure the active absorption of calcium across the duodenum, passive absorption may also occur during the experiment in these fasted mice.

The diet may cause an increase in passive calcium absorption in two ways. First, a high calcium diet will increase the concentration of calcium in the lumen of the intestine. Even though the mice were fasted, remnants of the diet may still exist after fasting. This would increase the concentration gradient between the lumen and the blood and therefore increase paracellular calcium absorption across the mucosal cells. Secondly, the diet contains 20% lactose, a major disaccharide in milk, which is known to increase calcium absorption in the absence of vitamin D (36). The exact mechanism of how this occurs is a matter of controversy, however, the breakdown of lactose to glucose and galactose may be important (36). In this process lactose may increase the bioavailability of calcium in the intestine, making it more readily absorbed, which would prolong the passive vitamin D-independent absorption of calcium in the ileum (106). Alternately, lactose may act on the intestinal mucosa to increase its permeability, possibly by increasing the space of the intercellular tight junctions (107).

A diet-induced increase in the passive absorption of calcium across the duodenum could also explain the increase in BMC that was observed in non-pregnant mice. This would provide more calcium for mineralizing the skeleton, resulting in a steady increase in BMC in non-pregnant *Vdr* null mice with undermineralized skeletons.

4.2.2 Duodenal gene expression

To further investigate the cellular mechanisms involved in the upregulation of intestinal calcium absorption in *Vdr* null mice during pregnancy, I performed a whole

genome microarray analysis of gene expression in the duodenum of *Vdr* null and WT mice at baseline and late pregnancy. The microarray results for *Trpv6*, *Pmca1b* and *Sg100* are shown in Table 3.2. These results were confirmed using real time RT-PCR (*Table 3.3, Figure 3.7*).

The microarray data indicated that *Trpv6* expression was reduced in non-pregnant *Vdr* nulls as compared to WT ($p<0.005$). This agrees with other studies in Leuwen and Tokyo *Vdr* knockout mice on low, normal or high calcium diets (20, 99).

During pregnancy, *Trpv6* expression decreased in WT mice as compared to baseline ($p<0.005$). In contrast, *Trpv6* expression increased 4.8 fold during pregnancy in *Vdr* nulls as compared to baseline ($p<0.005$). As a result, *Trpv6* mRNA expression increased to equal (microarray) or surpassed (real time RT-PCR, *Figure 3.7*) WT baseline levels. These results indicate that *Trpv6* expression is upregulated in *Vdr* nulls independently of the *Vdr* during pregnancy, thus leading to an increase in the active absorption of intestinal calcium. Future studies will also determine if TRPV6 protein expression is upregulated in *Vdr* null mice during pregnancy.

The results from the microarray and real time RT-PCR analysis of *Trpv6* expression differ in magnitude and significance. Approximately 32 PCR cycles were required to amplify the template suggesting that *Trpv6* mRNA is expressed in very small amounts in the samples. Real time RT-PCR accurately detects very small amounts of mRNA and may produce more reliable results.

The increase in *Trpv6* expression in *Vdr* nulls during pregnancy does not appear to be diet-related. *Trpv6* expression was reduced in *Vdr* nulls at baseline, while receiving

the enriched diet. WT mice were also receiving the high calcium diet and did not experience an increase in *Trpv6* expression during pregnancy. Also, as mentioned, previous research by VanCromphaut *et al.* (20) and Song *et al.* (99) reported that *Trpv6* expression was reduced in non-pregnant Leuwen and Tokyo *Vdr* knockouts, regardless of the diet. This further supports that *Vdr* null *Trpv6* expression is increased during pregnancy and not as a consequence of the high calcium diet.

These data suggest that unique VDR-independent mechanisms are activated during pregnancy, which stimulate *Trpv6* expression leading to an increase in the active transport of calcium across the duodenum. Previous studies have shown that prolactin stimulates *Trpv6* expression (26). As placental lactogen has been shown to stimulate intestinal calcium absorption independently of $1,25(OH)_2D_3$ during pregnancy and act through the prolactin receptor, it may also be the factor that is responsible for stimulating the increase in *Trpv6* expression. To further investigate the mechanisms activating this system, future studies will focus on measuring the serum levels of these likely candidates.

The results also suggest that calbindin-D_{9K} is not required for the increase in duodenal calcium absorption in *Vdr* null during pregnancy. *Sg100* mRNA expression in *Vdr* nulls was normal at baseline and late pregnancy. This is not consistent with previous research which reported that intestinal *Sg100* mRNA expression was lower in Boston and Tokyo *Vdr* null mice as compared to WT (99, 108). These groups also showed, however, that *Sg100* mRNA expression is reduced in WT mice receiving the 2% enriched calcium as compared to WTs fed a regular diet. If my WT baseline expression values are

decreased due to the enriched diet, then *Vdr* null expression would appear normal. This may explain the why my results differ from previous research.

Pmca1b mRNA expression was also normal in *Vdr* nulls at baseline. These results agree with previous studies which also found that *Pmca1b* mRNA expression was normal in non-pregnant Leuwen and Tokyo *Vdr* nulls (20). Surprisingly, *Pmca1b* mRNA expression did not increase during pregnancy. This suggests that Ca^{2+}ATPase is not required for the upregulation of intestinal calcium transfer in *Vdr* nulls during pregnancy, however, Ca^{2+}ATPase expression may remain the same while its activity increases. In future studies, protein expression of calbindin-D_{9K} and Ca^{2+}ATPase and the activity of Ca^{2+}ATPase will be examined.

It is possible that I did not see changes in the expression of *Sg100* and *Pmca1b* because of the way I harvested the sample. Changes in expression that were directly related to the increase in calcium absorption would have occurred in the mucosal layer. Harvesting a section of the whole duodenum, which also contains the intestinal muscle wall and pancreatic tissue, may have masked important changes that could have occurred in the epithelium. This technique could be improved by obtaining duodenal epithelial scrapings, rather than harvesting the whole duodenum.

All other significant changes in duodenal gene expression are shown in Appendix A and B. Although the expression of these genes was not further explored in this thesis, some of them are deserving of future investigation. For example, the microarray analysis also appeared to support the theory that the lactose in the diet upregulates passive calcium absorption (Appendix A). The data indicated that lactase mRNA was upregulated 4.3

fold ($p<0.05$) in *Vdr* nulls at baseline as compared to WT (A1). Lactase expression was also 2.22 fold ($p<0.05$) in *Vdr* nulls during pregnancy as compared to pregnant WTs (A4) and 1.6 fold (NS, data not shown) in pregnant WTs as compared to baseline. Lactase is an enzyme which is expressed on the brush border membrane of the duodenal mucosal cell that is essential for the break down of lactose to glucose and galactose. Prolonged exposure to the diet may upregulate lactase expression, resulting in the breakdown of lactose that ultimately initiates signaling to cause an increase in paracellular calcium absorption.

In addition, duodenal expression of claudin-4 was decreased 0.46 ($p<0.005$) in pregnant *Vdr* nulls as compared to baseline (A2) and 0.42 ($p<0.05$) as compared to pregnant WTs (A4). The claudin family of proteins are important in the regulation of tight junctions (109). $1,25(OH)_2D_3$ has been shown to stimulate claudin-2 and claudin-12 expression to increase intestinal paracellular absorption (30). These results further support that claudin expression is regulatd by $1,25(OH)_2D_3$ and the *Vdr* but do not appear to explain the mechanism causing the increase in *Vdr* null intestinal calcium absorption during pregnancy.

Furthermore, duodenal expression of the uncharacterized cDNA sequence AY05357 is increased 3.42 ($p<0.05$) in *Vdr* nulls at baseline as compared to WT's (A1) but is decreased 0.27 ($p=0.005$) in pregnant *Vdr* nulls as compared to pregnant WT's (A2). The role of this gene in pregnant *Vdr* nulls may also deserve further exploration in the future.

It is possible that the analysis of the microarray data is limited due to the small sample sizes used in the experiment. This was caused by problems with RNA quality. The Centre for Applied Genomics' (The Hospital for Sick Children, Toronto) protocol recommends that only samples with a RIN≥7 be used for microarray analysis. Only 50% of my samples met this requirement because there was significant degradation observed in the other half of the samples. As a result, only two samples (as opposed to four) per genotype, per timepoint were chosen for microarray analysis, which greatly reduced the sample sizes for the experiment. Due to time constraints and the low probability of *Vdr* null survival to 10 weeks (~25%), acquiring more samples was not possible. Despite the small sample sizes, good quality RNA was used for these microarray experiments and the results were confirmed using real-time PCR, suggesting that the data are accurate.

4.3 Impact on calcium homeostasis

Non-pregnant *Vdr* null mice have hypocalcemia, secondary hyperparathyroidism, osteomalacia and rickets. Next I wanted to determine if the increase in intestinal calcium absorption during pregnancy also repaired calcium homeostasis in *Vdr* nulls.

4.3.1 Serum calcium

Serum ionized calcium was measured to determine if the increase in intestinal calcium absorption in *Vdr* nulls during pregnancy also normalized serum ionized calcium

levels. Unfortunately, only preliminary data could be obtained for ionized calcium. Reagents for the ionized calcium machine in our laboratory were no longer commercially available and no other ionized calcium measuring device was available locally. As a result, the sample sizes for my ionized calcium data were very small.

The non-pregnant *Vdr* null was hypocalcemic at baseline but normalized serum ionized calcium to WT levels by late pregnancy. These preliminary data suggest that pregnancy normalized ionized calcium levels in *Vdr* null mice, however, more data is needed to be conclusive.

To further examine if ionized calcium were normalized by the enriched diet, I measured ionized calcium in non-pregnant *Vdr* null mice on a regular calcium diet (10 weeks of age), after receiving the high calcium diet at 12 weeks, 20 weeks and 22 weeks of age. Non-pregnant *Vdr* null mice were hypocalcemic on the regular diet. *Vdr* null ionized calcium normalized to WT levels between 12 and 20 weeks of receiving the enriched diet. This suggests that the high calcium diet will eventually normalize ionized calcium in *Vdr* null mice. Others have shown that a high calcium diet normalized serum calcium in vitamin D deficient rats (110), *Vdr* knockout mice (87, 89) and 1,α-hydoxylase knockout mice (111) that would otherwise be hypocalcemic if fed a regular 1% calcium diet. Due to the lack of data between 12 and 20 weeks it is difficult to determine if the normalization of serum calcium would occur faster in pregnant *Vdr* nulls. It will be necessary to repeat this experiment to obtain more data. This will help distinguish how pregnancy and the diet independently influence serum calcium in *Vdr* null mice.

4.3.2 Urine calcium

I measured urine calcium to determine if calcium excretion was altered during pregnancy in *Vdr* null mice. At baseline, *Vdr* null urine calcium is not significantly different but appears reduced as compared to WT. This may suggest that because *Vdr* nulls have decreased duodenal calcium absorption, they need to reclaim more calcium back into the circulation. Conversely, it may indicate that WT mice are excreting more calcium because of the diet-induced increase in intestinal calcium absorption.

Early in pregnancy, urine calcium is increased in both *Vdr* null and WT mice. This supports the ^{45}Ca absorption results because an increase in duodenal calcium absorption would increase calcium availability in both genotypes and require that the kidneys remove more calcium from the circulation. By late pregnancy, urine calcium excretion shows a reducing trend in both null and WT mice, suggesting that more calcium is being reclaimed back into the circulation in order to meet the demands of the mineralizing fetal skeleton.

4.3.3 Secondary hyperparathyroidism and bone turnover

Non-pregnant *Vdr* null mice have secondary hyperparathyroidism which is associated with increased bone turnover or remodeling. I measured serum PTH and biomarkers of bone turnover to determine if secondary hyperparathyroidism was decreased in *Vdr* nulls during pregnancy.

Vdr null mice had secondary hyperparathyroidism at baseline; serum PTH was significantly elevated as compared to WT. During early and late pregnancy, serum PTH decreased to levels that were not statistically different from WT. This suggests that secondary hyperparathyroidism in *Vdr* nulls is lessened during pregnancy. These results were expected since an increase in intestinal calcium absorption during pregnancy would possibly increase serum calcium, leading to a decrease in secondary hyperparathyroidism.

The decreased PTH levels may be related to the enriched diet. If the diet increases the passive absorption of calcium, then serum calcium normalizes, resulting in a decrease in PTH. The diet was shown to prevent secondary hyperparathyroidism (maintain normal PTH levels) in both rats with diet-induced vitamin D deficiency (88) and *Vdr* null mice (fed diet at weaning) (87). However, Song *et al.* (99) observed that PTH levels remained elevated in Tokyo *Vdr* null mice that were fed the high calcium diet from weaning. To address this issue, further research is necessary to determine if serum PTH levels are altered in non-pregnant *Vdr* nulls receiving the calcium enriched diet.

Since there was a decrease in serum PTH in pregnant *Vdr* null mice, I wondered if there were also a decrease in bone turnover. I measured serum osteocalcin, a marker of bone formation, and urine DPD (*Figure 3.13*), a marker of bone resorption, to determine if these processes were decreased in pregnant *Vdr* nulls.

At baseline, serum osteocalcin was increased in *Vdr* nulls as compared to WT, suggesting that bone formation is increased. During pregnancy, *Vdr* null serum osteocalcin decreased to WT levels, indicating that bone formation decreased. This suggests that the increased BMC in *Vdr* nulls during pregnancy did not result from an

increase in the formation of new bone. It is possible, at baseline, osteoblasts are laying down the bone matrix at a high rate but due to hypocalcemia, calcium may not be available to mineralize the matrix. During pregnancy, *Vdr* null intestinal calcium transfer is increased, resulting in an increase in the availability of calcium in the serum and mineralization of the previously laid bone matrix at a time when osteoblast activity is decreasing.

Urine DPD was significantly increased in *Vdr* nulls at baseline suggesting that bone resorption is increased during this time. During pregnancy, *Vdr* null urine DPD decreased to WT levels suggesting that bone resorption was decreasing. These results support the BMC data. Bone resorption is decreasing, allowing bone mineral content to increase.

Collectively, the increased serum osteocalcin and urine DPD levels at baseline suggest that bone turnover is elevated in non-pregnant *Vdr* null mice. Likewise, the decrease in osteocalcin and DPD levels in *Vdr* nulls during pregnancy suggest that bone turnover is decreased. These data demonstrate that secondary hyperparathyroidism and bone turnover are reduced in *Vdr* null mice during pregnancy.

4.4 Bone histology and histomorphometry

The biomarker data indicated that bone turnover decreased in *Vdr* nulls during pregnancy. This suggests that the increased BMC during pregnancy was not due to an increase in bone formation but rather an increase in osteoid mineralization.

To further investigate this, I examined undecalcified tibias to determine if bone morphology improved in *Vdr* nulls during pregnancy and to further confirm that bone mineral content increased (*Figure 3.14*). At baseline, *Vdr* null tibias had an abnormal rachitic morphology (B), a disorganized growth plate (E) and marked fibrosis (not displayed) as compared to WT (A, D). This rachitic phenotype was also shown during pregnancy in *Vdr* null mice (C). This suggests that the increased BMC and reduced secondary hyperparathyroidism that occurred in *Vdr* nulls during pregnancy did not repair the rachitic bone phenotype. This data supports the biomarker results and suggests that the increase in BMC in *Vdr* nulls during pregnancy is a result of an increase in the mineralization of pre-existing osteoid, rather than an increase in the formation of new bone. Analysis of tibia von Kossa stains supported the BMC data. Pregnant *Vdr* nulls (I) showed increased mineral as compared to baseline (H).

Vdr null and WT undecalified tibias were also analysed using histomorphometry to confirm if the increased BMC during pregnancy was the result of an increase in osteoid mineralization in *Vdr* nulls (*Table 3.4*). Interestingly, there was no significant difference in bone volume, trabecular thickness, trabecular spacing or trabecular number in pregnant *Vdr* nulls as compared to baseline. These results indicate that bone volume did not change during pregnancy in *Vdr* nulls and support the notion that the increase in BMC was not due to the formation of new bone. Surprisingly, significant decreases were observed in osteoblast and osteoclast numbers and resorptive surface in pregnant *Vdr* nulls which further supports the view that bone turnover is decreased in *Vdr* nulls during pregnancy. Osteoid surface and osteoid thickness also significantly decreased in

pregnant *Vdr* nulls suggesting that the amount of osteoid is decreasing and thus being mineralized to form bone. This is also displayed histologically. The amount of osteoid was greater in *Vdr* null tibias at baseline (indicated by arrows in F) than late pregnancy (G). This supports that the increase in *Vdr* null BMC during pregnancy was due to an increase in the mineralization of osteoid rather than the formation of new bone.

4.5 Proposed model

In an attempt to explain the results of my experiments, I am proposing the following models (*Figure 4.1, 4.2*). *Figure 4.1* displays how the active transcellular transport of calcium is upregulated in *Vdr* nulls. During pregnancy, the presence of factors/hormones activate unique mechanisms in the *Vdr* null to increase the expression of duodenal *Trpv6*, thus driving an increase in the active absorption of calcium. I suspect that *Sg100* and *Pmca1b* are also upregulated at the protein level or show increased activity. As a result, serum PTH, urine calcium, bone turnover and BMC are normalized, allowing the *Vdr* null to follow through a normal pregnancy. *Figure 4.2* displays how the diet causes an increase in the passive paracellular absorption. The enriched calcium diet increases the concentration of calcium in the lumen, thus increasing the concentration gradient, favoring the movement of more calcium ions into the blood. I suspect that this is occurring in both *Vdr* null and WT mice. This is further encouraged by an increase in the expression of lactase. Lactase digests dietary lactose and increases paracellular

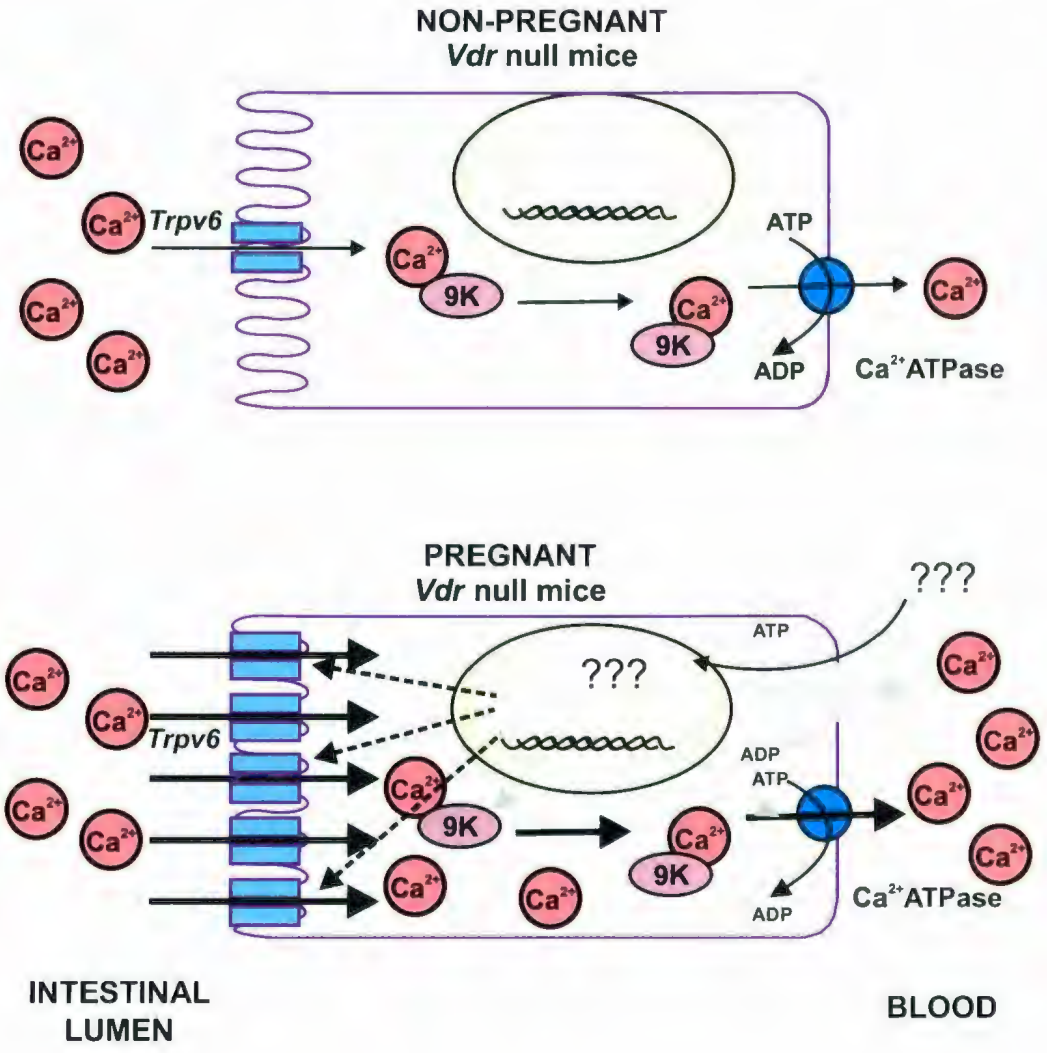

Figure 4.1 **Proposed model for the increase in transcellular absorption in *Vdr* null mice during pregnancy.** During pregnancy, the presence of factors/hormones activate unique mechanisms in the *Vdr* null during pregnancy increase the expression of duodenal *Trpv6*, thus driving an increase in the active absorption of calcium.

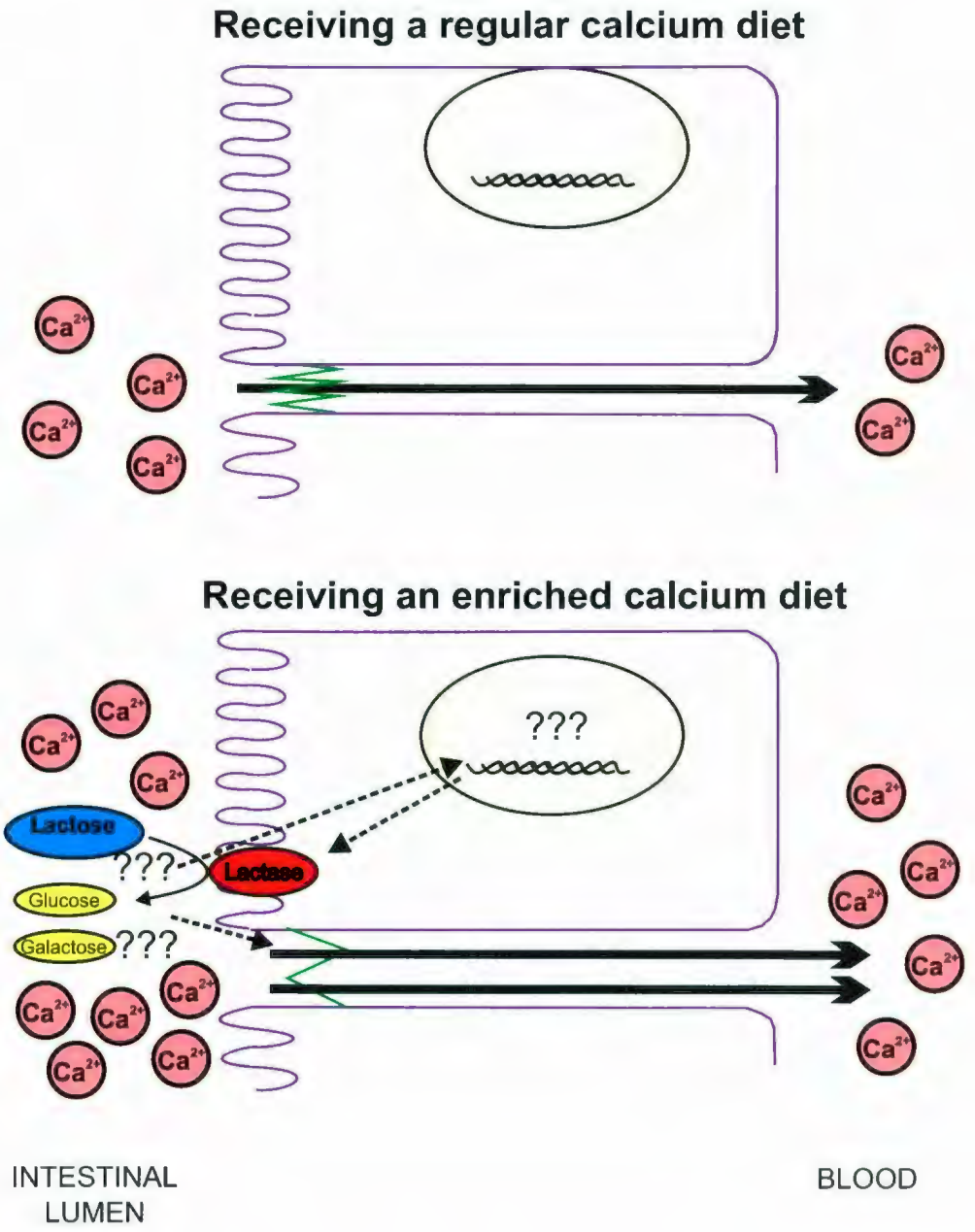

Figure 4.2 **Proposed model for the effect of the calcium and lactose enriched diet on paracellular absorption.** The enriched calcium diet increases the concentration of calcium in the lumen, thus increasing the concentration gradient, favoring the movement of more calcium ions into the blood. This is further encouraged by an increase in the expression of lactase. Lactase digests dietary lactose and increases paracellular absorption, probably through an increase in tight junction permeability.

absorption, probably through an increase in tight junction permeability. Over time, this small increase in calcium absorption would provide more calcium in the serum and eventually result in a steady increase in BMC in undermineralized *Vdr* null skeletons. For this reason, I believe that the diet is, at least in part responsible for the increase in BMC in pregnant and post-lactating *Vdr* null mice. The increase in passive absorption would have no visible effect on BMC in WT skeletons because they are not undermineralized.

4.6 Summary and conclusion

Vdr null mice were able to achieve a normal pregnancy, lactation and recovery. During pregnancy, *Trpv6* expression was increased in *Vdr* null mice leading to an increase in intestinal calcium absorption. The increase in calcium absorption increased serum calcium levels, resulting in a decrease in secondary hyperparathyroidism, an increase in osteoid mineralization and ultimately an increase in BMC. Experiments involving non-pregnant *Vdr* null mice suggest that the calcium and lactose enriched diet is partly responsible for the increase in BMC and normalization of calcium homeostasis, however, the contribution appears to be of a lesser magnitude than pregnancy.

In conclusion, the VDR is not required to regulate calcium and bone homeostasis during pregnancy.

REFERENCES

1. **Bischoff-Ferrari HA, Dietrich T, Orav EJ, Dawson-Hughes B** 2004 Positive association between 25-hydroxy vitamin D levels and bone mineral density: a population-based study of younger and older adults. Am J Med 116:634-9

2. **Bischoff-Ferrari HA, Willett WC, Wong JB, Giovannucci E, Dietrich T, Dawson-Hughes B** 2005 Fracture prevention with vitamin D supplementation: a meta-analysis of randomized controlled trials. Jama 293:2257-64

3. **Bikle D, Adams J, Christakos S** 2008 Vitamin D: Production, Metabolism, Mechanism of Action, and Clinical Requirements. In: Rosen CJ (ed) Primer on the Metabolic Bone Diseases and Disorders of Mineral Metabolism. American Society for Bone and Mineral Research, Washington DC; pp 141-149

4. **Holick MF** 2007 Vitamin D deficiency. N Engl J Med 357:266-81

5. **Favus MJ, Goltzman D** 2008 Regulation of Calcium Metabolism. In: Rosen CJ (ed) Primer on the Metabolic Bone Diseases an Disorders of Mineral Metabolism, 7th ed. American Society of Bone and Mineral Research, Washington, DC; pp 104-108

6. **Goltzman D, Cole DEC** 2003 Hypoparathyroidism. In: Favus MJ (ed) Primer on the Metabolic Bone Diseases and Disorders of Mineral Metabolism, 5th ed. The American Society for Bone and Mineral Research, Washington DC; pp 274-278

7. **Brown EM, MacLeod RJ** 2001 Extracellular calcium sensing and extracellular calcium signaling. Physiol Rev 81:239-297

8. **Kifor O, Diaz R, Butters R, Kifor I, Brown EM** 1998 The calcium-sensing receptor is localized in caveolin-rich plasma membrane domains of bovine parathyroid cells. J Biol Chem 273:21708-13

9. **Favus MJ, Bushinsky DA, Lemann J** 2006 Regulation of Calcium, Magnesium and Phosphate Metabolism. In: Favus MJ (ed) Primer on the Metabolic Bone Diseases an Disorders of Mineral Metabolism, 5 ed. American Society of Bone and Mineral Metabolism, Washington DC; pp 76-84

10. **Fraser DR, Kodicek E** 1973 Regulation of 25-hydroxycholecalciferol-1-hydroxylase activity in kidney by parathyroid hormone. Nat New Biol 241:163-6

11. **Prince RL** 2006 Secondary and Tertiary Hyperparathyroidism. In: Favus MJ (ed) Primer on the Metabolic Bone Diseases and Disorders of Mineral Metabolism, 6th ed. Society for Bone and Mineral Research, Washington, DC; pp 190-195

12. **Bronner F** 2009 Recent developments in intestinal calcium absorption. Nutr Rev 67:109-13

13. **Pansu D, Bellaton C, Bronner F** 1983 Developmental changes in the mechanisms of duodenal calcium transport in the rat. Am J Physiol 244:G20-6

14. **Hoenderop JG, Hartog A, Stuiver M, Doucet A, Willems PH, Bindels RJ** 2000 Localization of the epithelial Ca(2+) channel in rabbit kidney and intestine. J Am Soc Nephrol 11:1171-8

15. **Peng JB, Chen XZ, Berger UV, Vassilev PM, Tsukaguchi H, Brown EM, Hediger MA** 1999 Molecular cloning and characterization of a channel-like transporter mediating intestinal calcium absorption. J Biol Chem 274:22739-46

16. **Slepchenko BM, Bronner F** 2001 Modeling of transcellular Ca transport in rat duodenum points to coexistence of two mechanisms of apical entry. Am J Physiol Cell Physiol 281:C270-81

17. **Bronner F** 1996 Bioavailability of calcium supplements. Am J Clin Nutr 64:825-6

18. **Favus MJ** 2002 Intestinal Absorption of Calcium, Magnesium and Phosphorus. In: Coe FL, Favus MJ (eds) Disorders of Bone Mineral Metabolism, 2nd ed. Lippincott Williams Wilkins, Philadelphia, PA, USA; pp 48-73

19. **Haussler MR, Haussler CA, Jurutka PW, Thompson PD, Hsieh JC, Remus LS, Selznick SH, Whitfield GK** 1997 The vitamin D hormone and its nuclear receptor: molecular actions and disease states. J Endocrinol 154 Suppl:S57-73

20. **Van Cromphaut SJ, Dewerchin M, Hoenderop JG, Stockmans I, Van Herck E, Kato S, Bindels RJ, Collen D, Carmeliet P, Bouillon R, Carmeliet G** 2001 Duodenal calcium absorption in vitamin D receptor-knockout mice: functional and molecular aspects. Proc Natl Acad Sci U S A 98:13324-9

21. **Weber K, Erben RG, Rump A, Adamski J** 2001 Gene structure and regulation of the murine epithelial calcium channels ECaC1 and 2. Biochem Biophys Res Commun 289:1287-94

22. **Hoenderop JG, Vennekens R, Muller D, Prenen J, Droogmans G, Bindels RJ, Nilius B** 2001 Function and expression of the epithelial Ca(2+) channel family: comparison of mammalian ECaC1 and 2. J Physiol 537:747-61

23. **Wood RJ, Tchack L, Taparia S** 2001 1,25-Dihydroxyvitamin D3 increases the expression of the CaT1 epithelial calcium channel in the Caco-2 human intestinal cell line. BMC Physiol 1:11

24. **Hoenderop JG, Bindels RJ** 2008 Calciotropic and magnesiotropic TRP channels. Physiology (Bethesda) 23:32-40

25. **Pahuja DN, DeLuca HF** 1981 Stimulation of intestinal calcium transport and bone calcium mobilization by prolactin in vitamin D-deficient rats. Science 214:1038-9

26. **Ajibade DV, Dhawan P, Benn BS, Meyer MB, Pike JW, Christakos SS** 2006 Evidence for a role of prolactin in calcium homeostasis:regulation of intestinal TRPV6 and intestinal calcium absorption by prolactin ASBMR 30th Annual Meeting, Toronto, ON

27. **Madara JL, Trier JS** 1987 Functional Morphology of the Mucosa of the Small Intestine. In: Johnson LR (ed) Physiology of the Gastrointestinal Tract, 2nd ed. Raven Press, New York; pp 1209-1249

28. **Chirayath MV, Gajdzik L, Hulla W, Graf J, Cross HS, Peterlik M** 1998 Vitamin D increases tight-junction conductance and paracellular Ca2+ transport in Caco-2 cell cultures. Am J Physiol 274:G389-96

29. **Tudpor K, Teerapornpuntakit J, Jantarajit W, Krishnamra N, Charoenphandhu N** 2008 1,25-dihydroxyvitamin D(3) rapidly stimulates the solvent drag-induced paracellular calcium transport in the duodenum of female rats. J Physiol Sci 58:297-307

30. **Fujita H, Sugimoto K, Inatomi S, Maeda T, Osanai M, Uchiyama Y, Yamamoto Y, Wada T, Kojima T, Yokozaki H, Yamashita T, Kato S, Sawada N, Chiba H** 2008 Tight junction proteins claudin-2 and -12 are critical for vitamin D-dependent Ca2+ absorption between enterocytes. Mol Biol Cell 19:1912-21

31. **Krishnamra N, Lotinun S, Limlomwongse L** 1993 Acute effect and mechanism of action of prolactin on the in situ passive calcium absorption in rat. Bone Miner 23:253-66

32. **Krishnamra N, Wirunrattanakij Y, Limlomwongse L** 1998 Acute effects of prolactin on passive calcium absorption in the small intestine by in vivo perfusion technique. Can J Physiol Pharmacol 76:161-8

33. **Thongon N, Nakkrasae LI, Thongbunchoo J, Krishnamra N, Charoenphandhu N** 2008 Prolactin stimulates transepithelial calcium transport

and modulates paracellular permselectivity in Caco-2 monolayer: mediation by PKC and ROCK pathways. Am J Physiol Cell Physiol 294:C1158-68

34. **Thongon N, Nakkrasae LI, Thongbunchoo J, Krishnamra N, Charoenphandhu N** 2009 Enhancement of calcium transport in Caco-2 monolayer through PKCzeta-dependent Cav1.3-mediated transcellular and rectifying paracellular pathways by prolactin. Am J Physiol Cell Physiol 296:C1373-82

35. **Breslau NA** 1996 Calcium Magnesium and Phosphorus: Intestinal Absorption. In: Favus MJ (ed) Primer on the Metabolic Bone Diseases and Disorders of Mineral Metabolism, 3rd ed. American Society for Bone and Mineral Research, Washington; pp 41-49

36. **Breslau NA** 2008 Calcium, Magnesium and Phosphorus: Intestinal Absorption. In: Primer on the Metabolic Bone Diseases and Disorders of Mineral Metabolism, 3rd ed. American Society for Bone and Mineral Research, Washington; pp 41-49

37. **Marcus CS, Lengemann FW** 1962 Absorption of Ca45 and Sr85 from solid and liquid food at various levels of the alimentary tract of the rat. J Nutr 77:155-60

38. **Ireland P, Fordtran JS** 1973 Effect of dietary calcium and age on jejunal calcium absorption in humans studied by intestinal perfusion. J Clin Invest 52:2672-81

39. **McCormick CC** 2002 Passive diffusion does not play a major role in the absorption of dietary calcium in normal adults. J Nutr 132:3428-30

40. **Juppner H, Abou-Samra AB, Freeman M, Kong XF, Schipani E, Richards J, Kolakowski LF, Jr., Hock J, Potts JT, Jr., Kronenberg HM, et al.** 1991 A G protein-linked receptor for parathyroid hormone and parathyroid hormone-related peptide. Science 254:1024-6

41. **Dempster DW** 2006 Anatomy an FUnctions of the Adult Skeleton. In: Favus MJ (ed) Primer on the Metabolic Bone Diseases an Disorders of Mineral Metabolism, 6 ed. American Society for Bone and Mineral Research, Washington; pp 7-11

42. **Canalis E** 1996 Regulation of Bone Remodeling. In: Favus MJ (ed) Primer on the Metabolic Bone Diseases and Disorders of Mineral Metabolism, 3 ed. American Society of Bone and Mineral Research, Washington; pp 29-34

43. **Baron RE** 1996 Anatomy and Ultrastructure of Bone. In: Favus MJ (ed) Primer on the Metabolic Bone Diseases and Disorders of Mineral Metabolism, 3rd ed. American Society for Bone and Mineral Research, Washington, DC; pp 3-10

44. **Suda T, Takahashi N, Udagawa N, Jimi E, Gillespie MT, Martin TJ** 1999 Modulation of osteoclast differentiation and function by the new members of the tumor necrosis factor receptor and ligand families. Endocr Rev 20:345-57

45. **Boyle WJ, Simonet WS, Lacey DL** 2003 Osteoclast differentiation and activation. Nature 423:337-42

46. **Pixley FJ, Stanley ER** 2004 CSF-1 regulation of the wandering macrophage: complexity in action. Trends in Cell Biology 14:628-638

47. **Ross FP** 2008 Osteoclast Biology and Bone Resorption. In: Rosen CJ (ed) Primer on the Metabolic Bone Diseases and Disorders of Bone Metabolism, 7th ed. American Society of Bone and Mineral Research, Washington, DC; pp 16-22

48. **Kostenuik PJ, Shalhoub V** 2001 Osteoprotegerin: a physiological and pharmacological inhibitor of bone resorption. Curr Pharm Des 7:613-35

49. **Brown EM** 2006 Parathyroid Hormone: Synthesis, Secretion and Action. In: Favus MJ (ed) Primer on the Metabolic Bone Diseases and Disorders of Mineral Metabolism, 6th ed, Washington, DC; pp 90-99

50. **DeLuca HF** 1980 Vitamin D revisited. Clinical Endocrinology Metabolism 9:1-26

51. **Raisz LG, Trummel CL, Holick MF, DeLuca HF** 1972 1,25-dihydroxycholecalciferol: a potent stimulator of bone resorption in tissue culture. Science 175:768-9

52. **Ross FP, Teitelbaum SL** 2005 alphavbeta3 and macrophage colony-stimulating factor: partners in osteoclast biology. Immunol Rev 208:88-105

53. **Teitelbaum SL** 2005 Osteoporosis and integrins. J Clin Endocrinol Metab 90:2466-8

54. **Teitelbaum SL, Ross FP** 2003 Genetic regulation of osteoclast development and function. Nat Rev Genet 4:638-49

55. **Salo J, Lehenkari P, Mulari M, Metsikko K, Vaananen HK** 1997 Removal of osteoclast bone resorption products by transcytosis. Science 276:270-3

56. **Aubin JE, Lian JB, Stein GS** 2006 Bone Formation: Maturation and Functional Activities of Osteoblast Lineage Cells. In: Favus MJ (ed) Primer on the Metabolic Bone Diseases and Disorders of Mineral Metabolism. American Society for Bone and Mineral Research, Washington; pp 20-29

57. **Bonewald LF, Mundy GR** 1990 Role of transforming growth factor-beta in bone remodeling. Clin Orthop Relat Res:261-76

58. **Mohan S, Baylink DJ** 1996 Insulin-like growth factor system components and the coupling of bone formation to resorption. Horm Res 45 Suppl 1:59-62

59. **Locklin RM, Oreffo RO, Triffitt JT** 1999 Effects of TGFbeta and bFGF on the differentiation of human bone marrow stromal fibroblasts. Cell Biol Int 23:185-94

60. **Ooms ME, Roos JC, Bezemer PD, van der Vijgh WJ, Bouter LM, Lips P** 1995 Prevention of bone loss by vitamin D supplementation in elderly women: a randomized double-blind trial. J Clin Endocrinol Metab 80:1052-8

61. **Xiaoyu Z, Payal B, Melissa O, Zanello LP** 2007 1alpha,25(OH)2-vitamin D3 membrane-initiated calcium signaling modulates exocytosis and cell survival. J Steroid Biochem Mol Biol 103:457-61

62. **Boivin G, Mesguich P, Pike JW, Bouillon R, Meunier PJ, Haussler MR, Dubois PM, Morel G** 1987 Ultrastructural immunocytochemical localization of endogenous 1,25-dihydroxyvitamin D3 and its receptors in osteoblasts and osteocytes from neonatal mouse and rat calvaria. Bone Miner 3:125-36

63. **Goltzman D, Miao D, Panda DK, Hendy GN** 2004 Effects of calcium and of the Vitamin D system on skeletal and calcium homeostasis: lessons from genetic models. J Steroid Biochem Mol Biol 89-90:485-9

64. **Rubin MR, Bilezikian JP** 2003 New anabolic therapies in osteoporosis. Endocrinol Metab Clin North Am 32:285-307

65. **Cross NA, Hillman LS, Allen SH, Krause GF, Vieira NE** 1995 Calcium homeostasis and bone metabolism during pregnancy, lactation, and postweaning: a longitudinal study. Am J Clin Nutr 61:514-23

66. **Kent GN, Price RI, Gutteridge DH, Rosman KJ, Smith M, Allen JR, Hickling CJ, Blakeman SL** 1991 The efficiency of intestinal calcium absorption is increased in late pregnancy but not in established lactation. Calcif Tissue Int 48:293-5

67. **Kovacs CS** 2008 Vitamin D in pregnancy and lactation: maternal, fetal, and neonatal outcomes from human and animal studies. Am J Clin Nutr 88:520S-528S

68. **Halloran BP, DeLuca HF** 1980 Calcium transport in small intestine during pregnancy and lactation. Am J Physiol 239:E64-8

69. **Brommage R, Baxter DC, Gierke LW** 1990 Vitamin D-independent intestinal calcium and phosphorus absorption during reproduction. Am J Physiol 259:G631-8

70. **Takeuchi K, Morikawa H, Ueda Y, Mochizuki M** 1988 [Studies on the effects of placental lactogen on calcium metabolism during pregnancy]. Nippon Naibunpi Gakkai Zasshi 64:1175-86

71. **Sharpe CJ, Fudge NJ, Kovacs CS** 2003 A rapid 35% flux in bone mass occurs during pregnancy and lactation cycles in mice [abstract]. International Bone and Mineral Society Meeting, Osaka, Japan

72. **Woodrow JP, Sharpe CJ, Fudge NJ, Hoff AO, Gagel RF, Kovacs CS** 2006 Calcitonin plays a critical role in regulating skeletal mineral metabolism during lactation. Endocrinology 147:4010-21

73. **Kovacs CS, Kronenberg HM** 1997 Maternal-fetal calcium and bone metabolism during pregnancy, puerperium, and lactation. Endocr Rev 18:832-72

74. **Purdie DW, Aaron JE, Selby PL** 1988 Bone histology and mineral homeostasis in human pregnancy. Br J Obstet Gynaecol 95:849-54

75. **Laskey MA, Prentice A, Hanratty LA, Jarjou LM, Dibba B, Beavan SR, Cole TJ** 1998 Bone changes after 3 mo of lactation: influence of calcium intake, breast-milk output, and vitamin D-receptor genotype. Am J Clin Nutr 67:685-92

76. **VanHouten JN, Dann P, Stewart AF, Watson CJ, Pollak M, Karaplis AC, Wysolmerski JJ** 2003 Mammary-specific deletion of parathyroid hormone-related protein preserves bone mass during lactation. J Clin Invest 112:1429-36

77. **Macdonald HM, New SA, Campbell MK, Reid DM** 2005 Influence of weight and weight change on bone loss in perimenopausal and early postmenopausal Scottish women. Osteoporos Int 16:163-71

78. **Polatti F, Capuzzo E, Viazzo F, Colleoni R, Klersy C** 1999 Bone mineral changes during and after lactation. Obstet Gynecol 94:52-6

79. **Sowers MF, Hollis BW, Shapiro B, Randolph J, Janney CA, Zhang D, Schork A, Crutchfield M, Stanczyk F, Russell-Aulet M** 1996 Elevated parathyroid hormone-related peptide associated with lactation and bone density loss. Jama 276:549-54

80. **Halloran BP, DeLuca HF** 1980 Skeletal changes during pregnancy and lactation: the role of vitamin D. Endocrinology 107:1923-9

81. **Halloran BP, DeLuca HF** 1980 Effect of vitamin D deficiency on fertility and reproductive capacity in the female rat. J Nutr 110:1573-80

82. **Halloran BP, De Luca HF** 1981 Effect of vitamin D deficiency on skeletal development during early growth in the rat. Arch Biochem Biophys 209:7-14

83. **Dardenne O, Prud'homme J, Arabian A, Glorieux FH, St-Arnaud R** 2001 Targeted inactivation of the 25-hydroxyvitamin D(3)-1(alpha)-hydroxylase gene (CYP27B1) creates an animal model of pseudovitamin D-deficiency rickets. Endocrinology 142:3135-41

84. **Li YC, Pirro AE, Amling M, Delling G, Baron R, Bronson R, Demay MB** 1997 Targeted ablation of the vitamin D receptor: an animal model of vitamin D-dependent rickets type II with alopecia. Proc Natl Acad Sci U S A 94:9831-5

85. **Yoshizawa T, Handa Y, Uematsu Y, Takeda S, Sekine K, Yoshihara Y, Kawakami T, Arioka K, Sato H, Uchiyama Y, Masushige S, Fukamizu A, Matsumoto T, Kato S** 1997 Mice lacking the vitamin D receptor exhibit impaired bone formation, uterine hypoplasia and growth retardation after weaning. Nat Genet 16:391-6

86. **Kovacs CS, Woodland ML, Fudge NJ, Friel JK** 2005 The vitamin D receptor is not required for fetal mineral homeostasis or for the regulation of placental calcium transfer in mice. Am J Physiol Endocrinol Metab 289:E133-44

87. **Li YC, Amling M, Pirro AE, Priemel M, Meuse J, Baron R, Delling G, Demay MB** 1998 Normalization of mineral ion homeostasis by dietary means prevents hyperparathyroidism, rickets, and osteomalacia, but not alopecia in vitamin D receptor-ablated mice. Endocrinology 139:4391-6

88. **Kollenkirchen U, Fox J, Walters MR** 1991 Normocalcemia without hyperparathyroidism in vitamin D-deficient rats. J Bone Miner Res 6:273-8

89. **Amling M, Priemel M, Holzmann T, Chapin K, Rueger JM, Baron R, Demay MB** 1999 Rescue of the skeletal phenotype of vitamin D receptor-ablated mice in the setting of normal mineral ion homeostasis: formal histomorphometric and biomechanical analyses. Endocrinology 140:4982-7

90. **Dostal LA, Toverud SU** 1984 Effect of vitamin D3 on duodenal calcium absorption in vivo during early development. Am J Physiol 246:G528-34

91. **Johnson LE, DeLuca HF** 2001 Vitamin D receptor null mutant mice fed high levels of calcium are fertile. J Nutr 131:1787-91

92. **Irizarry RA, Hobbs B, Collin F, Beazer-Barclay YD, Antonellis KJ, Scherf U, Speed TP** 2003 Exploration, normalization, and summaries of high density oligonucleotide array probe level data. Biostatistics 4:249-64

93. **Jain N, Thatte J, Braciale T, Ley K, O'Connell M, Lee JK** 2003 Local-pooled-error test for identifying differentially expressed genes with a small number of replicated microarrays. Bioinformatics 19:1945-51

94. **Benjamini Y, Hochberg Y** 1995 Controlling the false discovery rate: a practical and powerful approach to multiple testing. Journal of the Royal Statistical Society. Series B (Methodological) 57:289-300

95. **Rummens K, van Cromphaut SJ, Carmeliet G, van Herck E, van Bree R, Stockmans I, Bouillon R, Verhaeghe J** 2003 Pregnancy in mice lacking the vitamin D receptor: normal maternal skeletal response, but fetal hypomineralization rescued by maternal calcium supplementation. Pediatr Res 54:466-73

96. **Miller SC, Halloran BP, DeLuca HF, Jee WS** 1982 Role of vitamin D in maternal skeletal changes during pregnancy and lactation: a histomorphometric study. Calcif Tissue Int 34:245-52

97. **Bronner F, Yost JH** 1985 Saturable and nonsaturable copper and calcium transport in mouse duodenum. Am J Physiol 249:G108-12

98. **Bronner F, Pansu D, Stein WD** 1986 An analysis of intestinal calcium transport across the rat intestine. Am J Physiol 250:G561-9

99. **Song Y, Kato S, Fleet JC** 2003 Vitamin D receptor (VDR) knockout mice reveal VDR-independent regulation of intestinal calcium absorption and ECaC2 and calbindin D9k mRNA. J Nutr 133:374-80

100. **Zhou LX, Nemere I, Norman AW** 1992 1,25-Dihydroxyvitamin D3 analog structure-function assessment of the rapid stimulation of intestinal calcium absorption (transcaltachia). J Bone Miner Res 7:457-63

101. **Christakos S, Dhawan P, Ajibade D, Benn BS, Feng J, Joshi SS** Mechanisms involved in vitamin D mediated intestinal calcium absorption and in non-classical actions of vitamin D. J Steroid Biochem Mol Biol

102. **Nemere I, Schwartz Z, Pedrozo H, Sylvia VL, Dean DD, Boyan BD** 1998 Identification of a membrane receptor for 1,25-dihydroxyvitamin D3 which mediates rapid activation of protein kinase C. J Bone Miner Res 13:1353-9

103. **Zanello LP, Norman AW** 2004 Rapid modulation of osteoblast ion channel responses by 1alpha,25(OH)2-vitamin D3 requires the presence of a functional vitamin D nuclear receptor. Proc Natl Acad Sci U S A 101:1589-94

104. **Fleet JC** 2004 Rapid, membrane-initiated actions of 1,25 dihydroxyvitamin D: what are they and what do they mean? J Nutr 134:3215-8

105. **Nguyen TM, Lieberherr M, Fritsch J, Guillozo H, Alvarez ML, Fitouri Z, Jehan F, Garabedian M** 2004 The rapid effects of 1,25-dihydroxyvitamin D3 require the vitamin D receptor and influence 24-hydroxylase activity: studies in human skin fibroblasts bearing vitamin D receptor mutations. J Biol Chem 279:7591-7

106. **Miller DD** 1989 Calcium in the diet: food sources, recommended intakes, and nutritional bioavailability. Adv Food Nutr Res 33:103-56

107. **Armbrecht HJ, Wasserman RH** 1976 Enhancement of Ca++ uptake by lactose in the rat small intestine. J Nutr 106:1265-71

108. **Li YC, Bolt MJ, Cao LP, Sitrin MD** 2001 Effects of vitamin D receptor inactivation on the expression of calbindins and calcium metabolism. Am J Physiol Endocrinol Metab 281:E558-64

109. **Turksen K, Troy TC** 2004 Barriers built on claudins. J Cell Sci 117:2435-47

110. **Johnson LE, DeLuca HF** 2002 Reproductive defects are corrected in vitamin d-deficient female rats fed a high calcium, phosphorus and lactose diet. J Nutr 132:2270-3

111. **Dardenne O, Prud'homme J, Hacking SA, Glorieux FH, St-Arnaud R** 2003 Correction of the abnormal mineral ion homeostasis with a high-calcium, high-phosphorus, high-lactose diet rescues the PDDR phenotype of mice deficient for the 25-hydroxyvitamin D-1alpha-hydroxylase (CYP27B1). Bone 32:332-40

APPENDIX A1

The complete list of significant changes in duodenal gene expression obtained by whole genome microarray analysis for the following comparison:

Vdr null baseline vs. WT baseline

gene_assignment	FoldChange	adj_pvalue
NM_181729 // Muc6 // mucin 6	0.01747005	2.78E-59
NM_009363 // Tff2 // trefoil factor 2 (spasmolytic protein 1)	0.01927562	2.78E-59
NM_026860 // 1190003M12Rik // RIKEN cDNA 1190003M12	0.02821670	3.36E-28
NM_011922 // Anxa10 // annexin A10	0.034501448	5.04E-20
NM_026336 // 2310057J18Rik // RIKEN cDNA 2310057J18	0.023529273	2.60E-14
NM_133184 // Slc5a4a // solute carrier family 5	8.201186911	8.20E-13
ENSMUST00000073350 // Ctse // cathepsin E (Ctse)	0.104399282	3.55E-12
NM_028593 // Cybrd1 // cytochrome b reductase 1	0.227837588	1.08E-11
NM_001081084 // Cubn // cubilin (intrinsic factor-cobalamin receptor)	5.363943522	1.75E-11
NM_025467 // Gkn2 // gastrokine 2	0.02398303	2.09E-10
NM_001033366 // Dpcr1 // diffuse panbronchiolitis critical region	0.07719625	3.93E-10
NM_001077424 // A4gnt // alpha-1	0.07988742	7.05E-10
NM_031188 // Mup1 // major urinary protein 1	0.10453278	3.24E-08
NM_025973 // Pgc // progastricsin (pepsinogen C)	0.09894057	3.24E-08
NM_025466 // Gkn1 // gastrokine 1	0.03398676	5.22E-08
NM_008647 // Mup2 // major urinary protein 2	0.10643236	5.29E-08
NM_008647 // Mup2 // major urinary protein 2	0.10896920	7.26E-08
NM_009362 // Tff1 // trefoil factor 1	0.04192548	1.32E-07
NM_008647 // Mup2 // major urinary protein 2	0.11794654	1.83E-07
NM_001045550 // Mup2 // major urinary protein 2	0.11781678	2.56E-07
NM_001045550 // Mup2 // major urinary protein 2	0.11935309	3.15E-07
NM_022413 // Trpv6 // transient receptor potential cation channel	**0.13015475**	**5.76E-07**
NM_021332 // Glp1r // glucagon-like peptide 1 receptor	0.07855238	7.22E-07
NM_010844 // Muc5ac // mucin 5	0.05660384	1.65E-06
NM_001081078 // Lct // lactase	**4.30155899**	**1.65E-06**
NM_145434 // Nr1d1 // nuclear receptor subfamily 1	4.34941603	1.65E-06
NM_023113 // Aspa // aspartoacylase (aminoacylase) 2	4.50334613	1.96E-06
NM_001042712 // Amy2-1 // amylase 2-1	0.18141119	1.98E-06
NM_001042712 // Amy2-1 // amylase 2-1	0.18141119	1.98E-06
NM_001042712 // Amy2-1 // amylase 2-1	0.18141119	1.98E-06
NM_001042712 // Amy2-1 // amylase 2-1	0.18141119	1.98E-06
NM_009669 // Amy2 // amylase 2	0.15934821	1.98E-06
NM_001045550 // Mup2 // major urinary protein 2	0.13446752	1.98E-06
NM_001024698 // Cpa2 // carboxypeptidase A2	0.13271512	3.30E-06
NM_023219 // Slc5a4b // solute carrier family 5	5.12868280	3.30E-06
NM_011036 // Pap // pancreatitis-associated protein	2.23110379	3.30E-06
NM_007969 // Expi // extracellular proteinase inhibitor	0.15164079	4.49E-06
NM_007860 // Dio1 // deiodinase	5.10719749	7.48E-06
NM_008647 // Mup2 // major urinary protein 2	0.14355542	8.85E-06
NM_009763 // Bst1 // bone marrow stromal cell antigen 1	4.34974844	1.21E-05
NM_008386 // Ins1 // insulin I	0.15279525	1.33E-05
XM_001477017 // LOC100046894 // similar to Igk-C protein	3.86183466	1.44E-05
NM_009504 // Vdr // vitamin D receptor	0.31357283	1.45E-05
NM_199252 // Unc93a // unc-93 homolog A (C. elegans)	4.3206215	3.76E-05

APPENDIX A1

The complete list of significant changes in duodenal gene expression obtained by whole genome microarray analysis for the following comparison:

Vdr null baseline vs. WT baseline

NM_007607 // Car4 // carbonic anhydrase 4	3.99433834	3.96E-05
BC128471 // Unc93a // unc-93 homolog A (C. elegans)	4.27087551	4.47E-05
NM_001045550 // Mup2 // major urinary protein 2	0.16491619	5.79E-05
ENSMUST00000080885 // Dbp //	3.75745354	7.07E-05
NM_013590 // Lyz // lysozyme	0.92222030	8.28E-05
NM_008486 // Anpep // alanyl (membrane) aminopeptidase	2.65777403	8.67E-05
NM_146198 // Slc5a11 // solute carrier family 5	3.73013222	0.00012729
NM_013605 // Muc1 // mucin 1	0.15906580	0.00017299
NM_133675 // 1110032A04Rik // RIKEN cDNA 1110032A04	0.13847562	0.00017389
NM_175344 // Tmem16f // transmembrane protein 16F	4.00810019	0.00019840
NM_001009546 // Naaladl1 // N-acetylated alpha-linked acid.	5.56544564	0.00020020
ENSMUST00000047812 // Dpp4 // dipeptidylpeptidase 4 (Dpp4)	3.78380407	0.00020263
BC129974 // Pla2g4c // phospholipase A2	0.20342232	0.00020702
NM_001081215 // BC013672 // cDNA sequence BC013672	3.61245200	0.00021289
NM_001012307 // Defcr23 // defensin related cryptdin 23	0.64361771	0.00023103
NM_001012307 // Defcr23 // defensin related cryptdin 23	0.64361771	0.00023103
NM_009127 // Scd1 // stearoyl-Coenzyme A desaturase 1	0.19572797	0.00025986
NM_007850 // Defcr3 // defensin related cryptdin 3	0.69235211	0.00026254
NM_007850 // Defcr3 // defensin related cryptdin 3	0.69235211	0.00026254
NM_029639 // 1600029D21Rik // RIKEN cDNA 1600029D21	0.15976842	0.00028923
NM_013492 // Clu // clusterin	0.18821250	0.00030887
NM_011783 // Agr2 // anterior gradient 2 (Xenopus laevis)	0.24771194	0.00035305
NM_007850 // Defcr3 // defensin related cryptdin 3	0.70232151	0.00036360
NM_025583 // Ctrb1 // chymotrypsinogen B1	0.24216203	0.00037328
NM_017474 // Clca3 // chloride channel calcium activated 3	0.54678265	0.00039333
NM_017399 // Fabp1 // fatty acid binding protein 1	2.63050644	0.00041867
NM_026925 // Pnlip // pancreatic lipase	0.18014525	0.00050268
BC061093 // 2210010C04Rik // RIKEN cDNA 2210010C04 gene	0.15188741	0.00051317
NM_008604 // Mme // membrane metallo endopeptidase	2.71201555	0.00060177
NM_007643 // Cd36 // CD36 antigen	3.18084723	0.00060177
NM_025989 // Gp2 // glycoprotein 2 (zymogen granule membr.)	0.24405391	0.00068
NM_177802 // Slc7a15 // solute carrier family 7	3.39864474	0.00073811
NM_018830 // Asah2 // N-acylsphingosine amidohydrolase 2	3.35455778	0.00073811
BC027527 // Iapp // islet amyloid polypeptide	0.17749638	0.00081990
NM_001038996 // Try10 // trypsin 10	0.17100693	0.00081990
NM_001081310 // 2010003H20Rik // RIKEN cDNA 2010003H20	2.97425922	0.00120473
NM_009885 // Cel // carboxyl ester lipase	0.19728624	0.00121499
NM_134072 // Akr1c14 // aldo-keto reductase family 1	3.02753525	0.00127240
NM_029706 // Cpb1 // carboxypeptidase B1 (tissue)	0.17206824	0.00136462
NM_008100 // Gcg // glucagon	0.20572990	0.00146894
NM_025350 // Cpa1 // carboxypeptidase A1	0.18659062	0.00167505
NM_033612 // Ela1 // elastase 1	0.25695612	0.00177088
NM_011584 // Nr1d2 // nuclear receptor subfamily 1	2.46028477	0.00181632
ENSMUST00000033806 // Vsig1 // V-set and immu	0.16036354	0.00312132
NM_028216 // Psca // prostate stem cell antigen	0.13506044	0.00390596
NM_011259 // Reg3a // regenerating islet-derived 3 alpha	3.07176108	0.00483194
NM_008360 // Il18 // interleukin 18	2.90460940	0.00531538

APPENDIX A1

The complete list of significant changes in duodenal gene expression obtained by whole genome microarray analysis for the following comparison:

Vdr null baseline vs. WT baseline

ENSMUST00000023820 // Fabp2 // fatty acid binding protein 2	2.09737262	0.00545217
NM_011646 // Try4 // trypsin 4	0.18131316	0.00547880
ENSMUST00000069800 // Fut2 // fucosyltransferase 2 (Fut2)	0.26230618	0.00586791
ENSMUST00000057410 // Fbln1 // fibulin 1 (Fbln1)	2.82130787	0.00608967
NM_018874 // Pnliprp1 // pancreatic lipase related protein 1	0.17649297	0.00608967
ENSMUST00000058865 // Pdzk1 // PDZ domain containing 1	2.86784845	0.00679448
NM_013697 // Ttr // transthyretin	0.27978811	0.00683306
NM_001029935 // Trim38 // tripartite motif-containing 38	3.71000847	0.00694405
NM_145424 // BC089597 // cDNA sequence BC089597 // 10 D3 // 216454	3.10134342	0.00725440
NM_001082976 // Tc2n // tandem C2 domains	0.21696727	0.00737180
NM_019792 // Cyp3a25 // cytochrome P450	2.98136243	0.00836170
NM_019741 // Slc2a5 // solute carrier family 2	2.33181374	0.00864126
NM_001003405 // 1810049H19Rik // RIKEN cDNA 1810049H19	0.19936053	0.00880099
ENSMUST00000031277 // Prkg2 // protein kinase	2.85337648	0.00881361
NM_019792 // Cyp3a25 // cytochrome P450	3.01156862	0.00958223
NM_020518 // Vsig2 // V-set and immunoglobulin domain	0.23832606	0.00989103
NM_008904 // Ppargc1a // peroxisome proliferative activated rec.	2.81746876	0.00993789
NM_031197 // Slc2a2 // solute carrier family 2	2.30744151	0.01007046
NM_139142 // Xtrp3s1 // X transporter protein 3 similar 1 gene	2.71230662	0.01276961
NM_139148 // Clca4 // chloride channel calcium activated 4	0.46366399	0.01283238
NM_022411 // Slc13a2 // solute carrier family 13	2.70564159	0.01396868
NM_009099 // Trim30 // tripartite motif protein 30	2.76072049	0.01407884
NM_007919 // RP23-395H4.4 // elastase 2A // 4 E1 // 13706	0.23778684	0.01423963
NM_019815 // Cldn18 // claudin 18 //	0.20724016	0.01440302
NM_013806 // Abcc2 // ATP-binding cassette	2.23000850	0.01536195
NM_199313 // AY053573 // cDNA sequence AY053573	**3.41771022**	**0.01536195**
NM_023182 // Ctrl // chymotrypsin-like	0.25273854	0.01619867
NM_009425 // Tnfsf10 // tumor necrosis factor (ligand)	2.84433391	0.01758792
AF027131 // Muc3 // mucin 3	1.75315936	0.01904898
NM_001024225 // Defcr24 // defensin related cryptdin 24	0.67961524	0.02015273
NM_019810 // Slc5a1 // solute carrier family 5	1.62782443	0.02137025
NM_178758 // Acsm5 // acyl-CoA synthetase member 5	3.18091254	0.02185137
NM_007689 // Chad // chondroadherin	0.23455815	0.02267048
NM_021353 // Slc26a3 // solute carrier family 26	0.45722137	0.02689101
NM_010478 // Hspa1b // heat shock protein 1B	0.27128338	0.02690976
NM_026947 // 1810022C23Rik // RIKEN cDNA 1810022C23	2.72691809	0.02873092
NM_011957 // Creb3l1 // cAMP respon. Elem. bind. prot. 3-like 1	0.28651191	0.03030682
NM_001081137 // 2010204N08Rik // RIKEN cDNA 2010204N08	1.54545348	0.03068960
NM_007468 // Apoa4 // apolipoprotein A-IV	1.34036702	0.03068960
NM_173388 // Slc43a2 // solute carrier family 43	2.65501427	0.03242977
NM_011271 // Rnase1 // ribonuclease	0.25005237	0.03300215
ENSMUST00000023328 // Retnlb // resistin like beta (Retnlb)	0.53050505	0.03862735
ENSMUST00000030303 // Cyp2j6 // cytochrome P450	2.57155346	0.04121532
BC060650 // Aldh4a1 // aldehyde dehydrogenase 4 family	2.55656463	0.04626171
NM_027464 // 5730469M10Rik // RIKEN cDNA 5730469M10	2.19434445	0.04759991
NM_010639 // Klk1 // kallikrein 1	0.36384408	0.04775212

APPENDIX A1

The complete list of significant changes in duodenal gene expression obtained by whole genome microarray analysis for the following comparison:

Vdr null baseline vs. WT baseline

NM_028341 // 2810439F02Rik // RIKEN cDNA 2810439F02 gene	2.49326872	0.04853589
BC024697 // Apoc2 // apolipoprotein C-II	1.98646010	0.04901649
BC039284 // Muc2 // mucin 2	0.63589496	0.05994525
NM_001081663 // Btnl7	2.56727736	0.06034437
ENSMUST00000075068 // Pepd // peptidase D (Pepd)	2.51893270	0.06072724
ENSMUST00000025054 // Spdef // SAM pointed domain	0.29919539	0.06078031
NM_026419 // Ela3 // elastase 3	0.29418322	0.06186280
NM_001037842 // Cml3 // camello-like 3	2.92983724	0.06186280
ENSMUST00000046233 // Bbox1 // butyrobetaine (gamma)	2.72412203	0.06527830
NM_133775 // Il33 // interleukin 33	2.19224544	0.07130141
NM_019631 // Tmem45a // transmembrane protein 45a	0.31920632	0.07401122
NM_011128 // Pnliprp2 // pancreatic lipase-related protein 2	0.35032868	0.07705987
ENSMUST00000025866 // Vldlr // very low density lipoprotein receptor	0.34018037	0.08077338
NM_153506 // Clec2e // C-type lectin domain family 2	2.43664304	0.08614172
NM_009801 // Car2 // carbonic anhydrase 2	0.44054038	0.08936203
NM_008331 // Ifit1 // interferon-induced protein	2.76191724	0.08977668
NM_009155 // Sepp1 // selenoprotein P	2.31996564	0.09019386
NM_146101 // Habp2 // hyaluronic acid binding protein 2	0.34356553	0.09288956
NM_001037842 // Cml3 // camello-like 3	2.80422705	0.0933689
BC064446 // Casc4 // cancer susceptibility candidate 4	0.30068677	0.0933689
NM_027816 // Cyp2u1 // cytochrome P450	2.65909900	0.1006185
NM_194058 // Nlrp9b // NLR family	3.05435946	0.1006185
NM_011463 // Spink4 // serine peptidase inhibitor	0.60337206	0.1006185
NM_177450 // Cndp1 // carnosine dipeptidase 1	2.57651149	0.1006185
NM_153546 / Mboat1 / membr. Bnd. O-acyltransferase dom. cont.	0.33076229	0.1006692

APPENDIX A2

The complete list of significant changes in duodenal gene expression obtained by whole genome microarray analysis for the following comparison:

Vdr null pregnancy vs. *Vdr* null baseline

gene_assignment	FoldChange	adj_pvalue
NM_028593 // Cybrd1 // cytochrome b reductase 1	6.120796484	0
XM_001477017 // LOC100046894 // similar to Igk-C	0.194693201	3.21E-18
NM_011036 // Pap // pancreatitis-associated protein	0.364926724	1.54E-17
NM_008732 // Slc11a2 // solute carrier family 11 (proton-coupled divalent metal ion transporters)	4.357052681	0
NM_011260 // Reg3g // regenerating islet-derived 3 gamma	0.357380812	2.52E-13
NM_010220 // Fkbp5 // FK506 binding protein 5	4.810803807	7.27E-10
NM_001081084 // Cubn // cubilin	3.144371463	1.39E-09
NM_022413 // Trpv6 // transient receptor potential cation channel	**4.836569021**	**1.56E-07**
NM_008570 // Mcpt1 // mast cell protease 1	0.177368356	1.90E-07
NM_007398 // Ada // adenosine deaminase	0.385993652	2.41E-06
NM_011044 // Pck1 // phosphoenolpyruvate carboxykinase 1	0.340746708	1.48E-05
NM_145474 // Cyp2d34 // cytochrome P450	3.75830429	1.48E-05
BC030378 // Slc38a1 // solute carrier family 38	2.582642546	1.48E-05
NM_134005 // Enpp3 // ectonucleotide pyrophosphatase/phosphodiesterase 3	0.456800652	5.38E-05
AF121081 // Slc37a2 // solute carrier family 37 (glycerol-3-phosphate transporter)	2.727759038	8.94E-05
ENSMUST00000095541 // Susd2 // sushi domain containing 2 (Susd2)	0.331456829	8.94E-05
NM_007643 // Cd36 // CD36 antigen	0.509312565	0.000102785
NM_008630 // Mt2 // metallothionein 2	2.349464459	0.000128643
M17782 // Igk-V38 // immunoglobulin kappa chain variable 38(V38)	0.438945778	0.000152924
NM_009903 // Cldn4 // claudin 4	**0.464922575**	**0.001107139**
NM_001039562 // Ankrd37 // ankyrin repeat domain 37	3.127352469	0.001308457
NM_207105 // H2-Ab1 // histocompatibility 2	1.598633517	0.001308457
NM_028064 // Slc39a4 // solute carrier family 39 (zinc transporter)	2.171937743	0.004393782
BC010818 // Sprr2a // small proline-rich protein 2A // 3 F1|3 45.2 cM // 20755 /// BC099393 // LOC100042514 // hypothetical protein LOC100042514 // 3 F1 // 100042514	1.988749457	0.004933078
NM_009155 // Sepp1 // selenoprotein P	0.44892077	0.004933078
NM_008571 // Mcpt2 // mast cell protease 2 // 14 C3|14 20.0 cM // 17225 /// ENSMUST00000015576 // Mcpt2 // mast cell protease 2 (Mcpt2)	0.316326101	0.004933078
NM_133675 // 1110032A04Rik // RIKEN cDNA 1110032A04 gene // 3 E3 // 66183 /// AF365876	3.082500491	0.004933078

APPENDIX A2

The complete list of significant changes in duodenal gene expression obtained by whole genome microarray analysis for the following comparison:

Vdr null pregnancy vs. *Vdr* null baseline

// 1110032A04Rik // RIKEN cDNA 1110032A04 gene // 3 E3 // 66183		
NM_011259 // Reg3a // regenerating islet-derived 3 alpha // 6 C3|6 33.5 cM // 19694 /// ENSMUST00000101272 // Reg3a // regenerating islet-derived 3 alpha (Reg3a)	0.450382837	0.004933078
NM_199313 // AY053573 // cDNA sequence AY053573 // 10 D3 // 380674 /// ENSMUST00000077287 // AY053573 // cDNA sequence AY053573 (AY053573)	**0.274387156**	**0.005164111**
NM_028247 // Slc16a10 // solute carrier family 16 (monocarboxylic acid transporters)	0.480292374	0.013657821
NM_029638 // Abp1 // amiloride binding protein 1	0.477382097	0.014907647
NM_018830 // Asah2 // N-acylsphingosine amidohydrolase 2	0.49268721	0.014907647
NM_016689 // Aqp3 // aquaporin 3	0.443522676	0.020582463
NM_010378 // H2-Aa // histocompatibility 2	1.451263167	0.021569196
BC099393 // LOC100042514 // hypothetical protein LOC100042514	1.854556384	0.022816924
BC099393 // LOC100042514 // hypothetical protein LOC100042514	1.854556384	0.022816924
AK008306 // 2010103J01Rik // RIKEN cDNA 2010103J01 gene	0.567813795	0.025066917
NM_017474 // Clca3 // chloride channel calcium activated 3	1.424921707	0.027133604
NM_207624 // Ace // angiotensin I converting enzyme (peptidyl-dipeptidase A) 1	0.497894932	0.033131966
NM_027872 // Slc46a3 // solute carrier family 46	0.497758459	0.041829041
NM_026853 // Asb11 // ankyrin repeat and SOCS box-containing protein 11	2.460587282	0.041829041
NM_009801 // Car2 // carbonic anhydrase 2	1.847275217	0.041829041
NM_026918 // 1810010M01Rik // RIKEN cDNA 1810010M01 gene	1.460379772	0.041829041
NM_199252 // Unc93a // unc-93 homolog A (C. elegans)	0.506478057	0.059743023
NM_133894 // Ugt2b38 // UDP glucuronosyltransferase 2 family	0.505940194	0.063167123
NM_008486 // Anpep // alanyl (membrane) aminopeptidase	0.621230968	0.063358982
ENSMUST00000066175 // Abcg5 // ATP-binding cassette	0.49614775	0.063358982
U00478 // Dnase1 // deoxyribonuclease I deoxyribonuclease I (Dnase1)	0.403125255	0.063358982
NM_011217 // Ptprr // protein tyrosine phosphatase	0.462060897	0.065369394
NM_011575 // Tff3 // trefoil factor 3	1.54392742	0.065369394
NM_025929 // 2010109I03Rik // RIKEN cDNA 2010109I03 gene	0.618897411	0.074406175

APPENDIX A2

The complete list of significant changes in duodenal gene expression obtained by whole genome microarray analysis for the following comparison:

Vdr null pregnancy vs. *Vdr* null baseline

NM_019571 // Tspan5 // tetraspanin 5	0.535970157	0.074406175
BC070401 // Sgk1 // serum/glucocorticoid regulated kinase 1	2.149360098	0.080625796
NM_177016 // Slc17a4 // solute carrier family 17 (sodium phosphate)	0.430614235	0.085909499
NM_001025573 // 2010107G12Rik // RIKEN cDNA 2010107G12 gene	0.568385314	0.087888829
ENSMUST00000073350 // Ctse // cathepsin E (Ctse)	2.364568278	0.100161896
NM_009026 // Rasd1 // RAS	2.321938218	0.111602411
NM_009127 // Scd1 // stearoyl-Coenzyme A desaturase 1	3.207585772	0.126707778
NM_133995 // Upb1 // ureidopropionase	0.482472774	0.126707778
NM_007468 // Apoa4 // apolipoprotein A-IV	0.822485326	0.13203257
NM_001042605 // Cd74 // CD74 antigen	1.433375945	0.139334994
NM_001004184 // Slc28a1 // solute carrier family 28 (sodium-coupled nucleoside transporter)	0.576600387	0.156833937
NM_001029867 // Ugt2b36 // UDP glucuronosyltransferase	0.461741821	0.167338872
NM_001030291 // Enpp7 // ectonucleotide pyrophosphatase/phosphodiesterase 7	0.432880612	0.170388428
BC128471 // Unc93a // unc-93 homolog A (C. elegans)	0.538743519	0.171153546
NM_001029935 // Trim38 // tripartite motif-containing 38	0.419777639	0.171153546
NM_001011790 // Olfr1382 // olfactory receptor 1382	2.246118106	0.171153546
NM_009467 // Ugt2b5 // UDP glucuronosyltransferase 2 family	0.459374996	0.176023503
U28490 // H2-Eb1 // histocompatibility 2	1.44783838	0.182752634
NM_001012306 // Hsd3b3 // hydroxy-delta-5-steroid dehydrogenase	2.533205788	0.191230299
BC039284 // Muc2 // mucin 2	1.37447149	0.201677977
BC028504 // Ccl20 // chemokine (C-C motif) ligand 20	2.214645926	0.206264102
NM_023149 // Cndp2 // CNDP dipeptidase 2 (metallopeptidase M20 family)	0.57289003	0.229955102
ENSMUST00000029076 // Car3 // carbonic anhydrase 3	2.88332321	0.254386067
NM_026436 // Tmem86a // transmembrane protein 86A	0.556995602	0.254386067
NM_007409 // Adh1 // alcohol dehydrogenase 1 (class I)	0.73610361	0.254386067
NM_011978 // Slc27a2 // solute carrier family 27 (fatty acid transporter)	0.541446695	0.284425108
NM_011463 // Spink4 // serine peptidase inhibitor	1.234398517	0.288099845
NM_172448 // Rnf43 // ring finger protein 43	1.723543195	0.300959248
NM_178661 // Creb3l2 // cAMP responsive	0.534638954	0.327872365

APPENDIX A2

The complete list of significant changes in duodenal gene expression obtained by whole genome microarray analysis for the following comparison:

Vdr null pregnancy vs. *Vdr* null baseline

element binding protein 3-like 2		
NM_009763 // Bst1 // bone marrow stromal cell antigen 1	0.607238644	0.397043434
NM_028610 // Dppa4 // developmental pluripotency associated 4	0.482665569	0.413424615
ENSMUST00000102925 // Uap1l1 // UDP-N-acteylglucosamine pyrophosphorylase 1-like 1	0.607234181	0.413424615
NM_007969 // Expi // extracellular proteinase inhibitor	2.356571653	0.508349257
NM_175606 // Hopx // HOP homeobox	1.900112033	0.532996437
NM_001024714 // Cma2 // chymase 2	0.477770443	0.532996437
NM_146811 // Olfr910 // olfactory receptor 910	2.16903618	0.53578644
NM_020010 // Cyp51 // cytochrome P450	1.857106275	0.53578644
ENSMUST00000030408 // Mfsd2 // major facilitator superfamily domain containing 2 (Mfsd2)	0.606406246	0.540126013
NM_010281 // Ggh // gamma-glutamyl hydrolase	2.241582894	0.552893515
NM_010281 // Ggh // gamma-glutamyl hydrolase	2.241582894	0.552893515
NM_001033286 // Slc30a10 // solute carrier family 30	1.621158014	0.567399573
AF045497 // Igh-6 // immunoglobulin heavy chain 6	0.593047469	0.585080453
NM_025968 // Ltb4dh // leukotriene B4 12-hydroxydehydrogenase	0.556631262	0.585080453
BC024348 // 1810030J14Rik // RIKEN cDNA 1810030J14 gene	1.989945419	0.593966682
NM_001034865 // Nek10 // NIMA (never in mitosis gene a)- related kinase 10	0.529989939	0.627814254
NM_176924 // 9530053A07Rik // RIKEN cDNA 9530053A07	1.743339339	0.63680537
NM_026180 // Abcg8 // ATP-binding cassette	0.57627302	0.669721707
NM_029555 // Gstk1 // glutathione S-transferase kappa 1	1.674602963	0.727016716
NM_139142 // Xtrp3s1 // X transporter protein 3 similar 1	0.603214874	0.740784355
NM_029494 // Rab30 // RAB30	0.438181746	0.740784355
NM_001009546 // Naaladl1 // N-acetylated alpha-linked acidic dipeptidase-like 1	0.410618198	0.740784355
NM_011783 // Agr2 // anterior gradient 2 (Xenopus laevis)	1.477811247	0.75587811
NM_153783 // Paox // polyamine oxidase (exo-N4-amino)	1.582987778	0.776269388
NM_008604 // Mme // membrane metallo endopeptidase	0.656235125	0.807241881
NM_009992 // Cyp1a1 // cytochrome P450	0.258502939	0.808358151
NM_010782 // Mcpt9 // mast cell protease 9	0.499582682	0.822362172
NM_021467 // Tnni1 // troponin I	1.970041867	0.82685767
NM_023219 // Slc5a4b // solute carrier family 5	0.564237844	0.833550467

APPENDIX A2

The complete list of significant changes in duodenal gene expression obtained by whole genome microarray analysis for the following comparison:

Vdr null pregnancy vs. *Vdr* null baseline

(neutral amino acid transporters		
NM_015747 // Slc20a1 // solute carrier family 20	0.640422524	0.87203211
NM_001033324 // Zbtb16 // zinc finger and BTB domain containing 16	2.314356519	0.87203211
ENSMUST00000080885 // Dbp // D site albumin promoter binding protein (Dbp)	0.64149821	0.900644927
ENSMUST00000021530 / Hif1a / hypoxia inducible factor 1	0.612177903	0.902049436
NM_153506 // Clec2e // C-type lectin domain family 2	0.636172035	0.9168243
NM_012055 // Asns // asparagine synthetase	1.564792917	0.951767909
NM_001033366 // Dpcr1 // diffuse panbronchiolitis critical region 1	2.198909891	0.98574557
NM_207208 // Clca6 // chloride channel Ca activated 6	0.740085392	0.98574557

APPENDIX A3

The complete list of significant changes in duodenal gene expression obtained by whole genome microarray analysis for the following comparison:

WT late pregnancy vs. WT baseline

gene_assignment	FoldChange	adj_pvalue
NM_009363 // Tff2 // trefoil factor 2 (spasmolytic protein 1)	0.076079	3.63E-44
NM_181729 // Muc6 // mucin 6	0.0685669	4.19E-44
NM_026860 // 1190003M12Rik // RIKEN cDNA 1190003M12	0.0758995	1.38E-21
NM_031188 // Mup1 // major urinary protein 1	0.0562791	3.04E-16
NM_008647 // Mup2 // major urinary protein 2	0.0635273	1.48E-14
NM_008647 // Mup2 // major urinary protein 2	0.0747501	1.27E-12
NM_008647 // Mup2 // major urinary protein 2	0.0792536	2.38E-12
NM_026336 // 2310057J18Rik // RIKEN cDNA 2310057J18	0.0392125	5.05E-12
NM_001045550 // Mup2 // major urinary protein 2	0.0856137	2.69E-11
NM_025973 // Pgc // progastricsin (pepsinogen C)	0.0861823	1.27E-10
NM_001045550 // Mup2 // major urinary protein 2	0.0923848	1.56E-10
NM_025466 // Gkn1 // gastrokine 1	0.0328597	3.49E-09
NM_001045550 // Mup2 // major urinary protein 2	0.1101184	8.97E-09
NM_001077424 // A4gnt // alpha-1	0.1032305	1.21E-08
NM_009362 // Tff1 // trefoil factor 1	0.0402426	1.29E-08
NM_025467 // Gkn2 // gastrokine 2	0.0321301	1.67E-08
NM_008647 // Mup2 // major urinary protein 2	0.1171555	4.96E-08
NM_021332 // Glp1r // glucagon-like peptide 1 receptor	0.0827272	3.60E-07
NM_001045550 // Mup2 // major urinary protein 2	0.130434	3.70E-07
NM_010844 // Muc5ac // mucin 5	0.059077	9.30E-07
NM_133894 // Ugt2b38 // UDP glucuronosyltransferase 2	0.2049445	5.79E-06
NM_009992 // Cyp1a1 // cytochrome P450	4.019687	0.00039495
NM_029494 // Rab30 // RAB30	4.4439749	0.0004176
NM_011922 // Anxa10 // annexin A10	0.4612434	0.00075875
NM_145434 // Nr1d1 // nuclear receptor subfamily 1	3.7113902	0.00104328
NM_013492 // Clu // clusterin	0.237617	0.0026941
AF027131 // Muc3 // mucin 3	1.9422252	0.00390347
NM_001033366 // Dpcr1 // diffuse panbronchiolitis critical r	0.3361816	0.00634644
NM_008732 // Slc11a2 // solute carrier family 11	4.3317996	0.01622183
NM_007689 // Chad // chondroadherin	0.2340061	0.03560548
NM_019815 // Cldn18 // claudin 18	**0.210068**	**0.0370079**
NM_007969 // Expi // extracellular proteinase inhibitor	0.2985981	0.0453826
NM_013697 // Ttr // transthyretin	0.3135062	0.04834296
NM_194058 // Nlrp9b // NLR family	3.4693963	0.05178443
NM_001039562 // Ankrd37 // ankyrin repeat domain 37	4.3029713	0.05178443
NM_022413 // Trpv6 // trans. Rec. potential cation channel	**0.3278776**	**0.05447083**
ENSMUST00000033806 // Vsig1 // V-set and immunoglobul	0.1976509	0.06687534
ENSMUST00000073350 // Ctse // cathepsin E (Ctse)	0.4356475	0.08248174
NM_021353 // Slc26a3 // solute carrier family 26	0.4324279	0.08248174

APPENDIX A3

The complete list of significant changes in duodenal gene expression obtained by whole genome microarray analysis for the following comparison:

WT late pregnancy vs. WT baseline

NM_009606 // Acta1 // actin	3.0888921	0.09073478
NM_133184 // Slc5a4a // solute carrier family 5	5.277091	0.10061168

APPENDIX A4

The complete list of significant changes in duodenal gene expression obtained by whole genome microarray analysis for the following comparison:

Vdr null late pregnancy vs. WT pregnancy

gene_assignment	Fold Change	adjusted_pvalue
NM_009992 // Cyp1a1 // cytochrome P450	0.144750297	5.19E-22
NM_001081084 // Cubn // cubilin	2.632802627	0
NM_008570 // Mcpt1 // mast cell protease 1	0.084159735	6.53E-21
NM_009669 // Amy2 // amylase 2	0.107816813	5.75E-19
NM_001042712 // Amy2-1 // amylase 2-1	0.123989583	2.71E-17
NM_001042712 // Amy2-1 // amylase 2-1	0.123989583	2.71E-17
NM_001042712 // Amy2-1 // amylase 2-1	0.123989583	2.71E-17
NM_001042712 // Amy2-1 // amylase 2-1	0.123989583	2.71E-17
NM_008571 // Mcpt2 // mast cell protease 2	0.129311353	6.58E-15
NM_145474 // Cyp2d34 // cytochrome P450	5.281988808	1.82E-11
NM_001024698 // Cpa2 // carboxypeptidase A2	0.168303901	4.15E-11
NM_026925 // Pnlip // pancreatic lipase	0.163160493	9.04E-11
NM_001024714 // Cma2 // chymase 2	0.174880492	3.26E-09
NM_025583 // Ctrb1 // chymotrypsinogen B1	0.215194531	9.66E-09
NM_013590 // Lyz // lysozyme	0.405176762	1.18E-08
NM_025350 // Cpa1 // carboxypeptidase A1	0.229307957	4.27E-08
NM_010782 // Mcpt9 // mast cell protease 9	0.200963355	4.79E-08
NM_033612 // Ela1 // elastase 1	0.220061251	2.11E-07
NM_133184 // Slc5a4a // solute carrier family 5	2.045040529	3.32E-07
NM_026419 // Ela3 // elastase 3	0.264457785	5.86E-07
NM_007919 // RP23-395H4.4 // elastase 2A	0.217514775	2.20E-06
NM_133894 // Ugt2b38 // UDP glucuronosyltransferase 2 family	3.441398623	2.90E-06
NM_029706 // Cpb1 // carboxypeptidase B1 (tissue)	0.243191637	3.83E-06
NM_018874 // Pnliprp1 // pancreatic lipase related protein 1	0.284470405	3.83E-06
NM_146466 // Olfr165 // olfactory receptor 165	3.340979451	5.01E-06
NM_025929 // 2010109I03Rik // RIKEN cDNA 2010109I03 gene	0.323773611	8.60E-06
NM_207105 // H2-Ab1 // histocompatibility 2	2.125903906	1.85E-05
NM_011851 // Nt5e // 5' nucleotidase	0.268256237	2.30E-05
NM_010855 // Myh4 // myosin	0.174464373	3.67E-05
NM_009504 // Vdr // vitamin D receptor	0.318740422	3.81E-05
NM_008386 // Ins1 // insulin I	0.262650899	4.59E-05
NM_011922 // Anxa10 // annexin A10	0.123263137	4.84E-05
NM_033149 // B3galt5 // UDP-Gal:betaGlcNAc beta 1	0.202186107	4.84E-05
NM_029494 // Rab30 // RAB30	0.308323186	5.43E-05
NM_023182 // Ctrl // chymotrypsin-like	0.232202136	5.67E-05
NM_009363 // Tff2 // trefoil factor 2	0.170749897	0.000131238
NM_001081070 // Pdia2 // protein disulfide isomerase associated 2	0.270424762	0.000176361
NM_009606 // Acta1 // actin	0.317530244	0.000225045
NM_175344 // Tmem16f // transmembrane protein 16F	2.3812495	0.000370033

APPENDIX A4

The complete list of significant changes in duodenal gene expression obtained by whole genome microarray analysis for the following comparison:

Vdr null late pregnancy vs. WT pregnancy

NM_001081078 // Lct // lactase	**2.215072107**	**0.000397973**
NM_007851 // Defcr5 // defensin related cryptdin 5	0.329219205	0.000803524
NM_177610 // Duox2 // dual oxidase 2	0.19841558	0.000803524
NM_007851 // Defcr5 // defensin related cryptdin 5	0.337572095	0.001430497
BC061093 // 2210010C04Rik // RIKEN cDNA 2210010C04	0.291147872	0.001658422
NM_008012 // Akr1b8 // aldo-keto reductase family 1	0.282697656	0.001749432
NM_001082531 // Pla2g2a // phospholipase A2	0.290720642	0.001837458
NM_025989 // Gp2 // glycoprotein 2	0.306901732	0.001852824
NM_010378 // H2-Aa // histocompatibility 2	1.835866052	0.001943024
NM_007851 // Defcr5 // defensin related cryptdin 5	0.347034051	0.002128099
BC061505 // Cyp2d9 // cytochrome P450	2.815884457	0.002167262
NM_001003405 // 1810049H19Rik // RIKEN cDNA 1810049H19 gene	0.338736238	0.002235172
NM_007851 // Defcr5 // defensin related cryptdin 5	0.354479134	0.002929417
NR_003552 // Cyp2d13 // cytochrome P450	2.931906359	0.002972871
ENSMUST00000071646 // Rdh16 // retinol dehydrogenase 16	0.365801646	0.003037992
NM_001004184 // Slc28a1 // solute carrier family 28 (sodium-coupled nucleoside transporter)	2.535691468	0.003147156
U28490 // H2-Eb1 // histocompatibility 2	1.952613941	0.003791021
M17782 // Igk-V38 // immunoglobulin kappa chain variable 38(V38)	0.445149626	0.003855784
NM_007398 // Ada // adenosine deaminase	0.401156553	0.003868697
BC129974 // Pla2g4c // phospholipase A2	0.244084452	0.004512411
NM_001042605 // Cd74 // CD74 antigen (invariant polypeptide of major histocompatibility complex	1.925183374	0.005580861
NM_207568 // Olfr1252 // olfactory receptor 1252	0.357548886	0.005852911
BC027527 // Iapp // islet amyloid polypeptide	0.32025137	0.007068486
NM_199313 // AY053573 // cDNA sequence AY053573	**0.380915976**	**0.010325867**
ENSMUST00000023328 // Retnlb // resistin like beta	0.330681868	0.012488591
NM_028089 // Cyp2c55 // cytochrome P450	2.451198104	0.012691854
NM_009903 // Cldn4 // claudin 4	**0.416058835**	**0.017892917**
ENSMUST00000087012 // Slc22a7 // solute carrier family 22 (organic anion transporter)	2.304580988	0.020202182
NM_001012306 // Hsd3b3 // hydroxy-delta-5-steroid dehydrogenase	2.721600478	0.022804121
NM_007844 // Defcr-rs1 // defensin related sequence cryptdin peptide (paneth cells)	0.382182492	0.022839009
NM_007844 // Defcr-rs1 // defensin related sequence cryptdin peptide (paneth cells)	0.381105298	0.023535089
NM_023219 // Slc5a4b // solute carrier family 5 (neutral amino acid transporters	2.09254852	0.023535089
NM_011921 // Aldh1a7 // aldehyde dehydrogenase family 1	2.257494199	0.023903424

APPENDIX A4

The complete list of significant changes in duodenal gene expression obtained by whole genome microarray analysis for the following comparison:

Vdr null late pregnancy vs. WT pregnancy

NM_009394 // Tnnc2 // troponin C2	0.401891089	0.024712789
NM_013467 // Aldh1a1 // aldehyde dehydrogenase family 1	2.167620942	0.026923285
NM_145424 // BC089597 // cDNA sequence BC089597	2.24890717	0.02711761
NM_013811 // Dnahc8 // dynein	2.343095921	0.028117789
NM_001039545 // Myh2 // myosin	0.359242086	0.028320723
ENSMUST00000071886 // AY761184 // cDNA sequence AY761184	0.430971342	0.032980916
NM_007818 // Cyp3a11 // cytochrome P450	2.014681295	0.035982979
NR_003146 // Defa-ps1 // defensin	0.412739885	0.039048153
NM_133775 // Il33 // interleukin 33	2.205855462	0.039048153
NM_178758 // Acsm5 // acyl-CoA synthetase medium-chain family member 5 // 7 F2 // 272428 /// ENSMUST00000066465 // Acsm5 // RIKEN cDNA C730027J19 gene (C730027J19Rik)	2.242711992	0.044485172
NM_009999 // Cyp2b10 // cytochrome P450	2.181679635	0.04782008
NM_008387 // Ins2 // insulin II	0.414741808	0.050187809
NM_007850 // Defcr3 // defensin related cryptdin 3	0.4865402	0.050187809
NM_007850 // Defcr3 // defensin related cryptdin 3	0.4865402	0.050187809
NM_007504 // Atp2a1 // ATPase	0.326970427	0.050294971
NM_178711 // Plscr4 // phospholipid scramblase 4	2.252201592	0.05267649
NR_003146 // Defa-ps1 // defensin	0.410552609	0.053215284
NM_011271 // Rnase1 // ribonuclease	0.46264114	0.054697354
NM_001024225 // Defcr24 // defensin related cryptdin 24	0.426518272	0.056585119
ENSMUST00000099472 // Cyp2c68 // cytochrome P450	1.985700378	0.057232405
NM_009430 // Prss2 // protease	0.438806909	0.06243781
NR_003146 // Defa-ps1 // defensin	0.423467943	0.063388438
NM_001033875 // Ctrc // chymotrypsin C (caldecrin)	0.418630142	0.066139322
NM_023113 // Aspa // aspartoacylase (aminoacylase) 2	2.168360691	0.067569894
NM_022413 // Trpv6 // transient receptor potential cation channel	**1.919931529**	**0.068088318**
NM_009043 // Reg2 // regenerating islet-derived 2	0.324583367	0.068679867
NM_181541 // Caprin2 // caprin family member 2	2.208558616	0.068711881
NM_007850 // Defcr3 // defensin related cryptdin 3	0.497610065	0.068711881
NR_003146 // Defa-ps1 // defensin	0.43951884	0.077515192
BC001996 // H2-DMa // histocompatibility 2	1.952197829	0.080778886
AF045503 // EG434609 // predicted gene	0.47549364	0.081097758
NM_029639 // 1600029D21Rik // RIKEN cDNA 1600029D21	0.305089058	0.090469903
NM_010416 // Hemt1 // hematopoietic cell transcript 1	0.33510227	0.094701369
NM_008885 // Pmp22 // peripheral myelin protein	0.653651719	0.096796679

APPENDIX B

Further analysis of the duodenal microarray data.

Similarities and differences of changes in gene expression between statistical comparisons.

B1.		*Vdr* null pregnancy vs. WT pregnancy	
		Decreased	Increased
Vdr null baseline vs. WT baseline	Decreased	NM_009669 // Amy2 // amylase 2 NM_001042712 // Amy2-1 // amylase 2-1 NM_001024698 // Cpa2 // carboxypeptidase A2 NM_026925 // Pnlip // pancreatic lipase NM_025583 // Ctrb1 // chymotrypsinogen B1 NM_013590 // Lyz // lysozyme NM_025350 // Cpa1 // carboxypeptidase A1 NM_033612 // Ela1 // elastase 1 NM_026419 // Ela3 // elastase 3 NM_007919 // RP23-395H4.4 // elastase 2A NM_029706 // Cpb1 // carboxypeptidase B1 (tissue) NM_018874 // Pnliprp1 // pancreatic lipase related protein 1 NM_009504 // Vdr // vitamin D receptor // 15 F1 NM_008386 // Ins1 // insulin I NM_011922 // Anxa10 // annexin A10 NM_023182 // Ctrl // chymotrypsin-like NM_009363 // Tff2 // trefoil factor 2 (spasmolytic protein 1) NM_029639 // 1600029D21Rik // RIKEN cDNA BC061093 // 2210010C04Rik // RIKEN cDNA NM_025989 // Gp2 // glycoprotein 2 (zymogen granule membrane) BC027527 // Iapp // islet amyloid polypeptide ENSMUST00000023328 // Retnlb // resistin like beta (Retnlb) NM_001012307 // Defcr23 // defensin related cryptdin 23 NM_011271 // Rnase1 // ribonuclease NM_007850 // Defcr3 // defensin related cryptdin 3	**NM_022413 // Trpv6 // transient receptor potential cation channel**
	Increased	**NM_199313 // AY053573 // cDNA sequence AY053573**	NM_001081084 // Cubn // cubilin (intrinsic factor-cobalamin receptor) NM_133184 // Slc5a4a // solute carrier family 5 **NM_001081078 // Lct // lactase** NM_023219 // Slc5a4b // solute carrier family 5 NM_133775 // Il33 // interleukin 33 NM_178758 // Acsm5 // acyl-CoA synthetase medium-chain family member 5

APPENDIX B

Further analysis of the duodenal microarray data.

Similarities and differences of changes in gene expression between statistical comparisons.

B2.		*Vdr* null pregnancy vs. *Vdr* null baseline	
		Decreased	Increased
WT pregnancy vs. WT baseline	Decreased	NM_133894 // Ugt2b38 // UDP glucuronosyltransferase 2 family	**NM_022413 // Trpv6 // transient receptor potential cation channel** ENSMUST00000073350 // Ctse // cathepsin E
	Increased		NM_008732 // Slc11a2 // solute carrier family 11 NM_001039562 // Ankrd37 // ankyrin repeat domain 37

B3.		*Vdr* null pregnancy vs. *Vdr* null baseline	
		Decreased	Increased
Vdr null baseline vs. WT baseline	Decreased		NM_028593 // Cybrd1 // cytochrome b reductase 1 **NM_022413 // Trpv6 // transient receptor potential cation channel** NM_017474 // Clca3 // chloride channel calcium activated 3 NM_009801 // Car2 // carbonic anhydrase 2 ENSMUST00000073350 // Ctse // cathepsin E
	Increased	XM_001477017 // LOC100046894 // similar to Igk-C protein NM_011036 // Pap // pancreatitis-associated protein NM_007643 // Cd36 // CD36 antigen NM_153506 // Clec2e // C-type lectin domain family 2 NM_011259 // Reg3a // regenerating islet-derived 3 alpha **NM_199313 // AY053573 // cDNA sequence AY053573** NM_018830 // Asah2 // N-acylsphingosine amidohydrolase 2 NM_199252 // Unc93a // unc-93 homolog A (C. elegans) NM_008486 // Anpep // alanyl (membrane) aminopeptidase	NM_001081084 // Cubn // cubilin (intrinsic factor-cobalamin receptor)

APPENDIX B

Further analysis of the duodenal microarray data.

Similarities and differences of changes in gene expression between statistical comparisons.

B4.		*Vdr* null pregnancy vs. *Vdr* null baseline	
		Decreased	Increased
Vdr null pregnancy vs. WT pregnancy	Decreased	NM_008570 // Mcpt1 // mast cell protease 1 NM_008571 // Mcpt2 // mast cell protease 2 NM_007398 // Ada // adenosine deaminase M17782 // Igk-V38 // immunoglobulin kappa chain variable 38 **NM_009903 // Cldn4 // claudin 4** **NM_199313 // AY053573 // cDNA sequence AY053573** NM_025929 // 2010109I03Rik // RIKEN cDNA 2010109I03 gene	
	Increased	NM_133894 // Ugt2b38 // UDP glucuronosyltransferase 2 family	NM_145474 // Cyp2d34 // cytochrome P450 NM_001081084 // Cubn // cubilin (intrinsic factor-cobalamin receptor) NM_010378 // H2-Aa // histocompatibility 2 **NM_022413 // Trpv6 // transient receptor potential cation channel** NM_207105 // H2-Ab1 // histocompatibility 2